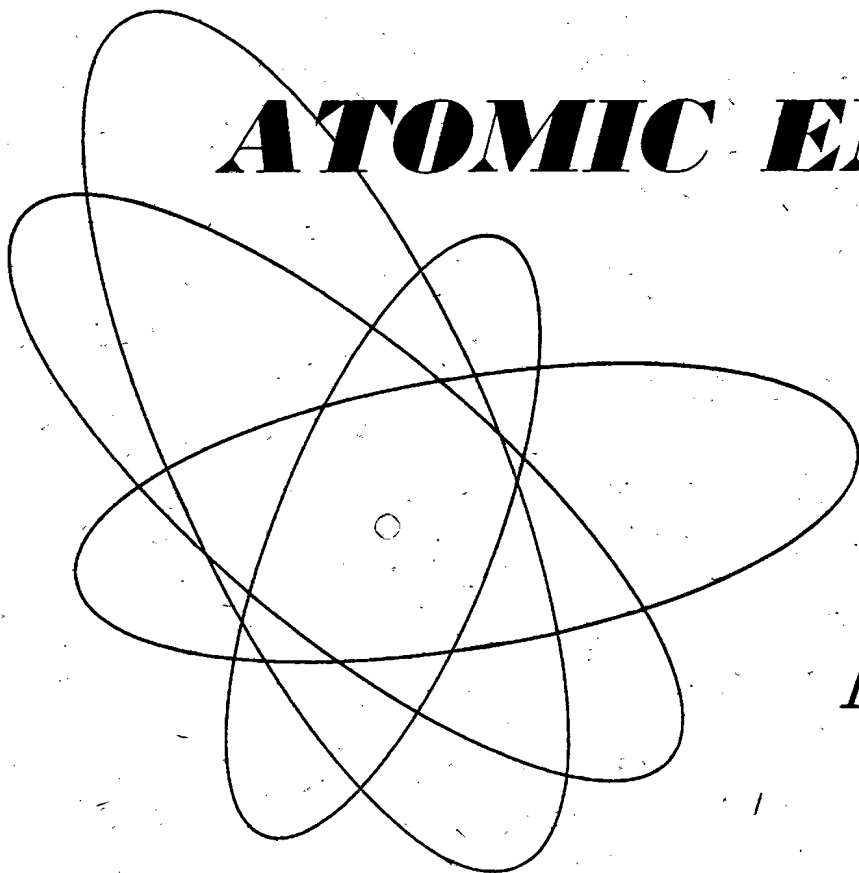# THE SOVIET JOURNAL OF

ATOMIC ENERGY

Атомная энергия

TRANSLATED FROM RUSSIAN

CONSULTANTS BUREAU

2 outstanding new Soviet journals

KINETICS AND CATALYSIS

The first authoritative journal specifically designed for those interested (directly or indirectly) in kinetics and catalysis. This journal will carry original theoretical and experimental papers on the kinetics of chemical transformations in gases, solutions and solid phases; the study of intermediate active particles (radicals, ions); combustion; the mechanism of homogeneous and heterogeneous catalysis; the scientific grounds of catalyst selection; important practical catalytic processes; the effect of substance — and heat-transfer processes on the kinetics of chemical transformations; methods of calculating and modelling contact apparatus.

Reviews summarizing recent achievements in the highly important fields of catalysis and kinetics of chemical transformations will be printed, as well as reports on the proceedings of congresses, conferences and conventions. In addition to papers originating in the Soviet Union, KINETICS AND CATALYSIS will contain research of leading scientists from abroad.

Contents of the first issue include:

Molecular Structure and Reactivity in Catalysis. A. A. Balandin

The Role of the Electron Factor in Catalysis. S. Z. Roginskii

The Principles of the Electron Theory of Catalysis on Semiconductors. F. F. Vol'kenshtein

The Use of Electron Paramagnetic Resonance in Chemistry. V. V. Voevodskii

The Study of Chain and Molecular Reactions of Intermediate Substances in Oxidation of n-Decane. Z. K. Maizus, I. P. Skibida, N. M. Emanuél' and V. N. Yakovleva

The Mechanism of Oxidative Catalysis by Metal Oxides. V. A. Roiter

The Mechanism of Hydrogen-Isotope Exchange on Platinum Films. G. K. Boreskov and A. A. Vasilevich

Nature of the Change of Heat and Activation Energy of Adsorption with Increasing Filling Up of the Surface. N. P. Keier

Catalytic Function of Metal Ions in a Homogeneous Medium. L. A. Nikolaev

Determination of Adsorption Coefficient by Kinetic Method. I. Adsorption Coefficient of Water, Ether and Ethylene on Alumina. K. V. Topchieva and B. V. Romanovskii

The Chemical Activity of Intermediate Products in Form of Hydrocarbon Surface Radicals in Heterogeneous Catalysis with Carbon Monoxide and Olefins. Ya. T. Éidus

Contact Catalytic Oxidation of Organic Compounds in the Liquid Phase on Noble Metals. I. Oxidation of the Monophenyl Ether of Ethyleneglycol to Phenoxyacetic Acid. I. I. Ioffe, Yu. T. Nikolaev and M. S. Brodskii

Annual Subscription: $150.00

Six issues per year — approx. 1050 pages per volume

JOURNAL OF STRUCTURAL CHEMISTRY

This significant journal contains papers on all of the most important aspects of theoretical and practical structural chemistry, with an emphasis given to new physical methods and techniques. Review articles on special subjects in the field will cover published work not readily available in English.

The development of new techniques for investigating the structure of matter and the nature of the chemical bond has been no less rapid and spectacular in the USSR than in the West; the Soviet approach to the many problems of structural chemistry cannot fail to stimulate and enrich Western work in this field. Of special value to all chemists, physicists, geochemists, and biologists whose work is intimately linked with problems of the molecular structure of matter.

Contents of the first issue include:

Electron-Diffraction Investigation of the Structure of Nitric Acid and Anhydride Molecules in Vapors. P. A. Akishin, L. V. Vilkov and V. Ya. Rosolovskii

Effects of Ions on the Structure of Water. I. G. Mikhailov and Yu P. Syrnikov

Proton Relaxation in Aqueous Solutions of Diamagnetic Salts. I. Solutions of Nitrates of Group II Elements. V. M. Vdovenko and V. A. Shcherbakov

Oscillation Frequencies of Water Molecules in the First Coordination Layer of Ion in Aqueous Solutions. O. Ya. Samilov

Second Chapter of Silicate Crystallochemistry. N. V. Belov

Structure of Epididymite NaBeSi$_3$O$_7$OH. A New Form of Infinite Silicon —Oxygen Chain (band) [Si$_6$O$_{15}$]. E. A. Podedimskaya and N. V. Belov

Phases Formed in the System Chromium—Boron in the Boron-Rich Region. V. A. Épel'baum, N. G. Sevast'yanov, M. A. Gurevich and G. S. Zhdanov

Crystal Structure of the Ternary Phase in the Systems Mo(W)—Fe(CO,Ni)—Si. E. I. Gladyshevskii and Yu. B. Kyz'ma

Complex Compounds with Multiple Bonds in the Inner Sphere. G. B. Bokii

Quantitive Evaluation of the Maxima of Three-Dimensional Paterson Functions. V. V. Ilyukhin and S. V. Borisov

Application of Infrared Spectroscopy to Study of Structure of Silicates. I. Reflection Spectra of Crystalline Sodium Silicates in Region of 7.5-15μ. V. A. Florinskaya and R. S. Pechenkina

Use of Electron Paramagnetic Resonance for Investigating the Molecular Structure of Coals. N. N. Tikhomirova, I. V. Nikolaeva and V. V. Voevodskii

New Magnetic Properties of Macromolecular Compounds with Conjugated Double Bonds. L. A. Blyumenfel'd, A. A. Slinkin and A. E. Kalmanson

Annual Subscription: $80.00

Six issues per year — approx. 750 pages per volume

Publication in the USSR began with the May-June 1960 issues. Therefore, the 1960 volume will contain four issues. The first of these will be available in translation in April 1961.

THE SOVIET JOURNAL OF

ATOMIC ENERGY

A translation of ATOMNAYA ENERGIYA,
a publication of the Academy of Sciences of the USSR

(Russian original dated January, 1960)

Vol. 8, No. 1   **April, 1961**

CONTENTS

CONTENTS (continued)

NOTE

The Table of Contents lists all material that appears in Atomnaya Énergiya. Those items that originated in the English language are not included in the translation and are shown enclosed in brackets. Whenever possible, the English-language source containing the omitted reports will be given.

Consultants Bureau Enterprises, Inc.

INFLUENCE OF THE REACTOR TEMPERATURE CHARACTERISTICS UPON THE CHOICE OF THE OPTIMUM THERMODYNAMIC CYCLE OF AN ATOMIC-ELECTRICAL GENERATING STATION

D. D. Kalafati

In this article we investigate the possible temperature changes in a nuclear energy station as a function of the thermal power of the reactor when there are two limiting temperatures: for the shell and for the center of the heat-emitting elements. We find the changes in the allowed thermal and electrical power of the unit as a function of the parameters of the thermodynamic cycle. We give the reader an understanding of the boundary thermal power of the reactor and the efficiency of the generator.

We also give the conditions under which the formulas which we have derived may be used for a preliminary calculation of the optimum parameters of the thermodynamic cycle. Our analysis gives the curves which show the increase in the parameters and the efficiency of the electrical generating station as a function of the material of which the shell is constructed and of the type of nuclear fuel used.

Changes in the initial parameters of the thermodynamic cycle of atomic-electrical generating stations and, consequently, of the temperature of the heat carriers leads to changes in the thermal power of the reactor as well as to changes in the efficiency of the cycle; therefore, the optimum parameters of the thermodynamic cycle and of the heat carriers are determined only by a simultaneous analysis of the operating conditions of the cycle and the reactor. Besides, in order to calculate the thermal operation of the reactor we must first know the optimum initial parameters of the cycle and of the heat carriers. This is difficult to do merely by means of variational calculations.

The following formula (1) was obtained on the basis of using the condition of minimum cost of electrical energy in a preliminary calculation of the optimum mean temperature of the heat supply for the heat cycles in the steam turbines of the atomic-electrical generating stations

$$T_{1\,cy}^{op.\ m} = \sqrt{\frac{T_r^1 T_{2cy}}{1-z}} \text{°K}, \qquad (1)$$

where T_r^1 is the limiting temperature of the shell T_s^1 or of the center T_c^1 of the heat-emitting elements (HEEL) of the reactor; T_{2cv} is the temperature in the condenser; $z = \eta_t + c_T$ (η_t is the thermal efficiency of the cycles, c_T is the thermal component of the cost of the electrical energy).

For a small thermal component where we can assume that $c_T = 0$, formula (1) corresponds to the condition of maximum electrical power of the generating station [2]:

$$T_{1\,cy}^{op.\ m} = \sqrt{T_r^1 T_{2cy}} \text{°K}. \qquad (2)$$

Formula (2) gives the value of the optimum mean temperature not of the heat carriers, as in the formula obtained by G. Melets [3, 4], but of the thermodynamic cycle. As a result of the completely identical results for limiting temperatures of the center and periphery [1, 2], in formulas (1) and (2) the temperature T_r^1 must correspond to the limiting shell temperature or the limiting center temperature and which of the temperatures is the limiting one in a given reactor. Since the optimum temperature of the cycle differs basically, it is necessary to establish which optimum is preferable for nuclear energy installations: that determined on the basis of the limiting temperature of the shell or that determined on the basis of the limiting temperature of the center.

In addition to this we often assume that the optimum temperatures exist simultaneously at the periphery and at the center. The question then arises as to how we can, in such a case, determine the optimum cycle parameters.

Possible Temperature Characteristics of the Nuclear Energy Station

Let us examine the possible temperature changes in a given nuclear energy installation for changes in the

1

thermal power of the reactor, due to changes in the initial parameters and to the thermodynamic cycle. Let the form, the surface, the number of HEEL be given and let us choose the velocity and consumption of heat carriers. Under these conditions, the thermal power of the reactor is proportional to the difference in the limiting temperatures of the shell (or center) of the HEEL and the average temperature of the heat supply pipes in the cycle [1]:

$$Q_r = k_r n k_t F_s \omega (T_r^1 - T_{1cy}^m) \qquad (3)$$

where k_r is the coefficient of nonuniformity of heat emission with respect to the reactor radius, $\underline{n}$ is the number of HEEL, k_t is the coefficient of heat transmission, F_s is the surface of the HEEL, and ω is the coefficient of utilization of the possible reactor power.

The electric power of the station is equal to

$$P_e = Q_r \eta_{st}^{pr} - \Delta P_{sn} = k_r n k_t F_s \omega (T_r^1 - T_{1cy}^m) \times$$
$$(1 - \frac{T_{2cy}}{T_{1cy}^m}) \eta_{ri} \eta_m \eta_g - \Delta P_{sn} \qquad (4)$$

where $\eta_{ri} \eta_m \eta_g$ is the product of three efficiencies: the relative inner, the mechanical and the generator efficiency; and ΔP_{sn} is the power required for the operation of the station. If we change the thermal power Q_r for the given constant thermal resistances of the HEEL, constant heat transmission to the heat carriers and the steam generator, then all the temperature drops in the indicated elements change proportionally to the thermal power of the reactor. However, the temperature changes of these elements cannot be the same (Fig. 1) since they depend upon the conditions under which the changes occur in the thermal power of the reactor.

For a small thermal power (Zone I) an increase in the thermal flux leads to an increase in all the temperatures of the unit except the condenser temperature T_{2cy} = const. In Zone I an increase in the thermal power of the reactor leads to an increase in the average temperature of the cycle, i.e., in this zone there is no maximum electrical power. In the indicated zone we may operate reactors that are used for study purposes, but as far as the operation of power reactors is concerned, it is always advantageous to increase the thermal power until the maximum peripheral power T_s^{max} up to the limiting value. A further increase in the thermal power of the reactor must occur for T_s^1 = const. This can only be accomplished by lowering the mean temperature of the heat carriers in the cycle, while at the same time increasing the maximum temperature of the center HEEL T_c^{max}. Since in this process the thermal power increases and the cycle efficiency drops, then in Zone II, according to equation (4), we get the maximum electrical power of the station which corresponds to the optimum mean temperature of the cycle, equation (2), if we substitute in the formula T_s^1 for T_r^1. Then the point A, corresponding to the optimum thermal reactor power, is determined by the

Fig. 1. Possible temperature changes in a nuclear energy installation with $T_{1cy}^{op\,m}$ in Zone II.
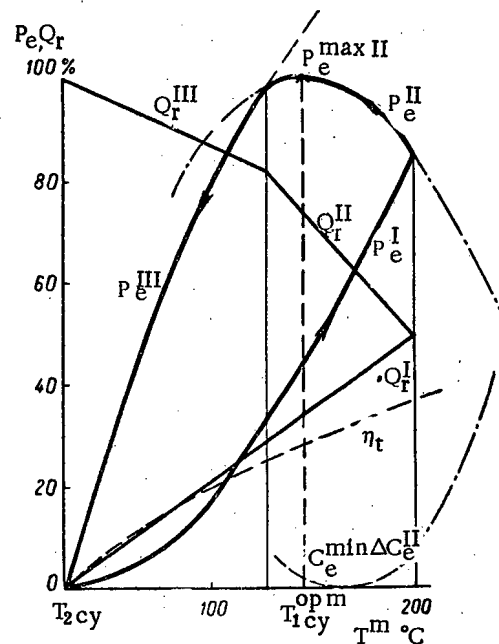
Fig. 2. Dependence of the thermal and electrical power of a reactor with $T_{1cy}^{op\,m}$ in Zone II upon T_{1cy}^m.

point of intersection of the lines of the optimum and allowed temperature cycles (see Fig. 1).

The dependence of the thermal and electrical power of the station upon the average temperature of the cycle for one limiting temperature of the shell or of the HEEL of the center is discussed in papers [1, 2]. For two limiting temperatures, the allowed changes in the thermal and electrical power have been computed from equations (3) and (4), for the case of an optimum in the average power Zone II, as a function of the mean temperature of the heat conductor for the cycle T_{1cy}^m and are shown in Fig. 2. We can see from Figs. 1 and 2 that an

2

increase in the thermal power in Zone II for T_s^1 = const. is possible until we reach the limiting temperature of the center of the HEEL, after which possible changes in thermal and electrical power can occur only for T_c^1 = const, i.e., in the high thermal power Zone III. in this case we must substitute T_c^1 for T_r^1 in equations (3) and (4).

Since the limiting shell temperature is bounded by the quality of the materials used or the properties of the heat carriers and often does not exceed 300 - 400°C, then for a condenser pressure p_2 = 0.04 atm (t_s = 28.6°C) and T_s^1 = 300°C we get from equation (2):

$$T_{1cy}^{op\ m} = \sqrt{573 \cdot 302} = 416\,°K = 143\,°C,$$

this corresponds (for the cited temperature range of the shell) to a saturated steam cycle with an initial pressure of 5 - 10 atm. Such steam parameters would lead to low efficiencies (of the order of 20% and less), therefore the operation of atomic-electrical generating stations in Zone II would not be economical. For the same thermal reactor power an increase in the efficiency of the station [the factor η_{st}^{pr} in equation (4)] increases proportionately, or lowers the specific capital losses. For a given electrical power for the station using nuclear fuel, i.e., for the same depth of burning (degree of fuel utilization), the duration of the reactor charge is directly proportional to the efficiency of the station. Therefore an increase in the efficiency of atomic generating stations is significant even for the small fuel cost component of electrical generating stations.

Since the limiting temperatures of the center of the HEEL are significantly higher than those of the shell (from T_c^1 = 660°C for metallic uranium to T_c^1 = 2800°C for uranium dioxide) then the optimum mean temperature of the heat conductor during the cycle, as given by formula (2) according to the limiting temperature of the center of the HEEL, increases discontinuously as for

example, for T_c^1 = 1000°C, $T_{1cy}^{op\ m}$ = $\sqrt{1273 \cdot 302}$ = 623°K = 350°C. This mean temperature necessitates the use of steam with ultra-high parameters, with station efficiency of the order of 40% which is twice as great as the efficiency of the station during operation in Zone II. In connection with this it is expedient to take such possible temperature characteristics of the nuclear energy installation so that the lines of the optimum and possible temperature cycles cross in Zone II and in Zone III; in Zone III both the thermal power of the reactor and the optimum cycle efficiency are greater (Fig. 3).

Upon reaching the limiting temperature of the shell and of the center of the HEEL simultaneously, the thermal power, which we shall henceforth call the boundary thermal power of the reactor, Q_r^b, does not as yet reach its maximum possible value, as has sometimes been indicated in the literature, but lies only at the beginning of Zone III. A further increase in the thermal power of the given reactor in Zone III for T_c^1 = const is possible if we decrease the maximum shell temperature as well as the mean temperatures of the cycle and of the heat carriers.

Possible changes in the thermal and electrical powers of the nuclear energy installation in the presence of an optimum in Zone III as a function of the changes in the mean temperature of the cycle are given in Fig. 4. As we see from the figure, if we increase the mean temperature of the cycle, when operating in Zone III, the electrical power of the installation increases at first, reaches a maximum $T_{1cy}^{op\ m}$ (determined from equation (2) by substituting T_c^1 for T_r^1), and then decreases. After we reach the boundary thermal power of the reactor, changes in the thermal and electrical power are possible only for the conditions of Zone II.

Thus the economy in the operation of atomic electrical generating stations operating in Zone III at a higher thermal power and greater efficiency is significantly
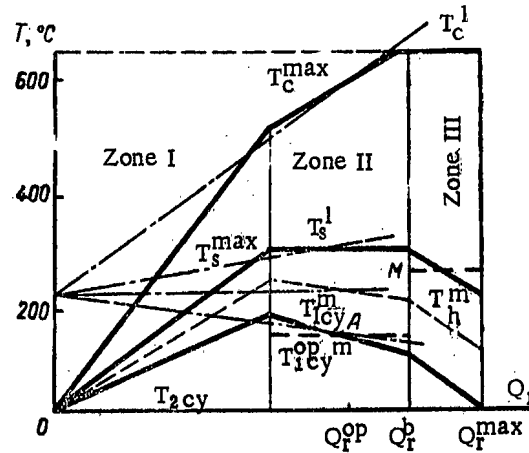

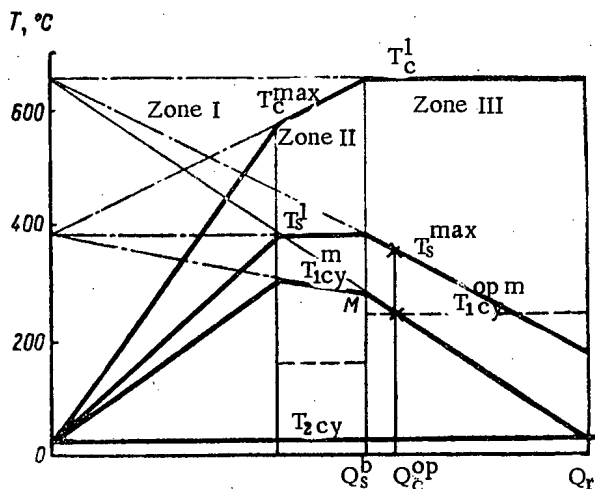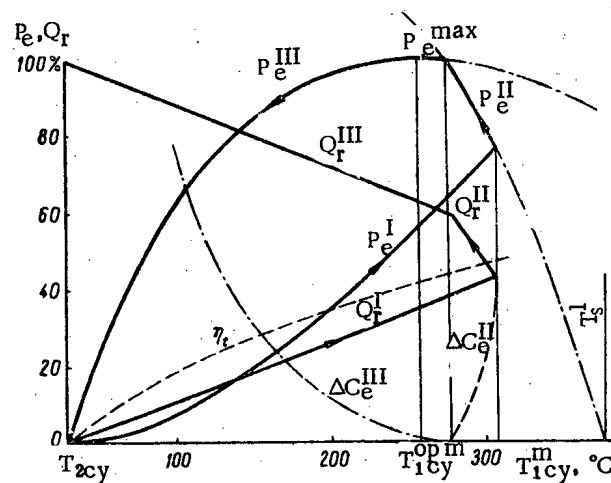Fig. 3. Possible temperature changes in a nuclear energy installation with $T_1^{op}c_y^m$ in Zone III.

Fig. 4. Dependence of the thermal and electrical power of a reactor with $T_1^{op}c_y^m$ in Zone III upon $T_1^m{}_{cy}$.

3

greater than that for electrical generating stations operating in Zone II where the optimum cycle parameters are determined by the limiting temperature of the shell. Therefore the best conditions for the operation of atomic-electrical generating stations are the conditions prevailing in Zone III where the optimum cycle parameters are determined by equation (2) according to the limiting temperature of the center of the HEEL. Since in Zone III the temperatures of the shell and cycle decrease relatively slowly, it is more probable that the operation in Zone III will be in the vicinity of point M (Fig. 5).

Due to the independence of the coefficients of conductivity and thermal emission of the mean temperature, the possible temperature characteristics take the form of line segments, Fig. 3. If the indicated coefficients change somewhat with temperature, then these lines will have an insignificant curvature, but the shape of the diagram and the division of the characteristics into three characteristic zones will not change. We wish to underline the fact that the diagram we have shown is not a diagram of the changing mode of operation of the reactor during power regulation in the exploitation process (for example, at average heat carrier temperatures $T_h^m = \mathrm{const}$, see dotted line in Fig. 1) but the characteristic temperature changes in the unit due to the choice of thermal power of the reactor.
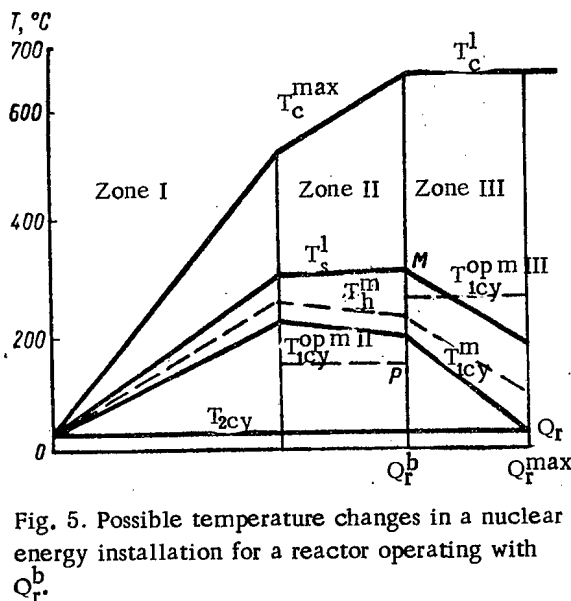
Fig. 5. Possible temperature changes in a nuclear energy installation for a reactor operating with Q_r^b.

Limiting Thermal Power of the Reactor and Greatest Electrical Power of the Station

Depending upon the relationships between the limiting temperatures of the shell and the center, the relationships between the thermal resistances of the HEEL,

the processes of heat transfer to the thermal carriers and the resistances of the steam generator, an intersection of the lines giving the possible changes in the mean temperatures of the cycle with the lines of optimum mean temperature in Zone III is not always possible. In particular, this is impossible when the limiting temperature of the shell of a given reactor in Zone III is lower than the optimum mean temperature of the cycle according to (2) with respect to the limiting temperature of the center, i.e., if

$$\sqrt{T_c^1\, T_{2cy}} > T_s^1. \qquad (5)$$

The indicated temperature relationship occurs, for example, in uranium dioxide water-water reactors. Since, for WWER (water-water element reactors) $T_c^1 = 2200°C$ and due to the absence of the boiling away of the heat carriers for $p_T = 100$ atm, it follows that $T_s^1 = 309°C$ [5]. Then according to the equation (5)

$$\sqrt{2473 \cdot 302} = 860°K > 582°K,$$

i.e., for the indicated type of reactor it is impossible to obtain the optimum mean temperature of the cycle in Zone III, due to the low limiting temperature of the HEEL of the shell. For this case, the mean temperature of the cycle must be as near as possible to the limiting temperature of the shell, since it is entirely expedient to raise the possible temperature characteristics, and the extent to which they are raised is limited only by the necessary optimum temperature drop in the steam generator Δt_{sg}^m. The temperature characteristics of such a unit are shown in Fig. 5, while the possible changes in thermal and electrical power, as a function of the mean cycle temperature or of the heat carriers, are shown in Fig. 6. For the case under consideration, there is no maximum electrical power either in Zone II or in Zone III, since the limiting temperatures of the HEEL of the shell and center are reached simultaneously for the point when, in one of these zones, the maximum is obtained. However, on the boundary of Zones II and III, for the limiting thermal power of the reactor, the greatest electrical power is obtained at the point of intersection of the curves which show the changes in electrical power in Zones II and III (Fig. 6).

The optimum mean temperature of the cycle, corresponding to the value of greatest electrical power, is always located between the two values of optimum mean temperature of the cycle which are determined from equation (2) if we substitute first the value of the limiting shell temperature and then the limiting temperature of the center of the HEEL. The value of the mean temperature of the cycle corresponding to the maximum electrical power cannot be found from equation (2). Therefore, the attempt [6] to find P_e^{max} by introducing, in equation (2), the limiting temperature of the shell plus a correction factor cannot be successful.

4

However, for the case of the limiting thermal power we get from the condition of the simultaneous existence of the limiting temperatures of the shell and of the center of the HEEL a single-valued determination of the mean temperature of the heat carriers. This solves the problem. For this case the optimum mean temperature of the cycle is determined from the expression

$$T_{1cy}^{opm} = T_h^{mb} - \Delta t_{sg}^{opm} \tag{6}$$

If, for the maximum electrical power there was a flat part of the power curve for which it would be possible that a small deviation of the mean temperatures of the cycle and of the heat carriers from the optimum would not result in a drop in the electrical power, then the derivative dP_e/dT_{1cy}^m would have a discontinuity. At this point E on the electric power curve we get a sharp peak (see Fig. 6) Therefore, even a small deviation of the mean temperature of the heat carriers from the optimum can lead to a noticeable lowering of the electrical power of the installation. For example, the maximum temperature of the center of the HEEL, 1200°C, for the atomic generating station in Shippingport [7], had not yet reached the limiting value for uranium dioxide, i.e., the steam pressure $p_1 = 39.2$ atmospheres, which was too high for the given installation, corresponds to point III on Fig. 6, and does not insure the maximum possible electrical power of the station.

Thus in the case under study, when the limiting temperature of the center of the HEEL is reached, it is expedient to raise the temperature characteristics for the mean cycle temperature, but if for the given installation $T_c^{max} < T_c^1$, it is expedient to lower the mean temperature of the cycle so that the limiting temperature of the center is not reached.

Power Efficiency of the Steam Generator

For the greatest electrical power output of the installation there is a boundary value for the thermal power of the reactor, but for a constant consumption of heat carriers there exists a mean temperature to which the heat carriers are raised. For this case, changes in the parameters and in the efficiency per cycle of the installation can occur only as the result of changes in the temperature drop within the steam generator due to changes in its surface heating or in the coefficient of heat transmission k_{ht}.

If, during alternations in the thermal power of the reactor, changes in the steam generator temperature drop influence the coefficient of utilization of the thermal power of the reactor [1, 2], then for a limiting thermal power, changes in the mean temperature drop in the steam generator, due to changes in its surface heat, influence only the changes in the thermal efficiency of the cycle.

Evaluations made in the literature regarding the quality of the steam generator sometimes make use of a value of the steam generator which takes into account the heat losses. These can usually be neglected.

For a given reactor, thermal power $Q_r^b = const$ due to the fact that the heat exchange process in the steam generator is not reversible, the index of thermodynamic perfection of the steam generator must be set up not in terms of the heat but in terms of the power efficiency of the steam generator and be equal to the ratio of the maximum work capability of the heat, before and after the heat exchange in the steam generator:

$$\eta_{sg}^{en} = \frac{AL_t^{cy}}{AL_t^{rev}} = \frac{\eta_t^{cy}}{\eta_t^{rev}} = \frac{(T_{1cy}^m - T_{2cy})T_h^m}{(T_h^m - T_{2cy})T_{1cy}^m}, \tag{7}$$

where AL_t^{cy} represents the operation of an ideal steam cycle (Fig. 7) and AL_t^{rev} represents the maximum possible work capability of the heat received by the heat carrier, which is equivalent to the operation of the reversible cycle, abcda, with an alternating temperature in the heat carrier heat supply. The work ratio in equation (7) is equal to the ratio of the efficiencies of the steam and reversible cycles expressed in terms of the temperature, since they represent the same amount of supplied heat.

In order to evaluate the thermodynamic perfection of the steam generators in atomic-electrical generating stations, we wish to point out, for example, that the power efficiency of the steam generator for a station with (WWER) computed from equation (7) is $\eta_{sg}^{en} = 0.92$, that for the atomic icebreaker "Lenin" is $\eta_{sg}^{en} = 0.835$, i.e., the power efficiency of the steam generators is close to the thermal efficiency of the boilers. The optimum
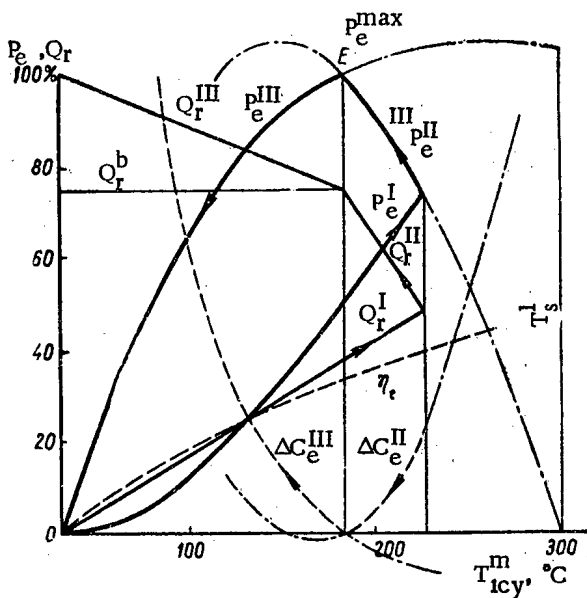

Fig. 6. Dependence of the thermal and electrical power of a reactor with Q_r^b upon T_{1cy}^m.
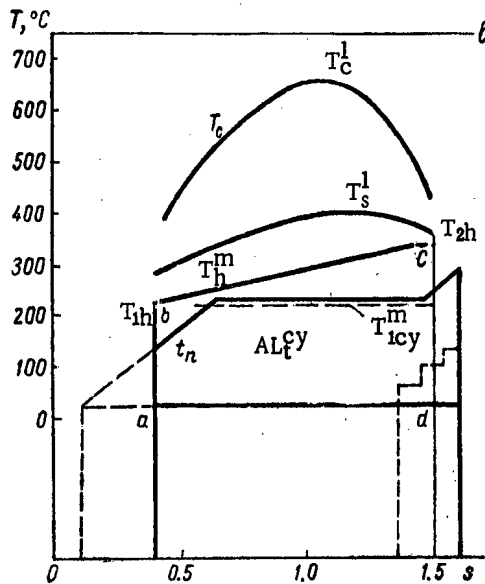
5

Fig. 7. Loss in the working capability of
the heat during nonreversible heat exchange
in the steam generator.

temperature drop in a steam generator is uniquely determined by comparing the surface heating of the steam generator and the energy losses during heat exchange, however, this requires a special derivation.

Influence of the Fuel Component Cost of Electrical Energy Upon the Optimum Cycle Parameters

Previously we have, for simplicity, examined installations in which the cost of the fuel components of the electrical energy was so small that it could be neglected, i.e., for which the optimum parameters were determined by the condition of maximum electrical power.

When the cost of the fuel component reaches 0.1 - 0.2 and higher, the optimum mean temperature of the cycle must be determined from the condition of the minimum electrical energy cost. Changes in the cost of the electrical energy may be expressed as a function of the electrical power and the efficiency of the station [1]:

$$C_e = C_K + C_T = \frac{K}{P_e} + \frac{V}{\eta_{st}} \text{ cents/kw hour,} \qquad (8)$$

where K denotes the capital outlay,* amortization, salaries, and other exploitation expenses which are proportional to time and computed per hour of operation of the atomic power generating station, and V is the cost of nuclear fuel used per kilowatt hour of heat generated.

The optimum mean temperature of the cycle, taking the cost of the nuclear fuel into account for K = const, is determined from equation (1). This preserves all the previously obtained conclusions regarding the influ-

ence of the possible temperature characteristics of the installation upon the optimum mean temperature of the cycle.

The optimum mean temperature and efficiency of the cycle corresponding to a minimum cost of electrical energy for either Zones II or III (determined respectively from the limiting temperature of the shell and the central HEEL) will be somewhat higher than the temperature and the efficiency corresponding to maximum electrical power (2).

However, if the unit operates at the limiting thermal reactor power, then as a result of the discontinuity in the power derivative dP_e/dT_{icy}^m at the point E (see Fig. 6) then the derivative of the costs dC_e/dT_{icy}^m will also have a discontinuity at this point. Instead of obtaining the minimum cost for the limiting thermal reactor power, we will get the minimum value of the cost of the electrical energy (except for the boundary portions at points M and P, Fig. 5). Thus, for the limiting thermal power of the unit the maximum electrical power usually coincides with the condition of minimum cost of electrical energy.

For uranium, for $T_c^l = 650°$, $c_T = 0.40$ and $\eta_t = 0.45$, the coefficient z is 0.18. Under these conditions, the optimum mean temperature of the heat supply is equal to

$$T_{icy}^{op\ m} = \sqrt{\frac{923 \cdot 302}{1 - 0.18}} = 585° \text{ K} = 312° \text{ C}.$$

At the same time for the cycle we have used for p_1 = 90 atm, t_1 = 500°C and t_h = 215°C (temperature to which the water is heated), the mean temperature of the heat supply is given by:

$$T_{icy}^m = \frac{i_1 - i_n}{s_1 - s_n} = \frac{810.1 - 220.4}{1.5934 - 0.5866} = 585° \text{ K} = 312° \text{ C}.$$

It follows from the example cited, that the optimum initial cycle parameters for atomic-electric generating stations, using metallic uranium with T_c^l = 650°C as determined from the conditions for the minimum electrical energy cost, consist, for example, of 90 atm pressure and 500°C. For the type of fuel considered a further increase in the initial steam parameters would be inadvisable. This conclusion coincides with the data of the project for the possible improvement in the cycle of an atomic-electric generating station using uranium with a sodium graphite reactor SGR [8]; in this project an increase in the initial steam parameters from 56 atm (440°C) to 88.5 atm (510°C) was foreseen. In this process the electrical power of the station does not increase, and an increase in the steam parameters results only in a decrease in the cost of the electrical energy. A further increase in the cycle parameters was advisable only for an increase in the temperature of the central HEEL, i.e., in the case where another nuclear fuel or an alloy with a greater limiting temperature was used.

* The amortization time of an electrical generating station is taken as eight years.

6

The Line of Optimum Temperatures for the Heat Supply During the Operating Cycle of an Atomic-Electric Generating Station

All the positions which we have examined for the line giving the optimum mean cycle temperature in the various zones, can be connected with one line of optimum mean cycle temperatures in TQ_r coordinates, this is the heavy line in Fig. 8.

The point of intersection of the line of possible temperature characteristics of the cycle, which can be drawn during the planning of the unit, with the line of optimum cycle temperatures will correspond to the optimum operating conditions of the given atomic-electric generating station. For the case of operation at the limiting thermal reactor power, the point of intersection of the possible changes in the mean temperature of the heat carriers with the vertical portion of the line giving the optimum conditions corresponds also to the mean optimum temperature of the heat carriers.

If we take into account the component giving the fuel costs of the electrical generating stations, the line showing the optimum cycle temperature in Zones II and III is raised, depending upon the coefficients $z = c_T \eta_t$ in formula (1); this corresponds to the dotted lines in Fig. 8. We wish to underline however, that all the points on the optimum temperature line of the cycle are of equal weight. The best conditions, which insure simultaneously the maximum thermal power and efficiency of the unit, lie in Zone III near point M.

The optimum mean temperatures of the cycle or of the heat carriers, for a given nuclear energy installation having a given form of, number of and type of surface
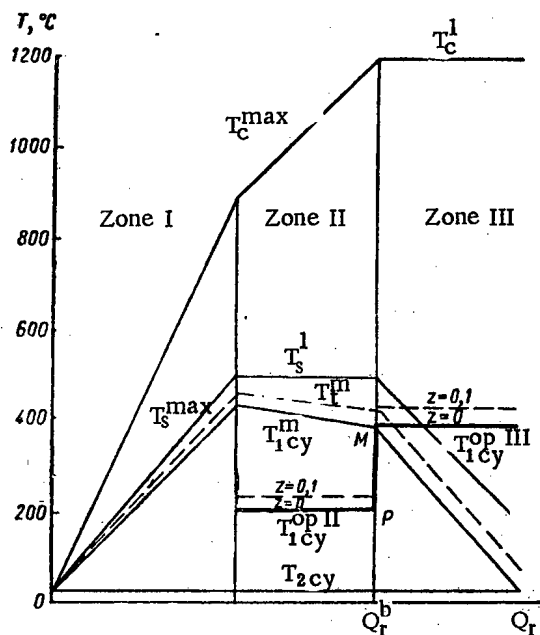
HEEL, and with a given velocity and utilization of heat carriers and with a constant surface heating of the steam generator, were considered previously.

If the characteristics of the possible temperature changes in a nuclear energy installation do not insure an optimum mean cycle temperature in Zone III (determined by equation (2) from the limiting center temperature), then we should raise the line of the possible temperature characteristics of the heat carriers in the cycle by changing the ratios of the thermal resistances of the HEEL, the heat transmission to the heat carriers, and the steam generator resistance, in order to insure the choice of the optimum parameters. Such an increase in the temperature characteristics of the heat carriers and of the cycle is possible if we change the diameter and heat conduction of the HEEL, the surface temperature of the steam generator, and the coefficient of heat transmission, depending upon the speed and parameters of the heat carriers and the working substance. It is possible to entirely eliminate Zone II and obtain only Zone III and its left boundary.

The method of obtaining more favorable thermodynamic operating conditions for the nuclear energy installation consists in raising the possible temperature characteristics. The expediency of such an increase in the indicated characteristics must be verified by calculations.

In order to evaluate the applicability of the previously derived conclusions, we show in Fig. 9 curves of the optimum mean temperatures of the heat supply during the cycle computed from equation (1) as a function of the limiting temperature of the shell and of the central HEEL and the fuel cost component of the electrical energy. Points 1 - 17 , Fig. 9, correspond to given mean temperatures of the thermodynamic cycles of the constructed or proposed electric generating stations listed in the table.

The computations for points 1 - 4 (Fig. 9), which we have carried out either as examples or to be used for double-purpose stations agree well with the theoretical curves computed using the limiting shell temperature; and points 5 - 11 characterize stations using uranium as a fuel, computed using the optimum cycle temperature for the limiting temperature of the central HEEL and for a fuel cost component of electrical energy from 0 – 30%.

When we considered the case of uranium dioxide as the nuclear fuel, we assumed that the temperature of the center was 2200 – 2760°C, and that the optimum mean temperature of the operating cycle of the atomic-electrical generating station (points 12 - 17, Fig. 9) was higher than the limiting temperature of the shell. Therefore such stations operate at the limiting thermal reactor power.

For a limiting temperature of the central HEEL, of the order of 1000 - 1200°C, the optimum parameters

Fig. 8. Line of optimum temperatures for $T_{1cy}^{op \cdot m}$ of an atomic-electric generating station.

7

Mean Temperature of the Heat Supply over the Heat Cycles in the Installation

Condition	Point No. (see Fig.9)	Name of Reactor or Station	T_r^1, °C	T_{1cy}^m, °C
For a limiting temperature of the shell HEEL	1	Uranium-graphite reactor (calculations in [9])	230	118
	2	Uranium-graphite reactor (calculations in [4])	300	137
	3	Two-purpose reactor at Marcoule (France)	400	157
	4	Reactor at Calder Hall (England)	408	165
For a limiting temperature of the central HEEL	5	First atomic generating station (USSR)	370	185*
	6	Station at Henderstone (England)	569	227
	7	Heavy water reactor with organic heat carriers (Switzerland)	600	224
	8	Uranium-graphite reactor using superheated steam (USSR)	550	312
	9	Sodium-graphite reactor at Santa Susana (USA)	642	245
	10	Reactor SGR (USA), variation 1 [8]	650	269
	10'	Reactor SGR (USA), variation 3 [8]	650	297
	11	Reactor "Enrico Fermi" (USA), variation 1	713	262
	11'	Reactor "Enrico Fermi" (USA), variation 2	713	287
For a limiting thermal power of the reactor	12	Generating station at Shippingport (USA)	1200	241
	13	Boiling reactor at Kale (FRG)	1760	247
	14	WWER reactor (USSR) [5]	2200	235
	15	Dresden reactor (USA)	2520	258
	16	"Yankee Atomic" station (USA)	2600	243
	17	Reactor SGR (USA)	2760	297

* For points 5, 8, 10, 12, and 14 in paper [6] the values given for T_{1cy}^m are not correct: 40–60°C lower without taking regeneration into account

** Point 6, Fig. 3, paper [1] for the station in Shippingport is erroneous.
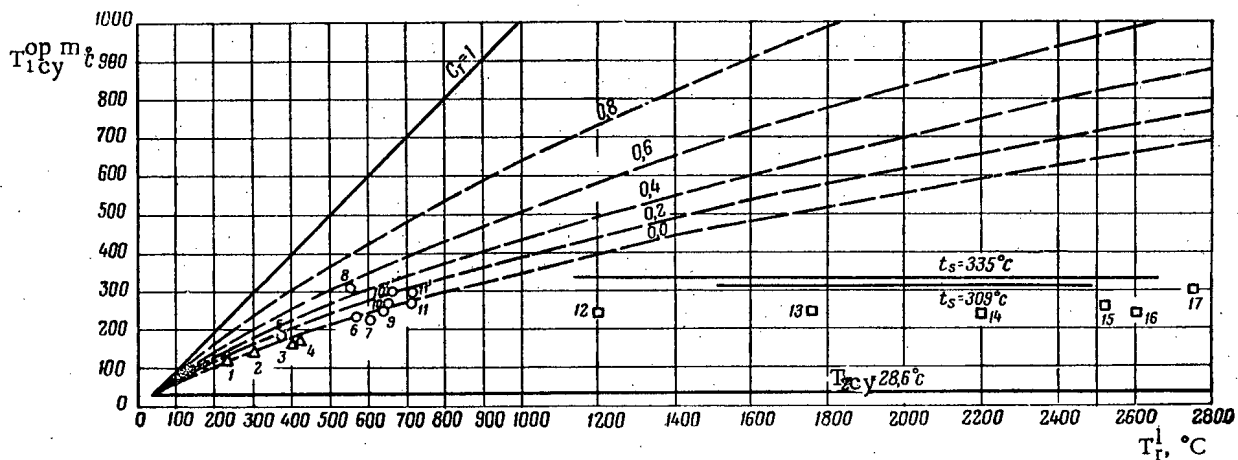
Fig. 9. Comparison of T_{1cy}^m for stations in operation, being planned or being built, with the theoritical curves for $T_{1cy}^{op\,m}$ for various fuel components.

will become so high that they will be unattainable for cycles utilizing ultrahigh parameter steam. Then the choice of the cycles for steam turbine installations may be based on the parameters attainable for steam and the determination of the optimum parameters will be necessary only for gas-turbine installations.

We have so far considered the temperature limitations of HEEL. There are also other limitations, for example, the critical thermal loading, the limiting temperature of the moderator, the radiational instability, etc., which affect the temperature characteristics which we have presented in TQ_r coordinates and which require a special analysis for each case.

On the basis of the data presented and also of the typical computations shown in papers [1, 2], we can conclude that equations (1) and (2) may be used to obtain a

8

preliminary estimate of the optimum parameters for the thermodynamic cycle of the steam turbine installations of atomic electric generating stations. A theoretical analysis using the indicated formulas enables us to find the factors which influence the optimum cycle parameters and also shows us how to develop and improve the thermodynamic operating cycles of atomic-electric generating stations.

LITERATURE CITED

1. D. D. Kalafati, Symposium Physics and Thermal Engineering of Reactors [in Russian] (Atomizdat, Moscow, 1958) p. 164.
2. D. D. Kalafati, Works of the Moscow Power Institute [in Russian] (1958) Vol. 30, p. 186.
3. Zh. Ibon, Materials of the International Conference on the Peaceful Uses of Atomic Energy (Geneva, 1955) [in Russian] (Fizmatgiz, Moscow, 1958) p. 397.
4. P. A. Petrov, Nuclear Power Installations [in Russian] (Gosénergoizdat, Moscow, 1958).
5. S. A. Skvortsov, Atomnaya Énerg. 5, 3, 245 (1958).†
6. Yu. D. Arsen'ev and K. E. Averin, Teploénergetika 5, 29 (1959).
7. George Simpson, et al., Materials of the International Conference on the Peaceful Uses of Atomic Energy (Geneva, 1955) [Russian translation] (Gosénergoizdat, Moscow-Leningrad, 1958) Vol. 3 p. 269
8. Ch. Starr, Materials of the International Conference on the Peaceful Uses of Atomic Energy (Geneva, 1955) [Russian translation] (Gosenergoizdat, Moscow-Leningrad, 1958) Vol. 3, p. 131.
9. A. I. Alikhanov, V. V. Vladimirskii, P. A. Petrov, and P. I. Khristenko, Atomnaya Énerg. 1, 5 (1956).†

---

† Original Russian pagination. See C. B. translation.

NUMBER OF NEUTRONS EMITTED BY INDIVIDUAL
FISSION FRAGMENTS OF U²³⁵

V. F. Apalin, Yu. P. Dobrynin, V. P. Zakharova
I. E. Kutikov, and L. A. Mikaelyan

A large detector filled with a liquid organic scintillator containing cadmium has been used to
measure the number of neutrons emitted by individual fragments in U²³⁵ fission   by thermal
neutrons. Using 4π geometry the dependence of the number of neutrons emitted by fragment
pairs on the mass ratio has been measured. The excitation energy used in neutron evaporation
is determined on the basis of the semiempirical Weizsäcker formula. A sharp asymmetry in the
distribution of excitation energy between the heavy and light fragments is noted. The data
which are obtained are found to be in disagreement with the statistical theory of fission pro-
posed by Fong.

Introduction

The distribution of excitation energy between frag-
ments is an important characteristic of the fission pro-
cess in heavy nuclei. In fission by thermal neutrons, the
initial excitation energy of the nucleus is equal to the
binding energy of the the neutron in the intermediate
nucleus which is formed and is approximately 6 Mev,
a figure which is many times smaller than the mean
value of the excitation energy of the fragment pair
which, in fission of uranium isotopes, is approximately
30 Mev. Considerations based on a quasi-static process
[1] indicate that the fragments remain in an unexcited
state up to the moment directly preceding the division
of the neck which connects them.

Bohr and Wheeler [2] have indicated that the exci-
tation of the fragments is basically connected with the
fact that the shape of the fragments directly after for-
mation does not correspond to equilibrium; the energy
of deformation is consequently transformed into energy
of internal degrees of freedom. B. T. Geilikman [3]
has considered this question in detail, relating the ex-
citation energy of each fragment with the deformation
parameters and the shape of the nucleus at the instant
preceding the actual division into fragments. The ex-
citation energy E_e is, as is well known, dissipated in the
emission of "prompt" neutrons and γ rays:

$$E(M)_e = \bar{\nu}(M)\,\varepsilon(M) + \varepsilon_\gamma(M),$$

where M is the mass of the fragment; $\bar{\nu}$ is the mean
number of neutrons emitted by the fragments and ε_γ
is the energy carried away by the γ photons; $\varepsilon(M)$ is
the mean energy required for the evaporation of a sin-
gle neutron. The energy carried away by the γ pho-

tons is a very weak function of the ratio of fragment
masses [4] and their excitation energies [5]. On the
other hand, direct experiments show [6] that an increase
in the excitation energy of the nucleus leads to an in-
crease in the number of neutrons emitted in fission and
that on the average the emission of a single neutron re-
quires an energy of approximately 7 Mev. Hence, an
investigation of the neutron yield from the separate
fragments makes it possible to obtain data on the dis-
tribution of excitation energy from the individual frag-
ments and thereby, information on the deformation of
the fragments at the time of formation. The depen-
dence of excitation energy of a fragment pair on mass
ratio is of interest from the point of view of checking
the statistical theory of fission proposed by Fong [7];
this theory predicts an increase in the excitation energy
of the fragment pair characterized by the most probable
mass ratio.

The neutron yield from individual fragments in
U²³³ fission by thermal neutrons was first measured by
Fraser and Milton [8] in 1954. The results obtained by
these authors indicate that in fission, which is almost
symmetrical in mass, the excitation energy is distributed
between the fragments in a manner which is far from
symmetrical: for a fragment mass ratio of 1:1 the light
fragment emits approximately four times more neutrons
that the heavy fragment. The total neutron yield is a
weak function of the mass ratio. In the region of the
most probable mass ratio there is apparently a small in-
crease in the number of emitted neutrons. This last
feature has been interpreted by Fong [7] as evidence of
the validity of his theory. From the point of view of
fission physics it is interesting to determine whether the
pattern observed by Fraser and Milton is an accidental

one, and is characteristic only of the fissile nucleus U^{234} or whether the excitation energy distribution, which has been observed, is a general feature which pertains under certain conditions for all nuclei (similarly, for the fission asymmetry).

In the present work we have measured the average number of neutrons emitted by the individual fragments and the fragment pairs, in fission of U^{235} by thermal neutrons.

Experimental Apparatus

The measurement of the neutron yield $\nu(M)$ from individual fragments is based on the fact that the angular distribution of the neutrons with respect to the direction of motion of the fragment is highly anisotropic: approximately seven times more neutrons are emitted in the direction of motion than at an angle of 90°, while the emission of neutrons in the backward direction is essentially negligible [9]. A schematic arrangement of the apparatus is shown in Fig. 1. A layer of U^{235}, $30\mu g/cm^2$ thick is deposited by evaporation on a colloidal film $20 \mu g/cm^2$ thick which is placed on the central electrode of a double grid ionization chamber. The chamber is filled with a mixture of carbon dioxide and argon (partial pressures of 50 and 900 mm Hg respectively). The angle of emission of the fragments with respect to the normal to the layer is defined by

iron   lead   water   con-   boron plus
                              crete paraffin
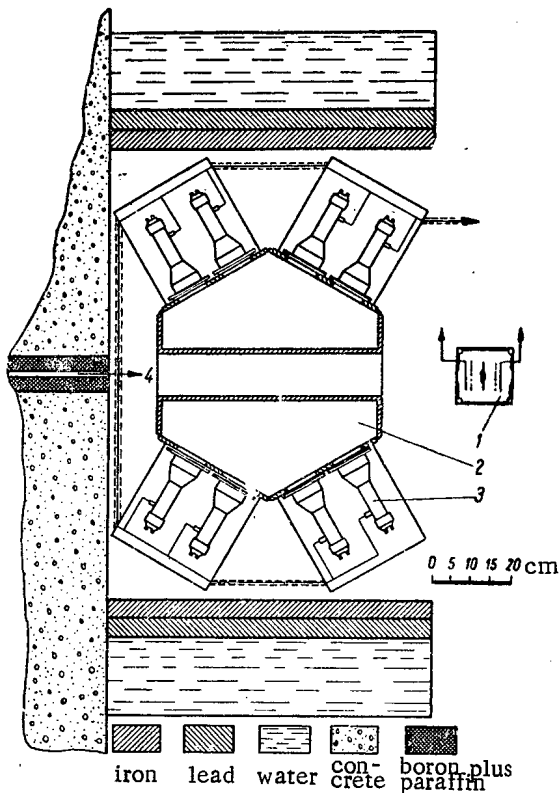
Fig. 1. Diagram of the apparatus: 1) double grid ionization chamber; 2) scintillation tank for neutron detection; 3) photomultipliers; 4) collimated neutron beam.

the collimator; this is a plate of phosphor bronze 0.4 mm thick in which an aperture 0.4 mm in diameter has been drilled. The most probable emission angle for the fragments is approximately 25°. The uranium layer is located at a distance from the neutron detector such that the most probable angle at which neutrons are detected is also approximately 25°.

The neutron detector is a hexagonal tank with a volume of 200 liters which is filled with a liquid scintillator. The scintillator is a solution of 2,5-diphenyloxazole (PPO) in dioxane with a concentration of 4 g/ liter which contains an almost saturated water solution of cadmium nitrate in amounts such that there is one cadmium atom for each 400 hydrogen atoms. The scintillation flashes, produced by the captured γ photons, are recorded by 32 FEU-24 photomultipliers with cathodes 78 mm in diameter. At the center of the detector there is an aperture 113 mm in diameter through which the collimated neutron beam passes. The lifetime of the neutrons in the scintillator is 11μ sec. The measured efficiency for detection of neutrons from U^{235} fission in the detector is 62%. The efficiency is determined by locating the layer of fissile material at the center of the detector. With the exception of the scintillator, the detector is essentially the same as that described in detail by Reines, Cowan, et al. [10].

The operation of the electronic system is controlled by the coincidence pulse from the fragments. This pulse opens for 25 μ sec a gate which transmits pulses from the detector to a high-speed counting system and pulses from the double ionization chamber to the input of the ratio analyzer. The gate is opened after a delay of approximately 0.6 μ sec from the fission time in order to avoid detection of the prompt γ rays. The resolution time of the neutron counting channel is approximately 0.4 μ sec. Information for each event (the magnitude of the ratio and the number of neutrons) is recorded on a recording system. The ratio range from 2.2 to 1/2.2 is covered by 30 channels of the analyzer. Cases in which the light fragment is emitted in the direction of the detector for ratios from 1/2.2 to 1 are analyzed by the first 15 channels while cases in which the heavy fragment is emitted in the direction of the detector for ratios from 1 to 2.2 are recorded by the remaining 15 channels. Under operating conditions approximately 80 fissions/min are recorded.

We measured 500,000 fission events in the course of these measurements; this corresponds to approximately 215,000 neutron pulses of which 85,000 were caused by fission neutrons, with the remainder due to the background of scattered γ rays and neutrons from the beam.

The data on the total yield of neutrons from fragment pairs can be obtained by measuring the neutron yield from the individual fragments $\nu(M)$. However, in order to obtain the quantity $\nu(M)$, it is necessary to introduce a correction in the experimental results; this

11

correction takes account of the dependence of neutron detection efficiency on angular distribution with respect to the fragments. To determine the total yield independent measurements are made in which the ionization chamber containing the layer of fissile material is placed at the center of the detector and the neutrons are detected in a 4π geometry. The apparatus is operated in the same way as in the measurements of neutron yield from the individual fragments with the only difference being that the ratios x and $1/x$, corresponding to the same mass ratio for the heavy and light fragments, are entered in the same channel of the analyzer. In these measurements the counting rate for coincidences between fragments is 15/min while the background is equal to one count per fission. In all approximately 70,000 fission events were recorded.

Corrections for Absorption in the Layer and Ionization Defect

In the ionization chamber used to measure the neutron yield from individual fragments, one of the fragments passes through the colloidal film and the collimator whereas the other loses energy only in the uranium layer. The average energy loss in the uranium layer is less than 0.4% and no corrections for this effect have been made. The energy loss in the film and the collimator are determined from the displacement of the point corresponding to symmetric fission with respect to the analyzer channel which records equal-amplitude pulses. The energy losses of the fragment in symmetric fission are found to be approximately 5 Mev. The appropriate corrections are introduced in the experimental distribution of fragment mass ratios. In introducing the corrections account has been taken of the dependence of initial ionization of the fragments on velocity

In the measurement of the total neutron yield, one of the fragments passes through the collimator while the other passes through the film. The energy losses of the fragments are approximately the same in magnitude and the displacement of the mass-ratio distribution curve is less than 1%. Hence, we have not deemed it necessary to introduce corrections for absorption, and record events characterized by the ratio x and $1/x$ in the same channel.

The yield curve for the fragments is also corrected for the ionization defect. In introducing this correction we use the values 5.7 and 6.7 Mev [11] for the ionization defect of the most probable light and heavy fragments respectively. It is assumed that the defect is a linear function of fragment mass: $\Delta E(M) = (4 + 0.019M)$ Mev [8].

Correction for Neutron Detection Efficiency

This correction must be introduced only in the measurements of neutron yield from the individual fragments. The larger the fragment velocity, the greater the

fraction of the neutrons emitted by it which enter the detector and are recorded.

The angular distribution of isotropically emitted neutrons from a fragment converted to the laboratory coordinate system has been given, for example, in [9]. In introducing corrections, we assume that the neutron detection efficiency $\eta(M,q)$ for neutrons which are emitted in the coordinate system of a fragment with energy q is proportional to the probability for emission of a neutron at an angle 0° in the laboratory coordinate system. Under these conditions

$$\eta(M,q) = \text{const}(1+r)^2, \quad r = \sqrt{\frac{E(M)}{Mq}}, \quad (1)$$

where E(M) is the kinetic energy of a fragment with mass M. For the most probable energies q and E the value of r is slightly smaller than unity. In going from symmetric to the most probable fission the efficiency η varies by approximately 20%. It can easily be shown that the magnitude of this variation is a very weak function of the energy q in the range 0.5 - 2.0 Mev, which covers most of the neutrons. Hence, although the neutron spectrum is continuous, it may be assumed that the detector efficiency is determined by the mean neutron energy q(M) emitted by a fragment of a given mass. The mean value of q(M) for the most probable mass depends on the excitation energy and is given by $0.62(\bar{\nu}+1)^{\frac{1}{2}}$ Mev, where $\bar{\nu}$ is the mean number of neutrons which appear per fission event (Terrel [12]). For U^{235} q is 1.15 Mev. Since, experimentally, one observes a strong dependence of fission excitation energy on mass, the corresponding change in mean neutron energy is taken into account. It is assumed that

$$q(M) = 1.5 + \left[\nu(M) - \frac{\nu}{2} \right] k.$$

The factor k can be found either from the relation $q = 0.62(\bar{\nu}+1)^{\frac{1}{2}}$ Mev or from the experimental results by studying the change in fragment temperature as a function of excitation energy [13]. The quantities found by these two methods differ somewhat and the average value is taken: k = 0.25 Mev/neutron. Thus

$$q(M) = 0.84 + \nu(M)0.25.$$

Substituting the value of q(M) in Eq. (1) and expressing the fragment energy in terms of its mass and the total kinetic energy of the fragment pair $E_0(x)$ with respect to the mass ratio x, finally we have

$$\eta(M) = \text{const} \times$$
$$\times \left[1 + \sqrt{\frac{M_0 - M}{M}} \sqrt{\frac{E_0(x)}{M_0(0.84 + 0.25\nu(M))}} \right]^2, \quad (2)$$

12

where M_0 is the mass number of the fissile nucleus. The value of the constant is found from the normalization condition: the results must be normalized to the known average value of $\bar{\nu}$ for U^{235} which is taken to be 2.45.

Discussion of Results

The results of the measurements are shown in Figs. 2 and 3. The mass ratio of the fragments is plotted along the abcissa axis. The fragment yield per unit mass ratio, corrected for the ionization defect and absorption, is shown in Figs. 2a and 3a. For purposes of comparison we also show the results of radiochemical and mass-spectrometer studies of fission products [14] (Fig. 3a, dashed curve).

In Fig. 2b is shown the neutron yield for individual fragments corrected for the efficiency of the neutron detector. Analysis shows that on the average the light fragment emits about 17% more neutrons than the heavy fragment. In Fig. 3b the points indicate the measured neutron yield from the fragment pair while the crosses denote values of $\nu(x)$ computed from the results of the measurements of ν from individual fragments. A comparison of the calculated and measured values shows

that although the correction for detector efficiency is based on a large number of simplifying assumptions, the error is less than approximately 5% when these corrections are taken into account.

The following remarks should be made with regard to these results. The values of ν obtained experimentally are averaged over some range of ratios. This averaging takes place primarily because of the finite resolving power of the ionization chamber. The resolving power $\Delta x / x$ (Δx is the dispersion in the value of $\underline{x}$) can be determined from a comparison of the obtained fragment yield curve with the accurate data obtained by radiochemical and mass-spectrometer analysis. An analysis such as that carried out by Leachman [15] shows that in the present experiment $\Delta x / x = 0.08$. It is assumed that for all values of $\underline{x}$ the error distribution is given in a Gaussian form with dispersion Δx which depends linearly on the ratio: $\Delta x = const$

The effect of the finite resolving power is specially noticeable where the fragment yield falls off sharply. Hence, in the region close to symmetric fission ($x < 1.20$) the behavior of the quantity $\nu(M)$ is not well defined.

In Figs. 2c and 3c we also show the calculated val-
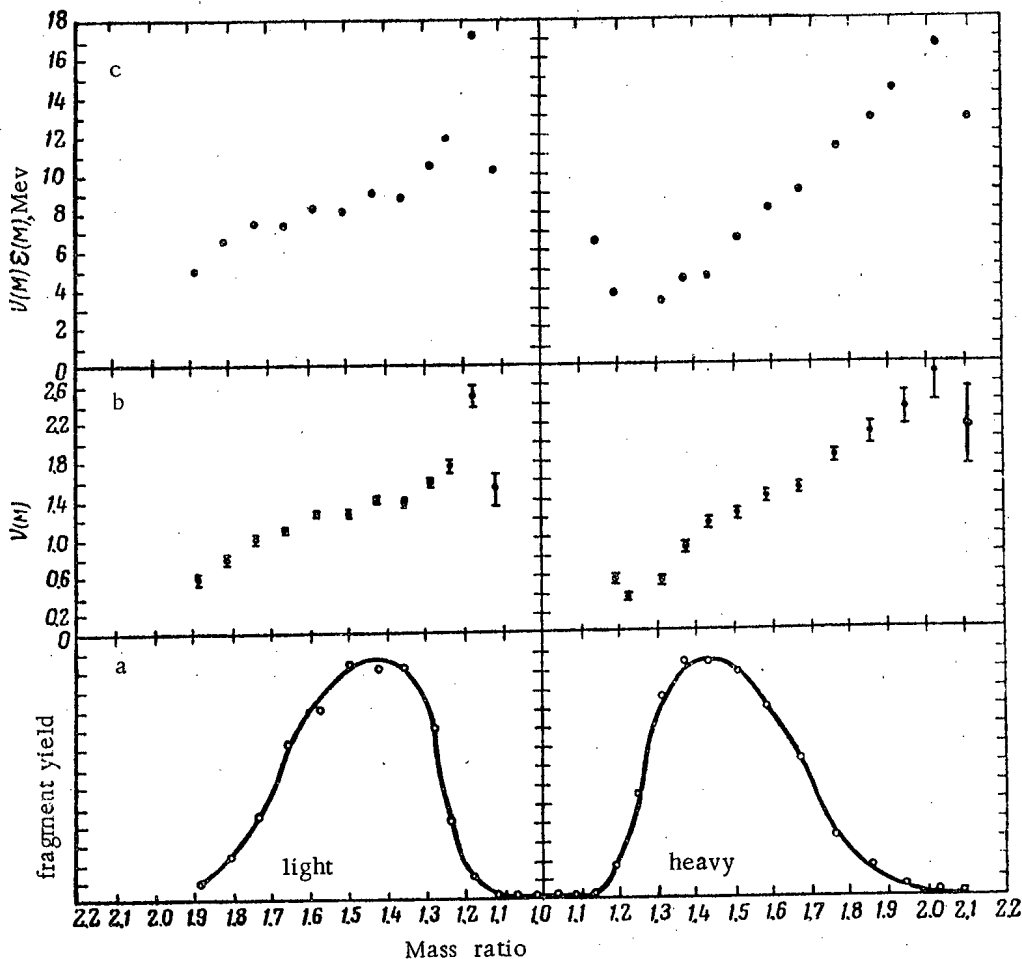
Fig. 2. Experimental data for the individual fragments: a) yield distribution for fission fragments; b) neutron yield; c) energy carried away by the neutrons.

13
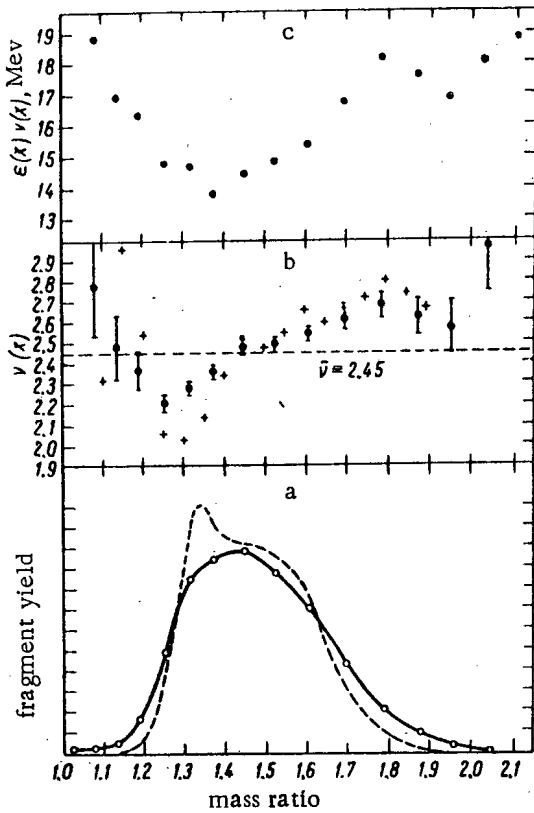
Fig. 3. Experimental data for fragment pairs: a) yield distribution of fission fragments; b) neutron yield; c) energy carried away by the neutrons.

ues of $\nu(M)$ $\epsilon(M)$ and $\nu(x)$ $\epsilon(x)$, the energy carried away by the neutrons from the individual fragments and the fragment pair. Stein and Whetstone [16] have attempted to determine experimentally the mean value of the energy $\epsilon(x)$ dissipated in evaporation of a single neu-

tron from a fragment pair. However, because of effects associated with the finite resolving power of the apparatus with which the velocity of the fragments was determined the value obtained by these authors is approximately 14 Mev/neutron, which is twice as large as the known value of approximately 7.0 Mev/neutron. The results contain a correction which amounts to approximately 100% of the quantity being measured. In the present work the resolving power is smaller than that of [16], and we find it more convenient to compute the value of $\epsilon(M)$.

The quantity $\epsilon(M)$ is equal to the sum of the neutron binding energy and its mean kinetic energy $q(M)$ in the fragment system. The Weizsäcker semiempirical formula can be used to compute the neutron binding energy. However, to carry out this procedure one must know the charge distribution between the fragments. The charge Z_l (M_l) is found from the relation

$$Z_1 = Z_h \frac{M_1}{M_h} + \Delta Z(M_1),$$
$$\Delta Z(M_1) = 5.9 - 0.05 M_1 , \tag{3}$$

where the subscripts "l" and "h" denote the light and heavy fragment, respectively. The coefficients in the expression for ΔZ are chosen to give equal lengths for the β-decay chains and to make ΔZ vanish for symmetric fission, unity for the most probable fission and equal to two for a mass ratio of two. Equation (3) gives detailed values of Z. For each mass the value of the binding energy is smoothed for the odd-even effect in the number of protons and interpolated to the exact value. The dependence of binding energy on fragment mass obtained in this way is shown in Fig. 4. The values of the binding energy for integral values of Z are taken from the table given by Cameron [17].
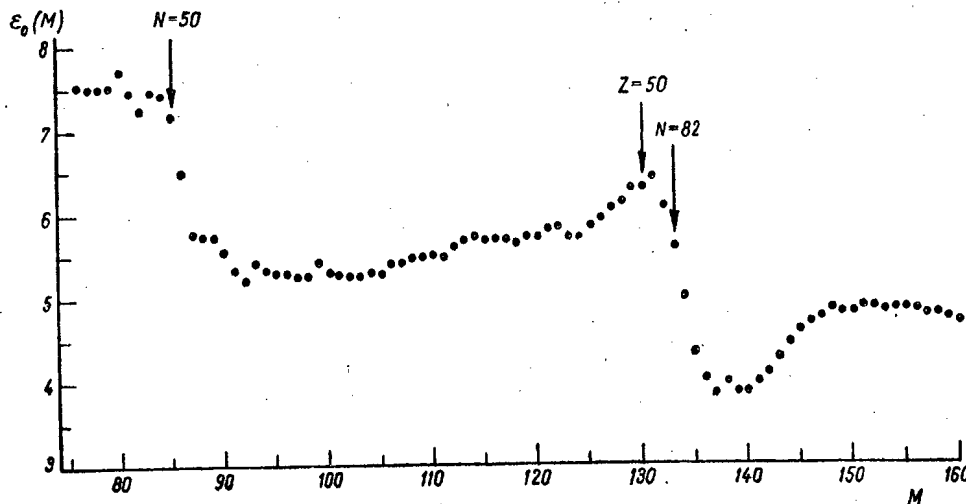
Fig. 4. Computed values of the neutron binding energy.

14
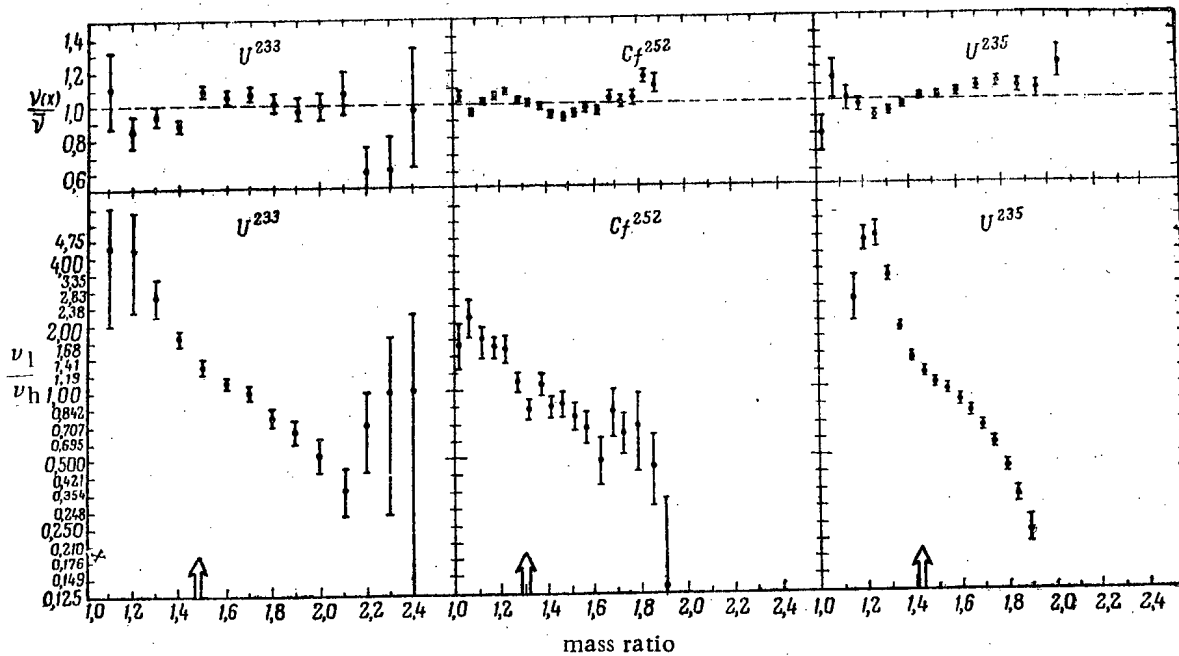
Fig. 5. Neutron yield from individual fragments ν_l/ν_h and total yield from the fragment pair $\nu(X)/\bar{\nu}$ for U^{233}, Cf^{252}, and U^{235}.

The values of $\epsilon(x)$ are given by the weighted average values:

$$\epsilon(x) = \frac{\epsilon(M)\,\nu(M) + \epsilon(M_0 - M)\,\nu(M_0 - M)}{\nu(M) + \nu(M_0 - M)};$$

$$\frac{M_0 - M}{M} = x.$$

Several months before the present work was finished data were published in [16] on the neutron yield from fragment pairs in spontaneous fission of Cf^{252}. At the Second International Conference on the Peaceful Uses of Atomic Energy, Leachman [12] reported on the results of measurements of neutron yield from Cf^{252} fragments obtained by Whetstone.

In Fig. 5 we show the results for U^{233} [8], Cf^{252} and U^{235} (data from the present work); the neutron yield from the individual fragments is converted into the ratio ν_l/ν_h while the total yield is given in units of $\nu(x)/\bar{\nu}$. The arrows on the abcissa axis indicate the most probable values for the fragment mass ratios.

As is apparent from the figure, the general characteristic for all fissile nuclei is the extremely sharp dependence of the number of emitted neutrons on fragment mass. For mass ratios of 1.20-1.25 practically all the neutrons are evaporated from the light fragment, while for strong asymmetry the neutrons are practically all emitted from the heavy fragment. At the same time the total number of neutrons emitted by the fragment pair is a weak function of fragment mass ratio. In the region of ratios which covers approximately 90% of all the fission cases, the value of $\nu(x)$ remains constant to ± 10%. For U^{235} and Cf^{252} no increase in $\nu(x)$ is found in the region of the most probable ratio; an in-

crease of this kind is predicted by the Fong theory. The results for U^{233} are obtained by combining the yields from the individual fragments and it is possible that the small increase in the yield is a consequence of a combination of experimental errors. As is apparent from Figs. 2, 3, and 4 the excitation energy of the fragments is approximately proportional to neutron yield. While the excitation energy of the fragments is basically associated with deformation, the nature of the excitation energy distribution between the fragments indicates that in fission which is almost symmetrical (in mass), the light fragment is deformed much more strongly than the heavy fragment. For the most probable mass ratio the deformation of the fragments is comparable while for high fission asymmetry the deformation of the heavy fragment is somewhat greater. It is possible that this pattern is connected with the oscillatory nature of the rupture of the neck of the fissioning nucleus.[*]

---

[*] The suggestion as to the oscillatory nature of the rupture of the neck of the fissioning nucleus was proposed by A. Bohr at the end of 1958 (private communication to V. M. Strutinskii).

15

LITERATURE CITED

1. B. T. Geilikman, Physics of Fission, Appendix No.1 of the Journal of Atomic Energy (Atomizdat, Moscow, 1957), p. 5

2. N. Bohr and J. Wheeler, Phys. Rev. 56, 426 (1939).

3. B. T. Geilikman, Atomnaya Énerg. 6 298 (1959)†

4. J. Fraser and J. Milton, Report No. 199, presented by Canadian Delegation to Second International Conference on the Peaceful Uses of Atomic Energy (Geneva, 1958)

5. A. I. Protopopov and B. M Shiryaev, Zhur. Éksp. i Teor. Fiz. 34, 331 (1958).

6. V. I. Kalashnikova et al., Conference of the Academy of Sciences USSSR on the Peaceful Uses of Atomic Energy (Session of the Division of Phys.-Math. Science) [in Russian] (Izd. AN SSSR, Moscow, 1955).

7. P. Fong, Phys. Rev. 102, 434 (1956).

8. J. Fraser and J. Milton, Phys Rev. 93, 818 (1954).

9. J. Fraser, Phys. Rev. 88, 536 (1952).

10. F. Reines et. al., Rev. Scient. Instrum. 25, 1061 (1954).

11. R. Leachman, Phys. Rev. 87, 444 (1952).

12. R. Leachman, Report No. 2467, presented by U. S. Delegation at the Second International Conference on the Peaceful Uses of Atomic Energy (Geneva, 1958).

13. I. I. Bondarenko et al., Second International Conference on the Peaceful Uses of Atomic Energy (Geneva, 1958) [in Russian] Nuclear Physics (Atomizdat, Moscow, 1959), Vol. 1, p. 438.

14. S. Katcoff, Nucleonics 16, 78 (1958).

15. R. Leachman, Phys. Rev. 83, 17 (1951).

16. W. Stein and S. Whetstone, Phys. Rev. 110, 476 (1958).

17. A. Cameron, A Revised Semiempirical Atomic Mass Formula (Chalk River, Ontario), 1957).

_____

†Original Russian pagination. See C. B. translation.

METHOD OF ESTIMATING THE CRITICAL PARAMETERS OF A BODY OF ARBITRARY SHAPE MADE FROM FISSIONABLE MATERIAL

V. G. Zagrafov

In this paper we consider an approximation method for determining the critical parameters of a body of arbitrary shape (or a group of bodies) made from fissionable material. In contrast with the variational method, the method described here is extremely simple and gives an error which is favorable from the point of view of safety as applied to fissionable materials; hence it is useful for engineering calculations.

The method has been applied to fast neutron systems where the single-velocity approximation gives good accuracy.

Derivation of the Basic Equation

The critical parameters of a body made from a material which is fissionable under neutron bombardment are described by the Peierls integral equation [1]

$$\varphi(\mathbf{r}) = \frac{1}{\gamma} \int_V \alpha(\mathbf{r'}) \varphi(\mathbf{r'}) K(\mathbf{r}, \mathbf{r'}) \, dV', \qquad (1)$$

where $\varphi(\mathbf{r})$ is an eigenfunction which coincides with the neutron density distribution function in the critical state; $\alpha(\mathbf{r})$ is the reciprocal mean free path length for the neutrons; γ is the eigenvalue of the equation.

The kernel $K(\mathbf{r}, \mathbf{r'})$ is defined by the expression

$$K(\mathbf{r}, \mathbf{r'}) = \frac{\exp\left(-\int \alpha \, dl\right)}{4\pi l^2}, \quad l = |\mathbf{r} - \mathbf{r'}|.$$

The integration is taken over the entire volume V.

Equation (1) is valid for a body or a material of uniform properties; the density need not be constant over the volume of the body.

In the critical state the first eigenvalue γ coincides with the material constant, which is equal to the reciprocal mean neutron multiplication factor for one collision with a nucleus:

$$\gamma_{\mathrm{m}} = \frac{\sigma_f + \sigma_s + \sigma_c}{\nu\sigma_f + \sigma_s},$$

where σ_f, σ_s and σ_c are the elementary cross sections for fission, scattering and capture; ν is the number of neutrons per fission. The difference between the eigenvalue and the material constant $\Delta\gamma = \gamma_{\mathrm{m}} - \gamma$ characterizes the departure of the system from the critical state. The excess value of the quantity being sought, γ, is favorable from the point of view of safety for application to fissionable materials because in this case the actual subcriticality of the system $\Delta\gamma$ is too low.

An upper estimate for the eigenvalue γ can be obtained from Eq. (1) if we know the local maximum for the neutron density $\mathbf{r_0}$. In this case, replacing $\varphi(\mathbf{r})$ by the constant value we find the following expression for the upper limit of γ.

$$\gamma = \int \alpha(\mathbf{r}) K(\mathbf{r_0}, \mathbf{r}) \, dV.$$

However, in practice this method is inconvenient because of the fact that it gives a large error and because the location of the neutron density maximum in a body of arbitrary shape is not, as a rule, known precisely. Generally we can only determine the region in which this maximum is located.

In order to obtain a more feasible method of making an estimate we consider region V_i, which includes the point which contains the neutron density maximum. For brevity, in what follows we will call the region V_i the primary inner region while the remaining volume of the body will be called the supplementary external region; we use the subscripts i and e to denote quantities referring to these regions.

We assume that $\varphi(\mathbf{r}) = $ const, and integrate Eq. (1) over the volume of the primary region:

$$\gamma = \frac{1}{V_i} \int_{V_i} dV \int_V \alpha(\mathbf{r'}) K(\mathbf{r_i}, \mathbf{r'}) \, dV'.$$

We transform the inner integral. We make use of the fact that the region of integration in it can be ex-

tended over the entire infinite space because outside the body $\alpha = 0$ (this factor is important for extension of the results to a system of interacting bodies). The integration is carried out in two steps: first we integrate over the direction Ω along a ray which originates at the point r_i, and then over the total solid angle:

$$\int \alpha(r')K(r_i, r')dV' =$$
$$= \int_{4\pi}\int_0^\infty \alpha(r')\frac{\exp\left(-\int \alpha dl\right)}{4\pi l^2}l^2\,dl\,d\Omega =$$
$$= \int_{4\pi}\frac{d\Omega}{4\pi}\int_0^{u_\infty}e^{-u}du,$$

where $u = \int_0^l \alpha dl$; $u_\infty = \int_0^\infty \alpha dl$; u_∞ is the optical path length along the line from the point r_i to infinity.[*]

Integrating along the ray we obtain

$$1-\gamma = \frac{1}{V_i}\int_{V_i}dV\int e^{-u_\infty}\frac{d\Omega}{4\pi}.$$

We now change the order of integration and divide the optical length of the ray u_∞ into two parts:

$$u_\infty = L + t,$$

where L is the optical distance along the ray from the point r_i to the surface of the primary region; t is the optical path length along the same ray from the surface of the primary region to infinity. Then we have

$$1-\gamma = \frac{1}{V_i}\int\frac{d\Omega}{4\pi}\int_{V_i}e^{-L}e^{-t}\,dV. \qquad (2)$$

We transform the inner integral which is a function of the direction Ω. We consider the case in which the density of matter is constant in the primary region. Expressing all linear dimensions in the primary region in free-path lengths, we set $dV = dLdS$, where dS is an element of area normal to the direction Ω. We integrate along dL:

$$1-\gamma = \frac{1}{V_i}\int\frac{d\Omega}{4\pi}\int(1-e^{-L_0})e^{-t}\,dS,$$

where L_0 is the "optical thickness" of the primary region along a ray which passes through the elementary area dS in the direction of Ω (Fig. 1). We replace the optical length t on the average value over the cross section S, by the value $\bar{t}(\Omega)$:

$$1-\gamma = \frac{1}{V_i}\int e^{-\bar{t}(\Omega)}\frac{d\Omega}{4\pi}\int_S(1-e^{-L_0})dS. \qquad (3)$$

The relation in Eq. (3) becomes simpler if we take the primary region to be a sphere. In this case, because of the spherical symmetry, the integral over S in Eq. (3) becomes independent of direction.

For an isolated primary sphere the critical parameter γ_0 is determined in our approximation by Eq. (3) with $t = 0$:

$$1-\gamma_0 = \frac{1}{V_i}\int_S(1-e^{-L_0})dS. \qquad (4)$$

Dividing Eq. (3) by Eq. (4), term by term, we obtain the relation between the quantity being sought, γ, and the value of γ_0 for an isolated primary sphere:

$$\frac{1-\gamma}{1-\gamma_0} = \int_{4\pi}e^{-\bar{t}(\Omega)}\frac{d\Omega}{4\pi}. \qquad (5)$$

In what follows, by γ_0 we will imply the eigenvalue of γ for a sphere determined by the exact equations, so that we satisfy the limiting case for the vanishing of the supplementary region.

In order to simplify Eq. (5), we make use of the fact that the average values of $\underline{t}$ are multiplied by the weighting function $(1 - e^{-L_0})$, that is, the largest contribution in the average value $\bar{t}(\Omega)$ comes from the central region of the cross section S. We assume that $\bar{t}(\Omega)$ coincides with the value $t_0(\Omega)$ for the ray which passes through the center of the primary sphere. There is some error associated with this approximation, but in the general case there will be different signs for the different directions of Ω and the error will average out in the integration over the total solid angle. It is shown later that this error does not change the sign of the total error.

The final relation assumes the following form:

$$\frac{1-\gamma}{1-\gamma_0} = \int_{4\pi}e^{-t_0(\Omega)}\frac{d\Omega}{4\pi}. \qquad (6)$$
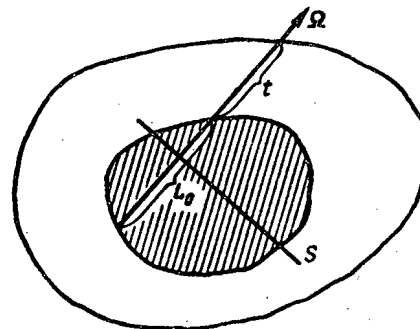

Fig. 1. Diagram for the integration process. The primary region is shown cross-hatched.

[*] For brevity, we will call the distances expressed in neutron mean-free path lengths the optical distance.

18

The dependence of γ_0 on the optical radius of an isolated primary sphere is shown in Fig. 2. The branch of the function $\gamma_0(R)$ for dimensions of a sphere large compared with the neutron free path length is obtained by the asymptotic diffusion method, which gives good accuracy in this region [2]. For $R \ll 1$, the following relation from [1] applies

$$\gamma_0 = R\,(0{,}78 - 0{,}39R).$$

Since both branches almost intersect each other, interpolation between them in the small intermediate region gives reliable results.

Equation (6) also applies when the density of the matter in the primary sphere is an arbitrary function of distance from the center of the sphere. We can convince ourselves of this if Eq. (6) is obtained directly from Eq. (2). This approach can be useful if the distribution of density in the primary sphere allows us to determine the quantity γ_0 by exact methods (for example, if there is a spherical cavity in the center of the primary sphere).

We may recall that Eq. (6) applies for an arbitrary distribution of density in the supplementary region. However, this relation can also be used for an arbitrary distribution of density over the total volume of the body. For this purpose it is sufficient to take as γ_0 a value which is too high, corresponding, for example, to the maximum density in the primary region; we can also reduce the primary region to dimensions such that the density becomes essentially constant. For this purpose we must use the requirement that there be a maximum
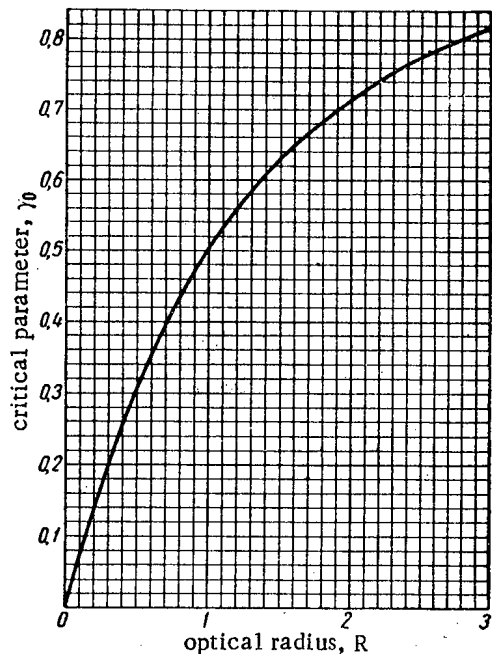
in the neutron density within the primary region. In the first approximation, the location of the maximum in the neutron density corresponds to a minimum in the quantity

$$\int e^{-u_\infty} \frac{d\Omega}{4\pi}$$

Errors of the Method

The errors in this method come from two sources. The basic error $\delta_1\gamma$, is caused by replacing the true neutron density distribution by a fixed quantity; this procedure leads to a value of γ which is too high. The second error $\delta_2\gamma$ is of the opposite sign and is due to the inexact averaging of the quantity $\underline{t}$ in Eq. (6). In order to determine the sign of the total error, we consider the behavior of these two errors as the dimensions of the primary region are changed.

In the limiting case, when the primary region shrinks to a point about the maximum in the neutron density, the error $\delta_2\gamma$ vanishes so that the averaging region for $\underline{t}$ (cross section of the primary sphere) approaches zero while $\delta_1\gamma$ assumes its maximum value. This is the case for which the error in this method is a maximum. In the other limiting case, in which $x = V_i/V = 1$, both errors vanish. Close to this limiting case the error $\delta_2\gamma$ is of greatest importance because of the smallness of the first error. In order to show that the absolute magnitude of the error $\delta_2\gamma$ is smaller than $\delta_1\gamma$ when $x \simeq 1$, we find the derivative $\dfrac{\partial}{\partial x}\left(\dfrac{\delta\gamma}{\gamma}\right)_{x=1}$

by comparison with the exact solution in the limiting case $(1 - x) = \Delta V/V \ll 1$, which we obtain by means of perturbation theory [3][†]

According to the perturbation theory analysis

$$\frac{\Delta\gamma}{\gamma} = k\frac{\Delta V}{V},$$

where

$$\Delta\gamma = \gamma - \gamma_0; \quad k = \frac{\varphi_e^2}{\overline{\varphi^2}}, \quad \overline{\varphi^2} = \frac{1}{V}\int \varphi^2\,dV. \quad (7)$$

We find $\Delta_1\gamma$ from Eq. (3) which does not include the error $\delta_2\gamma$. Considering the limiting case for the small supplementary region we obtain

$$\Delta_1\gamma = \gamma - \gamma_0 = \frac{\Delta V}{V}\int_{4\pi}(1 - e^{-L_0})\frac{d\Omega}{4\pi}, \quad (8)$$

where the integration is carried out over the rays which emanate from the volume ΔV. For a primary region in the form of a sphere of radius R, as an approximation we obtain[‡]

Fig. 2. The critical parameter γ_0 as a function of the optical radius R for an isolated sphere.

[†] This perturbation theory approach was developed independently by N. A. Dmitriev in 1948 (cf. [4]).

[‡] The accuracy of this approximation is discussed in the "two-sphere" section.

19

$$2 \int (1 - e^{-L_0}) \frac{d\Omega}{4\pi} = \frac{1}{S} \int (1 - e^{-L_0}) \, dS, \quad S = \pi R^2. \quad (9)$$

Taking account of Eqs. (4) and (9), we find that Eq. (8) assumes the following form:

$$\frac{\Delta_1 \gamma}{\gamma} = k_1 \frac{\Delta V}{V}, \quad k_1 = \frac{2}{3} R \frac{1 - \gamma}{\gamma}.$$

Similarly, from Eq. (6), including both errors we obtain

$$\frac{\Delta_{1,2} \gamma}{\gamma} = k_{1,2} \frac{\Delta V}{V}, \quad k_{1,2} = \frac{1}{3} R \frac{1 - \gamma}{\gamma}.$$

In Fig. 3 we show the dependence of the derivative

$$\frac{\partial}{\partial x} \left(\frac{\Delta \gamma}{\gamma} \right)_{x=1}$$

on the constant γ for the exact solution, the approximate solution neglecting the error $\delta_2 \gamma$, and for the solution which contains both errors. In the limiting case $\gamma \ll 1$, the values of the derivatives are determined by the method which has been described in [1]. In the region $0.3 < \gamma < 1$ we use the asymptotic diffusion method [2].

Comparing the derivatives of the first and second errors at $x = 1$

$$\frac{\partial}{\partial x} \left(\frac{\delta_1 \gamma}{\gamma} \right) = k - k_1 \quad \text{and} \quad \frac{\partial}{\partial x} \left(\frac{\delta_2 \gamma}{\gamma} \right) = k_1 - k_{1,2},$$

we see that the following relation always holds

$$\left| \frac{\partial}{\partial x} \left(\frac{\delta_1 \gamma}{\gamma} \right) \right| > \frac{\partial}{\partial x} \left(\frac{\delta_2 \gamma}{\gamma} \right) \quad \text{and} \quad \frac{\partial}{\partial x} \left(\frac{\delta_1 \gamma}{\gamma} + \frac{\delta_2 \gamma}{\gamma} \right) < 0,$$

as was to be demonstrated.
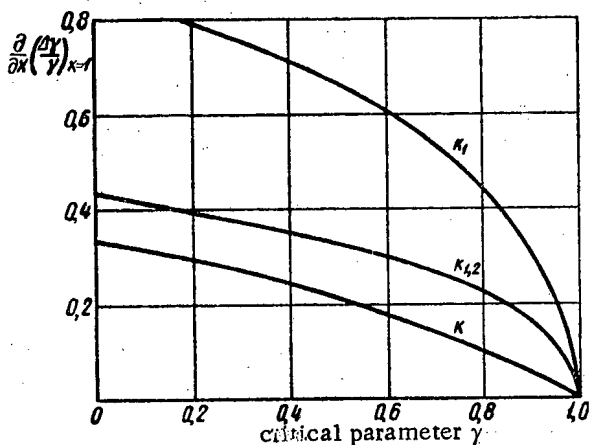
Fig. 3. The error derivatives for $x = 1$ as a function of γ for the exact solution (curve k) the approximate solution without the error $\delta_2 \gamma$ (curve k_1) and for the solution which contains both errors ($k_{1,2}$).

The total error increases as the dimensions of the primary region are reduced; the total error reaches a maximum when the primary region shrinks to a point, in which case the error due to averaging the neutron density becomes greatest while the error of opposite sign associated with the averaging of the quantity t vanishes. Hence, in taking solutions of actual cases it is convenient to choose the primary region to be a sphere of the largest possible dimensions, i.e., a sphere inscribed in the geometric shape of the body. In carrying out this procedure we must satisfy the basic requirement that the maximum neutron density is found within the primary sphere.

Comparison of the Theoretical and Experimental Results.

We compare the results obtained by the method described above with the experimental data for a system of different geometric shape of Oralloy - 93.5,which has been published in [5].**

The parameter γ_m is 0.74 for a sphere of Oy (93.5), in agreement with the experimental measurements of the mass of a critical sphere of Oy (93.5) of 51.3 kg. [5]. The neutron mean free path is $\alpha^{-1} = 4$ cm.

Infinite Plate. We inscribe the primary sphere in the plate as shown in Fig. 4. Carrying out the integration in the right-hand side of Eq. (6) we obtain the critical equation for the plate

$$\frac{1 - \gamma}{1 - \gamma_0 (R)} = 1 + R e^R Ei(-R). \quad (10)$$

For the value $\gamma = \gamma_m = 0.74$, from Eq. (10) we find that $R = 0.77$, i.e., the critical thickness of the plate $H = 2R\alpha^{-1} = 6.16$ cm.

The critical thickness of the plate found by the asymptotic diffusion method with the material constants in agreement with the experimental values of the critical mass of a sphere of Oy (93.5) is 6.57 cm. The critical thickness of the plate,obtained by extrapolation of the experimental data is $H \approx 6.1$ cm [5].

Infinite cylinder. In similar fashion, for an infinite cylinder of Oy (93.5), from Eq. (6) we find $R = 1.45$; $D = 2R\alpha^{-1} = 11.6$ cm.

The experimental value of the critical diameter D for an infinite cylinder of Oy (93.5) is 12.4 cm [5]. A calculation of the critical diameter of a cylinder by the asymptotic diffusion method also gives the value $D = 12.4$ cm.

Sphere. We estimate the radius a for a critical sphere of Oy (93.5) using Eq. (6). For this purpose the primary sphere of radius R is located eccentrically as shown in Fig. 5. Carrying out the integration in Eq. (6) for the supplementary region,we obtain:

_____

** Oralloy - 93.5 or Oy (93.5) is metallic uranium which contains 93.5% of the U^{235} isotope.

20

for $R = 0.75\,a$ $a = 1.9$, $r = a\alpha^{-1} = 7.6$ cm;

for $R = 0.5\,a$ $a = 1.95$, $r = 7.8$ cm.

Experimentally, for a density of 18.8 g/cm^3, the value of the radius r for a critical sphere of Oy (93.5) is 8.7 cm [5].

With a further reduction in R the error is reduced and the error changes sign when R < 0.37a. This feature serves to illustrate the fact that the requirement that the maximum in the neutron density be included in the primary sphere is a sufficient condition but not a necessary condition for obtaining an error whose sign is favorable in the sense of safety.

Two spheres. For a system consisting of two identical spheres, one of which is assumed to be the primary sphere, Eq. (6) assumes the following form:

$$\frac{1 - \gamma}{1 - \gamma_0} = 1 - \frac{\Omega}{4\pi}(1 - g), \quad g = \frac{1}{\Omega} \int_\Omega e^{-t}\, d\Omega, \quad (11)$$

where $\Omega = \frac{1}{2}\left(1 - \sqrt{1 - \left(\frac{R}{b}\right)^2}\right)$ is the solid

angle subtended by the second sphere at the center of the first sphere (b is the distance between the centers of the spheres). The function g characterizes the transparency of the sphere.
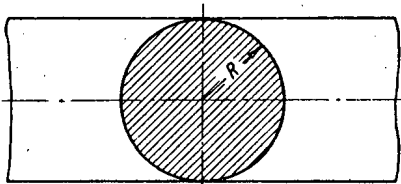
Fig. 4. Position of the primary sphere in the plate.

With fairly high accuracy we may assume that g is equal to the transparency factor g_0 of a sphere for a plane neutron beam:

$$g_0 = \frac{1}{S} \int_S e^{-t}\, dS = \frac{1 - e^{-2R}(1 + 2R)}{2R^2}, \quad S = \pi R^2. \quad (12)$$

Comparison with the results of the exact integration in Eq. (11) shows that replacing g by g_0 in the most unfavorable case for b ⇒ 2R leads to a negligibly small error which is less than 1% in the quantity 1 - g.[††] This result allows us to extend the analysis to the case of interaction of a large number of spheres.

In Fig. (6) we show the dependence of the critical radius of the spheres of Oy (93.5) (in neutron mean free paths) on the relative distance between the centers of the spheres b/R determined by Eqs. (11) and (12) (curve a). For comparison, we also show the critical radius R as a function of b/R obtained by the method described in [6] (curve b).
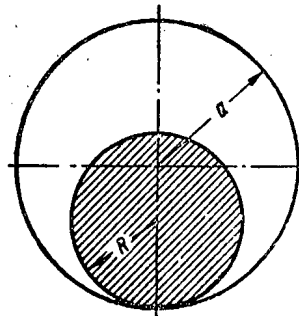
Fig. 5. Sphere with the eccentric primary sphere.

The relation given in Eq. (12) was verified experimentally by B. D. Stsiborskii and M. I. Kuvshinov for two spheres of Oy (93.5) located close to each other. The results of the measurements are in agreement with those obtained by Eq. (11) to within the limits of the experimental errors. The good agreement between the theoretical and experimental results is explained by the fact that the mean values of the neutron density in the primary and supplementary regions coincide because the spheres are identical.

Equation (11) also applies for a system consisting of several spheres. In this case, we choose one of the spheres in the center of symmetry where the neutron density is a maximum as the primary sphere while the solid angle Ω in Eq. (11) is summed over the remaining spheres (if they do not shield each other).

System of a large number of spheres. We apply Eq. (6) to a system consisting of a large number of spheres with radii R which are uniformly distributed over the volume of a sphere of radius a with a mean density of n spheres per unit volume. We take one of the spheres in the center of the system to be the primary sphere.
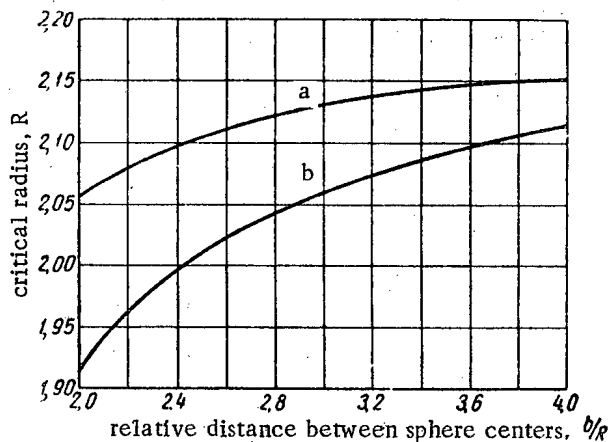
Fig. 6. The critical radius R as a function of the relative distance between centers b/R for two interacting spheres: a) according to Eq. (11); b) using the method of [6].

_____
†† The sign of this error is favorable as far as safety is concerned.

Each sphere of the system can be characterized by an effective cross section for neutron interaction:

$$\sigma = (1 - g_0)\, S, \quad S = \pi R^2, \tag{13}$$

where g_0 is determined from Eq.(12). In this case the neutron mean free path length is

$$\alpha^{-1} = [(1 - g_0)\, S n]^{-1}. \tag{14}$$

From Eqs. (13) and (14) we obtain the critical relation for a system of spheres:

$$\frac{1 - \gamma}{1 - \gamma_0} = e^{-(1 - g_0)\, S n a},$$

or, in more convenient form

$$\frac{3}{4} (1 - g_0)\, N \left(\frac{R}{a} \right)^2 = \ln \frac{1 - \gamma_0}{1 - \gamma}, \tag{15}$$

where N is the total number of spheres in the system.

Because the primary sphere is located at the neutron density maximum, Eq. (15) contains an error which is favorable from the point of view of safety, that is to say it either reduces the total number of spheres in the system N as compared with the critical value N_{crit} or reduces the radius of the system $\underline{a}$ for a given N.

In order to estimate the magnitude of the excess, we may note that the distribution of an average neutron density in the system as a function of radius is, in the first approximation, the same as the neutron distribution in an isolated sphere of fissionable material with a material constant $\gamma' = 1/Q$, where Q is the multiplication factor by each sphere in the system for an incident neutron flux.‡‡ Hence, having determined the critical radius of this sphere R′ by the same method as that used to determine the critical radius of a system of spheres $\underline{a}$, we obtain the same error in these two cases with respect to the critical radius.

We locate the primary sphere concentrically in a sphere of matter characterized by a constant γ' and allow the radius of the primary sphere to approach zero. From Eq. (6) we find the lowest value of the critical radius of the sphere R′:

$$R' = |\ln (1 - \gamma')|.$$

Comparing the magnitude of R′ with the exact value of the critical radius of the sphere and introducing

the same relative correction in Eq. (15) we obtain the corrected critical relation for our system of spheres

$$\frac{3}{4} (1 - g_0)\, N \left(\frac{R}{a} \right)^2 = \frac{R(\gamma')}{|\ln (1 - \gamma')|} \ln \frac{1 - \gamma_0}{1 - \gamma}, \tag{16}$$

where $\gamma' = 1/Q$, while $R(\gamma')$ is determined, for example, from Fig. 2.

We may emphasize, that because of the absence of experimental data, we must take Eq. (15) as a working relation and this provides a reliable excess. We can use Eq. (16) to estimate the magnitude of this excess.

CONCLUSIONS

The analysis which has been made of the above errors which arise and the comparison with experimental data verify the stability of the sign of the error as being independent of any given problem. This factor is of great value for solution of problems associated with safe handling of fissionable materials.

The method described above is particularly effective in calculations of the critical parameters for groups of bodies made from fissionable material, in which case other methods become very difficult. The method is applicable for an arbitrary distribution of the density of the fissionable material. Thus, this approximation method can be used for systems with a fissionable material, which is uniform in its properties, without moderators or reflecting shells.

LITERATURE CITED

1. R. Peierls, Proc. Cambridge Philos. Soc. 35, 610 (1939).
2. Codd, Sheford, Tait, "Fast neutron reactor physics," Coll : Progress in Nuclear Power [Russian translation] (IL, 1958) p.300.
3. K. Fuchs, Proc. Phys. Soc. 62A, 791 (1949).
4. L. N. Yschaev, Proceeding of the Second International Conference on the Peaceful Uses of Atomic Energy (Geneva, 1955) [in Russian] (Izd. AN SSSR, 1958) Vol. 5, p. 598.
5. G. Graves and H. Paxton, Nucleonics 15, 90 (1957).
6. G. Stuart, J. Appl. Phys. 27, 1294 (1956).

‡‡ The method of determining the multiplication factor has been described in [3].

REMOVAL OF OXIDES FROM SODIUM AND TESTS FOR THE OXIDE CONTENT

P. L. Kirillov, F. A. Kozlov, V. I. Subbotin, and N. M. Turchin

Oxides present in sodium, used as a heat carrier, accelerate the corrosion of the ducts and may cause blockage of the coldest sections of the circuit. The article gives the results of tests on cold oxide traps and work on an apparatus for determining the oxygen content in sodium. The results of the work can be used for planning experimental and industrial apparatuses in which sodium or sodium-potassium alloys are used as heat carriers.

Until recently, the use of sodium as a heat carrier was difficult because of the absence of methods of removing oxides from sodium and also tests for the oxide content. The presence of oxides in liquid sodium intensifies corrosion of structural materials (for example, stainless steel — see Table 1 [1]). When oxides are deposited from solution in the cold parts of the circuit, heat transfer to the liquid sodium or sodium-potassium alloy is lessened and the pipelines may become blocked [2].

The tests of apparatuses for determining the oxide content in sodium (indicators, oxides) and of oxide traps were carried out on a special testing installation (Fig. 1) with the following characteristics:

Volume of metal in the circuit, m^3	0.100-0.450
Oxygen content, wt. %	0.1-0.001
Working temperatures, °C	110-550
Pressure head of the pump, kg/cm^2	6-10
Length of the pipelines, m	~50
Diameters of the pipelines, mm	25-48

For preliminary heating of the metal all the lengths of the circuit were equipped with electric heaters. During the operation of the testing installation the metal was heated by electric or gas furances.

Apparatus for determining the oxygen content in liquid sodium. Methods for the chemical determination of the oxygen content in liquid sodium — mercury [3], butyl bromide [4], distillation [5], vacuum fusion [6] — are rather complicated, very time consuming and require special equipment. When operations are carried out with radioactive sodium the chemical analysis is markedly complicated. The most difficult operations are sodium sampling and the transfer and introduction of the samples into the apparatus without contamination of the metal to be analyzed by oxygen.

A stopper indicator method was used to determine the oxygen content. The idea is far from new [7, 8].

TABLE 1. Rate of Leaching of the Components of Stainless Steel in Sodium at 496°C

Components of stainless steel	Rate of leaching, $mg/cm^2 \cdot month$	
	In sodium with 0.003 wt.% O_2	In sodium with 0.01 wt. % O_2
Iron	2,5	40
Cobalt	0,2	1
Tantalum	1,0	4
Manganese	7,2	26

It is based on the fact that if the temperature of the sodium current passing through a finely perforated diaphragm is lower than the temperature of its saturation by oxides, the latter are deposited and block the holes in the diaphragm. This method does not require highly accurate apparatus and ensures the required accuracy within a wide range of oxide concentrations.

Employing the relation between the solubility of oxygen in sodium and temperature

$$W = 2.7 \cdot 10^{-4} \left(\frac{t}{100} \right)^{3.6} \qquad (1)$$

(where W is the solubility of oxygen, in wt%, t is the temperature, in °C) established from the data of a number of works [9 - 14]; the oxygen content in the metal can be found if the temperature at which the oxides are deposited from solution is determined. The deposition of the oxides is recorded at the moment the flow of metal through the stopper indicator, shown in Fig. 2, falls.

Valve 1 with several radial grooves is installed so as to facilitate washing out of the oxides from the holes after the determination. The metal is cooled by air from a fan. A somewhat altered ÉPP-09 electronic self-recording potentiometer with a path/time scale of 8 sec was used for simultaneous determination of tem-

23
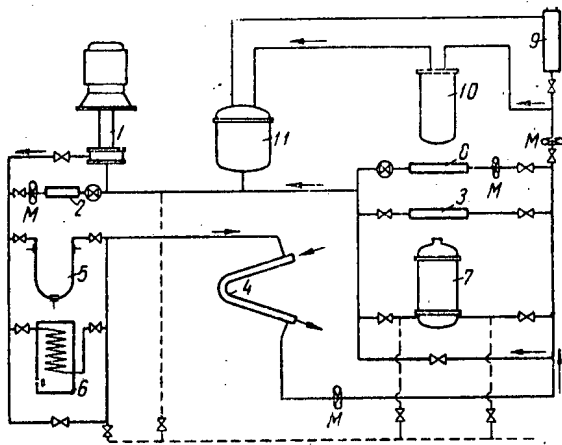
Fig. 1. Setup of the testing installation for tests of apparatuses for determining the oxide content of sodium:
1) pump; 2, 8) oxide indicators; 3) sampling device; 4) heat exchanger (sodium alloy, sodium-potassium); 5) electric heater; 6) gas heater; 7) sodium-water heat exchanger; 9) measuring tank; 10) cold trap; 11) pump tank; 12) magnetic flowmeters.

perature and flow of sodium (Fig. 3). The most characteristic parameters of different modifications of the apparatus are given in Table 2.

The relations between the apparatus readings and the rate of flow of metal through the holes, the dimensions of the holes, the number of holes and rate of cooling of the metal were determined in order to select the optimum design. During these tests the oxygen content of the sodium varied from 0.002 to 0.1 wt%, and the temperature of the sodium from 110 to 550° C. The re-

lations between the readings of the apparatus and the rate of flow of metal through the holes at two different oxygen contents were determined for each modification of the apparatus (for purposes of comparison, two designs were generally tested). The temperature at which the holes became blocked did not vary at flow rates of 2.5 to 14 m/sec (Fig. 4). At lower rates of flow the readings are too low, the cause of this being unknown as yet.

TABLE 2. Characteristics of the Oxide Indicators

Design characteristics	Modification		
	A	B	C
Number of grooves in the valve	16	16	34
Dimensions of the holes, mm.	1×1	1×1	$0,5\times0,5$
Diameter of the heat-exchanger tube	25	49	49
Total area of the heat-exchanger, m²	0,45	0,72	0,72

When the size of the holes was changed from 0.5 × 0.5 to 1 × 1 mm the readings of the apparatus were reduced by 2.5%. The number of grooves must be sufficiently high (10-15) to eliminate the effect of chance blockage of the holes. The readings of the apparatus are independent of the rate of cooling of sodium under the following conditions of the experiment: constant oxygen concentration (0.008-0.02 wt%), variation in the flow of metal from 2.5 to 13 m/sec, rate of fall of temperature in the valve from 0.3 to 37° C/min. A cooling rate of more than 10° C/min is undesirable because it

Unit A
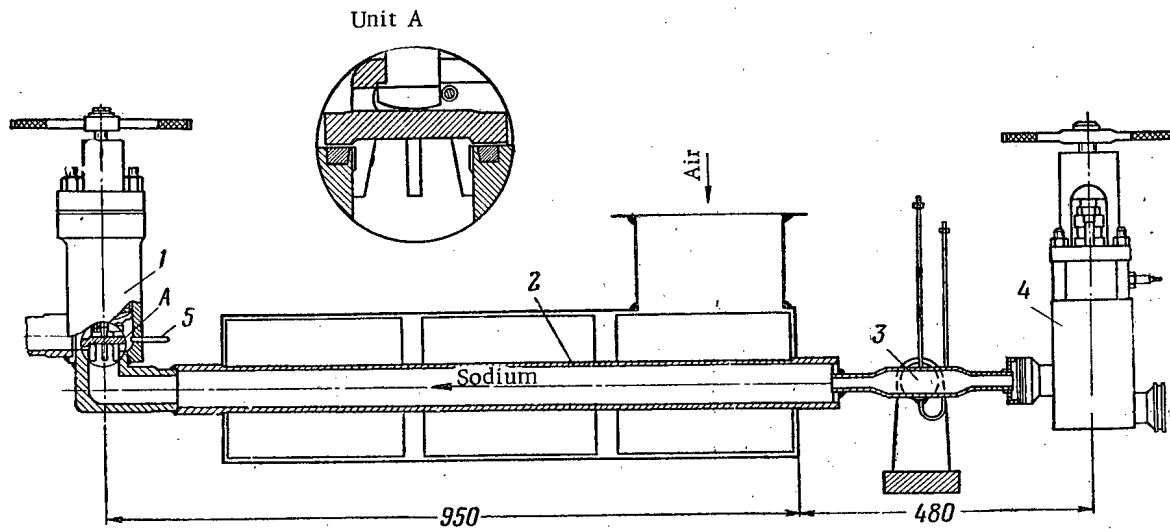
Fig. 2. Design of the stopper indicator for oxides: 1) main valve with radial grooves in the valve, retaining the oxides; 2) sodium-air heat exchanger; 3) flowmeter; 4) regulator valve; 5) thermocouple for measuring the temperature at the blocked point.

24
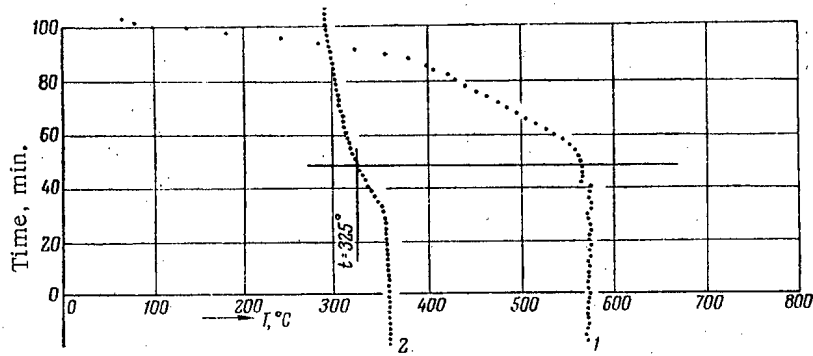
Fig. 3. Examples of recording of the curves of the flow and tempera-
ture of sodium in the secondary apparatus of the oxide indicator:
1) emf of the magnetic flowmeter; 2) temperature in the valve of the
main valve.

may lead to an error in the determination of the temp-
erature at which blockage of the holes occurs. The ac-
curacy of the indicator readings was checked by analy-
sis of the metal accumulated after a specific period of
operation of the trap. The results of chemical analysis
and the determinations of the stopper indicator are com-
pared in Table 3, which shows that they agree fairly
closely.

The majority of the components of the apparatus
were tested for several thousand hours at a temperature
of 300-500° C and showed quite satisfactory strength.

Cold traps for removal of oxides from sodium. The
working principle of cold traps [7, 8, 15] is that the me-
tal from the hot sections of the circuit is cooled and the
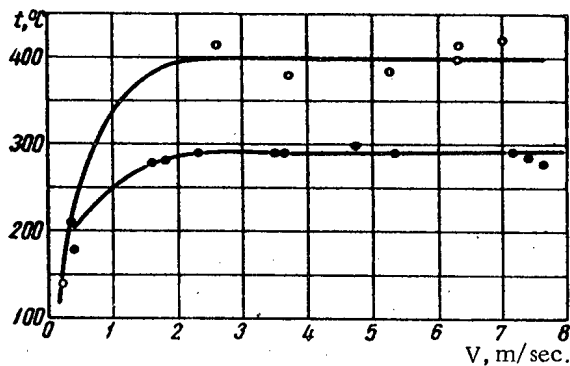
Fig. 4. Relation between the temperature of block-
age of the holes in the oxide indicator and the rate
of flow in the holes (approximate oxygen content:
O — 0.031%; O — 0.013%).

oxides deposited from the solution are then filtered.
Since the solubility of sodium oxides in sodium falls
with a reduction in temperature, the degree of removal
of the oxides is greater the lower the temperature of
the metal in the trap.

The trap (Fig. 5) is formed by a cylindrical contain-
er 2, consisting of two shells — an outer shell O and an

inner I — packed with stainless steel cuttings or wire.
The container is equipped with a jacket 1, containing
toluene for withdrawing heat from the sodium. The
toluene boils and its vapor condenses in the coil 5,
cooled by mains water. This complex cooling system

TABLE 3. Oxide Content in the Trap, Determined

Trap number	Data of the oxide indicator	Gas-analysis data
1	·890±100	1000±500
10	4750±700	6200±900

was used for reasons of safety in the event of leakage of
sodium. The lower part of the trap had a settling tank
6, in which the oxides are accumulated. The cone 7
reduces the rate at which the metal flows through the
settling tank. The trap is heated preliminarily by a ni-
chrome heater located in the shell 4.

The reduction in the oxygen content of the sodium
passing through the trap can be calculated from the
equation of the material balance:

$$\gamma V dc = \gamma Q (c - c') d\tau, \tag{2}$$

where V is the volume of sodium in the circuit, m^3; c is
the oxygen content in the sodium, wt%; c' is the solu-
bility of oxygen in the metal at a temperature t', wt%
(t' is the minimum temperature of the metal in the trap);
Q is the flow of metal through the trap, m^3/hr; γ is the
specific gravity of the metal at the temperature of the
circuit, kg/m^3; τ is the working time of the trap, hr.

Equation (2) was derived from the following pre-
mises: the volume of the trap is less than the volume of
the circuit; the flow of sodium through the trap is low
compared with the flow through the main circuit; all
the oxides deposted from the solution remain in the trap,

25

i.e., the oxygen content in the metal leaving the trap corresponds to its solubility at the minimum temperature in the trap.

Integrating equation (2) we obtain the following equation:

$$c = c' + (c_0 - c') e^{-n} \tag{3}$$

where c_0 is the oxygen content in the sodium before filtration; n is a number indicating the number of times the sodium present in the circuit has passed through the trap in time τ; $n = Q_\tau / V$.

The following factors had to be determined when the trap designs were tested: 1) the maximum degree of purification provided by the trap; 2) the maximum amount of accumulated oxides; 3) the suitability of the design as a whole, its thermotechnical and mechanical characteristics. The tests were carried out as follows. The initial oxygen content in the sodium was determined before filtration. The metal was then circulated through the trap at a predetermined rate for a specific time. The oxygen content in the metal was then redetermined. This procedure was repeated until the oxygen content had fallen to the required value. The results obtained were compared with the theoretical curve (3). If the oxides were removed from the trap the experimental curve appeared above the theoretical curve.

By reducing the flow of metal through the trap, a position was reached where the experimental points coincided with the theoretical or were fairly near to them.
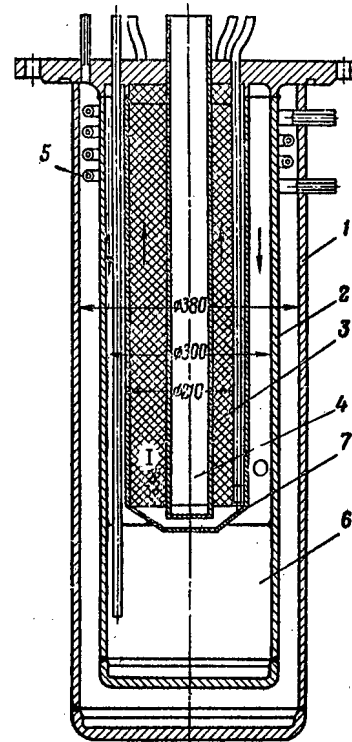
Fig. 5. Design of cold trap with a capacity of 32 liters of sodium.

Oxygen was added to the sodium either by mixing the pure metal with the oxidized metal or by introducing sodium peroxide into the circuit.

TABLE 4. Characteristics of the Traps Tested

Conditions and results of the tests	Metal capacity of the trap		
	32 liter trap*	47 liter trap	
Test time, hr.	624	720	1900
Circulation time of the metal, hr.	105	130	336
Flow of metal, m³/hr.	0,117—0,100	0,336—0,250	0,500—0,160
Rate of the metal, mm/sec:			
In the outer shell	1,75—1,5	2,82—2,1	11—3,5
In the inner shell	1,95—1,6	2,74—2,0	2,9—0,6
Temperature of the metal, °C:			
At the trap inlet	310—420	450—270	370—284
Inside the trap	140—217	200—120	226—160
At the trap outlet	148—280	300—180	180—125
Pressure of the toluene vapor, atm:			
Working	0,5—3	0,0—2	0,0—2
Maximum.	11	10	4,5
Oxygen content in the sodium before operation of the trap, wt.%:			
Working	0,044—0,02	0,04—0,02	0,03—0,015
Maximum.	0,083	0,055	0,045
Amount of oxides accumulated by the trap, g.	3010	4750	4850
Amount of oxides accumulated by the trap (wt. vol% of metal in the trap).	10	14	10

* 13.2 wt. vol. % of oxides of metal in the trap was found in the settling tank. The determination was made with respect to the density of the metal (the specific gravity of sodium oxide is more than twice that of the metal itself).

26

As a result of tests of different variants of the traps (Table 4) the following facts were established:

1) The cold trap can reduce the oxygen content in sodium to 0.002 wt%.

2) The required degree of purification can be easily obtained by selecting appropriate operating conditions.

3) The more oxides accumulated the better is the filtration capacity of the trap. At higher flow rates of metal there is a considerable entrainment of oxides.

4) The reduction of the temperature of the metal at the trap inlet, equivalent to a reduction in the mean temperature inside the trap, increases the filtration capacity of the trap.

5) The oxide capacity of the trap depends on its design, the type and density of the packing and the operating conditions.

6) For the same flow rates of metal, packing in the form of cuttings retains oxides more effectively than 0.5 mm diameter wire.

Only the inner shell was equipped with a packing (density 100 kg/m³). The volume of the settling tank was increased and the residence time of the metal in it was also increased. These measures made it possible to increase the oxide capacity of the trap to 10% .
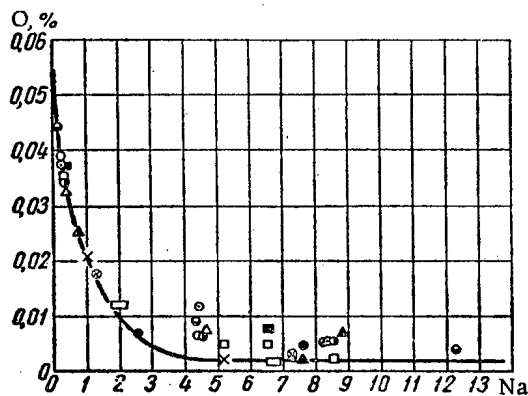
Fig. 6. Variation in the oxygen content in sodium during operation of the cold trap:
————) curve calculated from equation (3); the experiments were carried out at the following flow rates of sodium through the trap (m³/hr): ●) 0.168; ▲, ☐) 0.250; ■, ☐,×,⊕, ⊕, △) 0.285; ●, ⊙) 0.300; ○,⊙) 0.335.

When the oxygen content of the sodium was 0.1% or more the traps were blocked very rapidly. In such cases the metal was first pumped through the trap without toluene, i.e., the trap was used as a mechanical filter. After the oxygen content had been reduced to 0.06-0.05 wt%, toluene was added and filtration was continued. The typical characteristics of the trap operation are given in Fig. 6.

It should be noted that the operating conditions of the trap depend greatly on its oxide capacity. For ex-
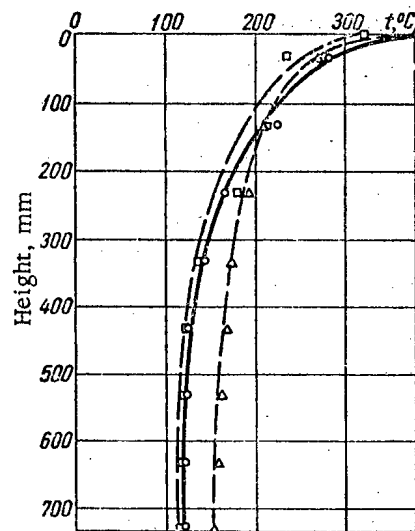
Fig. 7. Temperature distribution along the height of the trap at different sodium flow rates (m³/hr): ☐) 0.140; ○) 0.080; △) 0.060.

ample, during a test with a flow rate of sodium through the trap of 0.080-0.117 m³/hr its oxide capacity was only 4%; at flow rates of 0.270-0.500 m³/hr its capacity increased to 10%. This can be explained by the more uniform distribution of oxides in the volume of the trap at high rates.

To determine where exactly the oxides were accumulated, the inner and outer shells of the traps were flushed with gas after the tests and in some of them the content of the settling tank was analyzed. A comparison of the results of the tests of different traps and analyses of their contents and the contents of the settling tank after completion of the tests allows the following conclusion to be drawn with regard to the role of the different parts of the apparatus. The oxides are deposited from solution in the outer shell. The temperature distribution along the height of the trap was measured (Fig. 7). It was found that at a distance of 140 mm from the inlet the sodium temperature falls from 300-450° C to 180-200° C, i.e., nearly all the oxides are deposited immediately after entering the trap. This explains the fact, noted in [13], that the hydraulic resistance of traps increases as a result of blockage of the outer shell. But if the outer shell is packed nearly all the oxides are retained in it. The packing was, therefore, removed from the outer shell.

The cooled metal passes from the outer shell to the upper part of the settling tank, forming 10-40% of the volume of the whole trap. The results of the tests showed that the amount of oxides retained in the volume of the settling tank is negligible.

If dead-end and discharge lines are heated slightly they operate as diffusion traps, which can accumulate oxides or recycle them according to the oxygen content

27

in the sodium and the ratio between the temperatures of the dead ends and the temperature of the circulating metal.

LITERATURE CITED

1. R. Baus and A. Bogard, Reports to the International Conference on the Peaceful Uses of Atomic Energy (Geneva, 1955) [Russian translation] (Izd. AN SSR Moscow, 1957) p. 438.
2. P. L. Kirillov, V. I. Subbotin, M. Ya. Suvorov, and M. F. Troyanov, Atomnaya Énergiya 6, 382 (1959).*
3. L. Pepkowitz and W. Judd, Analyt. Chem. 22, 1283 (1950).
4. J. White, W. Ross, and R. Bowman, Analyt. Chem. 26, 210 (1954).
5. J. White, Nucl. Sci. Abstrs. 15, 8290 (1957).
6. Yu. A. Klyachko, Analysis of Gases, Nonmetallic Inclusions and Carbides in Steel [in Russian] (Metallurgizdat, 1953).
7. Liquid-Metallic Heat Carriers [in Russian] (IL, Moscow, 1958).
8. W. Bruggemann, J. Amer. Inst. Chem. Engr. 2, 153 (1956).
9. S. Siegel, R. Carter, F. Borman, and B. Heyford, Reports to the International Conference on the Peaceful Uses of Atomic Energy (Geneva, 1955) [Russian translation] (Izd. AN SSSR, Moscow, 1957) Vol. 9, p. 392.
10. I. Gray, R. Neal, and B. Voorhees, Nucleonics 14, 34 (1956).
11. S. McClean, Lectures on the Technique of Reactor Construction [in Russian] (Sudpromgiz, Moscow, 1957).
12. A. McIntosh and K. Bagley, J. Brit. Nucl. Energy Conference 3, 15 (1958).
13. F. Faris et al., Report No. 452, Given by the USA to the Second International Conference on the Peaceful Uses of Atomic Energy (Geneva, 1958).
14. O. Salmon and T. Cashman. J. Inst. Metals 84, 7 (1956).
15. Nuclear Reactors "Technique of nuclear reactors" Document of the Atomic Energy Commission of the USA (1955) Vol. 2, chap. 17.

*Original Russian pagination. See C. B. translation.

ON THE CHANGE IN THE COLOR AND TRANSPARENCY OF GLASSES WHEN BOMBARDED BY GAMMA RAYS FROM A Co60 SOURCE AND IN A NUCLEAR REACTOR

S. M. Brekhovskikh

Glasses of various types are widely used in radiation shielding. The problems involved in the effect of different types of radiation on glasses and the choice of glass with greatest radiation stability become important in this area. The present article deals with these questions. Results of experimental investigations where glasses of different types were subjected to bombardment from a Co60 source and to bombardment in a nuclear reactor are discussed. Glasses of different composition, products of several different glassworks in the USSR, were tested. Techniques for enhancing the radiation stability of the glasses are recommended in this article. Those characteristics of glasses which provide a fairly complete picture of the radiation response of the materials, e. g., index of stability, index of saturation, minimum transparency, coefficient of rate of darkening, are introduced.

Glasses darken or color upon exposure to radioactive radiations. The rate of darkening depends on the composition of the glass and the radiation dose; when radiation doses are large, transparency drops rapidly and the color characteristics of the glass are modified. Some data on the stability of industrial glasses to irradiation by γ rays may be found in [1].

The present article presents the results of additional investigations of color and transparency changes in glasses upon irradiation using a Co60 source in doses up to 10^6 r, and upon in-pile irradiation with doses reaching $5 \cdot 10^{10}$ r.

Polished glass specimens 30 mm in diameter and 5 ± 0.1 mm thick were used in the tests. Spectral absorbtion was determined in a quartz SF-4 spectrophotometer, and integral light transmission was found by using a tricolor VÉI colorimeter.

Change in Color of the Glass

Figure 1 shows the curves of the spectral transmittance of various glasses found prior to irradiation and following irradiation with a dose of 10^6 r from a Co60 source. Glass No. 10 from the "Krasnyi luch" works (Fig. 1a), used for the manufacture of extruded items of optical glass; polished (rolled) glass PG from the Dzerzhinskii glass works at Gusev (Fig. 1b); and green glass No. 18 (Fig. 1c) from the "Krasnyi luch" works were used. Both specimens of colorless glass darkened intensely and took on a dark brown coloration.

Figure 2a shows the curves of spectral transmittance prior to and following irradiation of red glasses colored with selenium and cadmium sulfate (selenium ruby

glass), Fig. 2b applies to orange cadmium OS-6 glasses, while Fig. 2c refers to blue (cobalt) glasses, No. 17.

Table 1 gives the color characteristics of red glasses of the "copper ruby" type prior to and following irra-
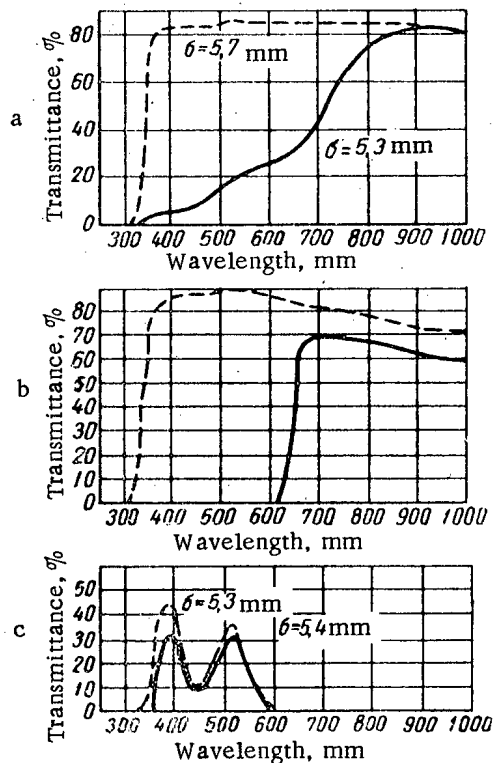

Fig. 1. Curves of spectral transmittance of glasses: (----) prior to irradiation; (——) following irradiation with a dose of 10^6 r.

29

diation with a dose of 10^6 r. We see from the Table that the color characteristics of the glasses suffered negligible change.

Change in Transparency of the Glass

Each glass specimen was exposed to various gamma-ray doses ranging from 10^2 to 10^6 r, emanating from a Co^{60} source, as well as irradiation in a nuclear reactor, in doses from 10^6 to $5 \cdot 10^{10}$ r.

Figure 3 shows the variation in the transparency of conventional window glass, OG from the Gorky glass-works (1), polished PG glass from the Gusev works (2),

and colorless No. 10 glass, for extruded items, from the "Krasnyi luch" works (3), as a function of radiation dose. The shape of the curves in Fig. 3 demonstrates that soda-lime glasses of compositions generally accepted in industry are stable to gamma-rays for doses of up to 10^4 r. Only at that dose limit is appreciable darkening of the glass observed. Further irradiation results in rapid darkening; within the $10^6 - 10^7$ r dose range, the slope of the curve dips, and at 10^{10} r the limit of color saturation sets in. For polished glass, color saturation sets in at lesser doses, at about 10^8 r.
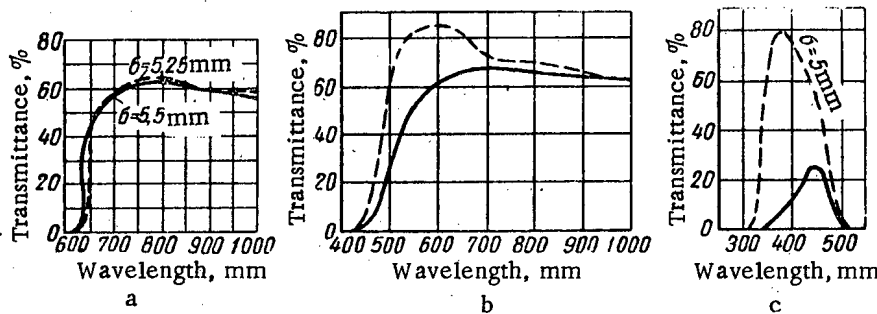
Fig. 2. Curves of spectral transmittance of glasses: (----) prior to irradiation; (———) after irradiation, dose 10^6 r.

The integral transparency of window glass irradiated with a maximum dose of $6 \cdot 10^{10}$ r is 7.1%, and for polished glass it is 12.8%, while it is 6.2% for glass No. 10.

Figures 4 to 6 show the curves characterizing the change in transparency of the glasses tested in response to irradiation with γ rays. Inspection of these curves shows clearly that there is an inflection point for each glass corresponding to the gamma dose at which appreciable darkening or an appreciable decrease in the transparency of the glasses begins.

The results of the test show that when a cation of larger ionic radius in the glass is replaced by a cation of smaller ionic radius, the stability of the glass to radiation bombardment is enhanced.

It is plausible to assume that the substitution of the Mg^{2+} ion with its radius of 0.78 A for the Na^+ ion of radius 0.98 A and the K^+ ion of radius 1.33 A explains the considerable stability to radiation of the rolled glass, compared to No. 10 glass.

Terminology

Hitherto, there has existed no unified terminology with respect to the determination of stability of glass to the effects of radioactive radiations. For the stability index (K_y) of the glass, it would be feasible to adopt the value of the logarithm of the dose, D_y, at which appreciable darkening of the glass sets in, i.e., $K_y = \log D_{sat}$. A decrease in transparency to visible light of 3-5% will

Table 1. Color Characteristics of Glasses of the "Copper Ruby" Type Prior to and Following Irradiation with a Dose of 10^6 r

Glass species	Thickness of glass σ mm	Wavelength λ, mm	Transparency τ, % in visible range	Color coordinates		Color saturation, %
				x	y	
Unglazed No. 13 copper ruby, from "Krasnyi luch":	} 5	620				
prior to irradiation			2,2	0,695	0,305	100
following irradiation			0,9	0,700	0,295	100
SKSG copper ruby, from the Chernyatinsk works:	} 5,1	638				
prior to irradiation			2,6	0,715	0,284	100
following irradiation			0,8	0,705	0,285	100
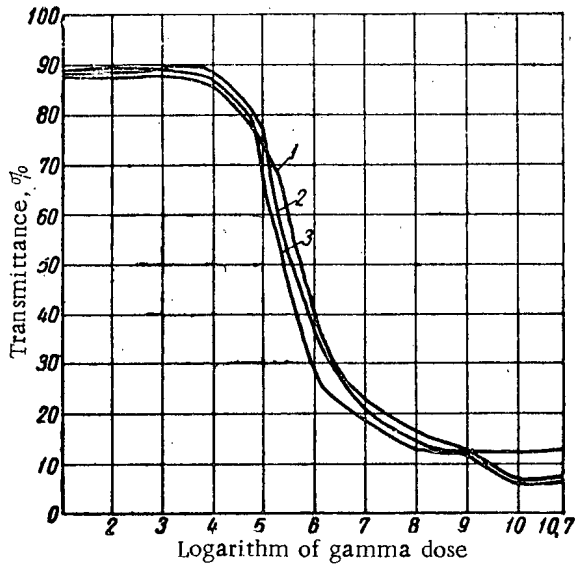
Fig. 3. Variation in the transparency of colorless glasses upon irradiation.
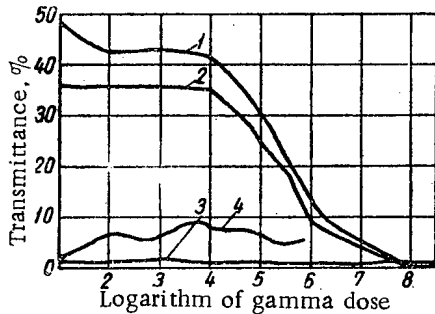
Fig. 4. Variation in the transparency of glasses in response to gamma irradiation. 1) Opal No. 14 glass from "Krasnyi luch"; 2) same type glass from Chernyatinsk works; 3) blue No. 17 (cobalt) glass from "Krasnyi luch"; 4) red No. 13 (copper ruby) glass from "Krasnyi luch".
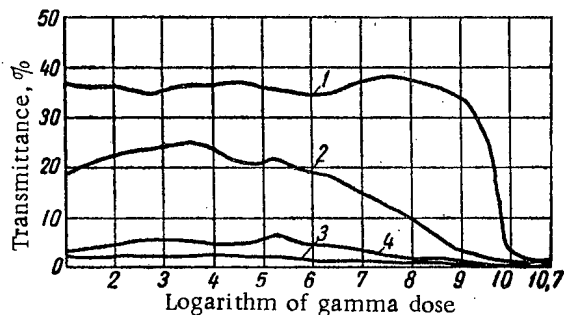
Fig. 5. Variation in the transparency of colored glasses in response to irradiation: 1) Blue-green SCh glass from Chernyatinsk works; 2) green 5A/Z glass from "Kransyi luch"; 3) red SKSG glass from Chernyatinsk works; 4) red K4/2 (selenium ruby) glass from "Krasnyi luch".

be adopted as criterion for the process of appreciable darkening.

As is clear from the graphs in Figs. 4-6, the rate of coloration of the glass increases continuously as the irradiation dose is stepped up. However, there is a certain limiting value to the irradiation dose for each glass species, any increase above which will fail to produce any further intensification in coloration.

This limiting value D_{sat} will not be the same for each glass species, and it would be advisable to introduce still another term to evaluate the response of the glass to radioactive bombardment; the saturation index (K_{sat}), which is of the form $K_{sat} = \log D_{sat}$. Furthermore, the minimum value of the total light transmittance T_m at the saturation dose D_{sat} is highly significant in the case of glass.
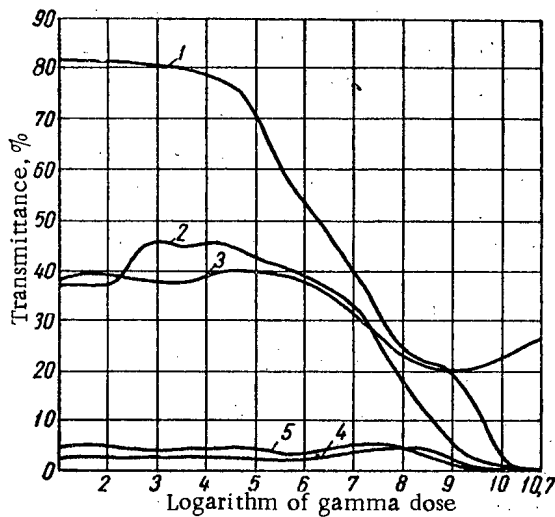
Fig. 6. Variation in transparency of colored glasses upon irradiation: 1) Orange OS-6 (cadmium) glass from Chernyatinsk works (unglazed); 2) same glass (glazed); 3) experimental US-4 glass, sulfur colorant; 4) red K 3/2 (selenium ruby) glass from "Krasnyi luch" works; 5) red Ks-1 (selenium ruby) glass from Chernyatinsk works.

Still one more criterion, the darkening rate or coefficient of rate of darkening Q, will be found useful in rounding out the description of the glass response, this quantity being accepted as the ratio of the transparency factor τ_0 prior to irradiation to the transparency factor τ following irradiation, at a dose of 10^6 r, i.e.,

$$Q = \frac{\tau_0}{\tau} .$$

The irradiation dose of 10^6 r is fully adequate for practical purposes.

These four quantities : the stability index K_y, the saturation index K_{sat}, minimum transmittance T_m, and coefficient of rate of darkening Q, give a fairly complete picture of the response of glass to irradiation. The

31

TABLE 2. Values of the Coefficients Characterizing the Response of Glass to Radioactive Bombardment

Glass species	Darkening rate, Q	Stability, Ky	Saturation, K_{sat}	Minimum transmittance, T_m %
OG window glass, Gor'kii glassworks	2.6	4	10	7.1
Polished (rolled) PG glass, Gusev glassworks	2.24	4	8.3	12.8
No. 10 (colorless) glass for extrusions, "Krasnyi luch" works	3.38	4	10	6.2
No. 14 opal glass, "Krasnyi luch"	4.25	3.9	8	0
OPLS opal glass, Chernyatinsk glassworks	3.98	3.9	8	0
Blue No. 17 (cobalt) glass, "Krasnyi luch"	1.26	10	10.7	0
Blue-green SCh glass, Chernyatinsk works	1.04	8.5	10.5	0
Green 5 A/3 glass, "Krasnyi luch"...................	1.04	3.7	10.5	0
Green No. 18 glass, "Krasnyi luch"	1.05	5.7	10.5	1.4
Red (selenium ruby) K 4/2 glass, "Krasnyi luch"	1.0	5.3	9.7	0.3
Red (copper ruby) SKSG glass, Chernyatinsk works	1.88	7.3	9.3	0
Orange (cadmium) OS-6 glass, unglazed, Chernyatinsk works	1.53	3.6	10.2	0
Orange (cadmium) OS-6 glass, glazed, Chernyatinsk works......	1.0	4.5	10.2	0
Red (selenium ruby) KS-1 glass, Chernyatinsk works	1.22	7.8	9.5	0.0
Red (selenium ruby) K 3/2 glass, "Krasnyi luch".............	1.07	8	9.5	0.0

values of these quantities are entered in Table 2.

It may be ascertained from the data in Table 2 that colored glasses with such colorants as selenium, cadmium sulfate, cobalt oxide, copper oxide and bichromates possess a high stability index and a low coefficient of rate of darkening. However, for irradiation doses of the order of $9\text{-}10^{10}$ r, they lose virtually all of their transparency in the visible portion of the spectrum.

The investigation presented in [2] contains an inaccurate statement that, on receiving doses of radiation close to 10^{10} r, the glass shatters. Not the least sign of shattering of the glass was observed in our experiments.

On Enhancing the Stability of Glass to Radiation.

The character and intensity of changes in the coloration of glass are dependent on the composition of the glass and the irradiation dose, and not on the form of the radiation. Industrial glasses, with the exception of special shielding glasses, absorb γ rays and neutrons weakly, and the effects of these forms of radiation therefore result in coloration of the glass through the entire thickness of the glass. The depth of penetration of α particles and β rays into the glass is negligible, and changes in glass coloration are observed only in the superficial layers. All forms of radiation lead to the formation of free electrons and excited atoms in the glass.

In the presence of ions free to change valency, the mechanism involved in the change in glass coloration may be explained by the attachment or ejection of electrons, as for example:

$$V^{3+} \text{ (green)} \quad + e^- \longrightarrow V^{2+} \text{ (pink)}.$$
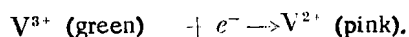
In the case of some ions, as Ce^{4+}, As^{5+}, Sb^{5+}, and Pb^{2+}, the change in valency fails to bring about any

change in the coloration of the glass:

$$Ce^{4+} \text{ (colorless)} \quad + e^- \longrightarrow Ce^{3+} \text{ (colorless)}.$$
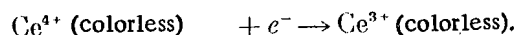
Transition from Ce^{4+} to Ce^{3+} does not result in any change in the absorption curve over the visible portion of the spectrum, since the absorption band for CeO_2 and Ce_2O_3 lies in the ultraviolet region.

Polyvalent ions in glass assume the role of electron acceptors, accepting electrons set free in response to radiation.

In glasses containing polyvalent ions, the energy of radiation is spent primarily in changing the valency, rather than in the formation of color centers. Such glass species accordingly exhibit high radiation stability.

The property of increasing the radiation stability of glasses is also possessed by Cr^{3+}, Mn^{4+}, As^{5+} and Sb^{5+} and Fe^{3+} ions. Ceric oxide is the only additive which has found practical use in industrial glasses as a material for sharply increasing the stability of glass to radiation. The intense effect of ceric oxide on the stability of glass to radiation was first disclosed as far back as 1926 [3], and in subsequent work [4] and [5]. Some very important work, in both theoretical and practical areas, has been done in this field by V. V. Vargin and his associates at the State Optics Institute.

At the present time, ceric oxide is used in amounts of 0.4-1.2 wt.% in the manufacture of glasses possessing increased radiation stability.

The status of shielding glasses with enhanced stability to γ rays is a more complex one. High-density glasses with a high lead oxide content are used as transparent shielding. Such glasses possess increased radiation stability in and of themselves. For example, the absorption coefficient of glass containing 69.5 wt.% lead

32

Appendix

Oxides	Glass species									
	№ 10	PG	К3/2	S-1	№ 18	5P/3	SKSG	№ 14	№ 17	№ 13
SiO$_2$	72,26	73,5	63,47	71	68,14	72,47	73,72	59,86	73,0	74,19
R$_2$O$_3$	0,32	1,0	—	—	0,23	0,33	—	10,46	0,24	0,20
CaO	8,4	9,0	—	—	9,31	8,58	7,94	0,78	8,22	0,34
MgO	0,15	3,3	—	—	0,24	0,14	3,76	0,19	0,25	0,24
Na$_2$O	17,63	13,2	2,64	16,0	11,11	13,76	11,7	9,11	16,3	14,7
K$_2$O	1,24	—	12,44	—	9,27	—	1,75	2,71	0,92	6,5
B$_2$O$_3$	—	—	2,88	2,0	—	3,23	—	0,69	1,07	—
ZnO	—	—	15,81	11,0	—	—	—	—	—	—
AlF$_3$	—	—	1,66	—	—	—	—	3,10	—-	—
NaF	—	—	1,41	—	—	—	—	2,64	—	—
PbO	—	—	—	—	—	—	—	10,4	—	—
CoO	—	—	—	—	—	—	—	—	0,24	—
BaO	—	—	—	—	—	—	—	—	—	2,73
Se (metal) . .	—	—	1,59	0,3	—	—	—	—	—	—
CdS	—	—	4,32	0,97	—	—	—	—	—	—
CuO	—	—	—	—	1,3	1,9	—	—	—	—
Cr$_2$O$_3$	—	—	—	—	0,35	0,11	—	—	—	0,7
Sn (metal) . .	—	—	—	—	—	—	0,5	—	—	—
Cu$_2$O	—	—	—	—	—	—	0,2	—	—	0,2

oxide is 1.48 cm^{-1} following an irradiation of 10^6 r, i.e., it is significantly less than that found for window and polished glasses. However, the ensuing darkening is inadmissible for a number of cases.

Ceric oxide additive in lead glass does not produce such noticeable results as in silicate glasses. In order to improve the γ stability of high-lead content glasses, arsenic and antimony are used as additives.

The transition of the As^{3+} ion to As^{5+} and the Sb^{3+} to Sb^{5+} transition calls for a high expenditure of energy above that required for the Ce^{4+} to Ce^{3+} transition. It is however possible that, when arsenic trioxide is added in combination with other polyvalent oxides, highly stable glasses may be successfully produced.

Cognizance must be taken of the desirability of replacing ions of larger dimensions by smaller ions, in working out the compositions of γ-stable glasses. The replacement of SiO$_2$ by P$_2$O$_5$; and B$_2$O$_3$ in glass improves the stability of the glass. Replacement of K$_2$O and Na$_2$O by Li$_2$O and MgO also has a salutary effect.

Our investigations resulted in the elaboration of a new technique for improving the γ stability of glass by addition of 0.5-1.5 wt% elemental sulfur. Electron attachment with the formation of polysulfides is postulated as an explanation.

Figure 7 shows the spectral transmission curves for the experimental glass US-4. The composition of this species is as follows (in wt.%): SiO$_2$ (71.5); B$_2$O$_3$ (1.5); CaO (8.5); MgO (1.5); Na$_2$O (17.0); sulfur above 100 wt.% (1.2).

Experiments have shown that the color of US-4 glass does not change in response to irradiation doses of $3 \cdot 10^8$ r. In this species of glass, the stability index K_y=

=5, the saturation index $K_{sat} > 10.7$, the darkening rate Q=1.0. The transparency of the glass following irradiation with a dose of $5 \cdot 10^{10}$ r is 27.7%, i.e., much higher than in the case of all other glasses investigated.

The processes involved in the change in coloration of the glass in response to irradiation have a reversible character. Coloration of the glass may be partially or completely reversed by heating the glass to temperatures close to the softening point, by exposing the glass to sunlight, or by exposing the glass to flourescent lamps. The first process proceeds very rapidly; a prolonged exposure is needed for sunlight to work its effect on the glass.

Polished glass from the Gusev works acquired, following γ irradiation with a dose of $5 \cdot 10^4$ r, a faint brownish-gray coloration, which disappeared completely when the specimen was left standing for four to five days of exposure to ordinary sunlight. The same glass, irradi-
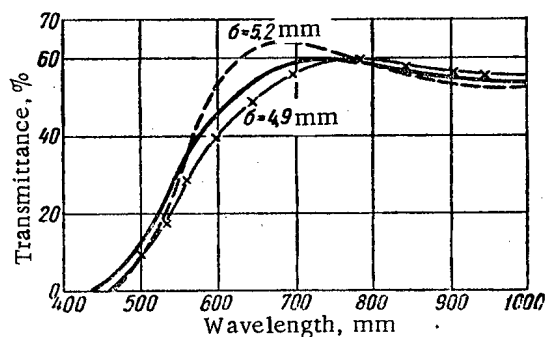
Fig. 7. Spectral transmittance of experimental glass US-4: – – – –) prior to irradiation; ————) after irradiation, dose 10^6 r; — x—) after irradiation, dose $3 \cdot 10^8$ r.

33

ated with a dose of 10^6 r, was successfully bleached only after 40 days of exposure.

Under the service conditions appropriate to shielding glasses, in the presence of low source activity, the rate of darkening of the glass is equal to the rate of fading, so that the transparency of the glass suffers no change.

In the manufacture of shielding glasses, it is sometimes necessary to glue separate plates of glass together into a sandwich. When the refractive indices of the glass and the film in the sandwich are approximately equal, reflection losses (4-6% on each surface) are absent, so that the transparency of the glued laminates is much higher than would be the case in a window made up of separate plates of glass with air layered in between.

Glass specimens glued to polyvinyl butyral film were subjected to γ irradiation in a nuclear reactor to study the γ stability of adhesives. As the experiments showed, polyvinyl butyral film exhibits excellent stability to γ rays, withstanding irradiation doses of 10^7 r without alteration. Bubble formation ensues when the film is exposed to a dose of 10^8 r.

In conclusion, I would like to express my acknowledgment to G. Ya. Vasil'ev and Yu. Ya. Zhelazova for their kind assistance in performing the experimental research discussed herein.

LITERATURE CITED

1. S. M. Brekhovskikh, Steklo i Keramika, 1, 3 (1958).
2. G. Formon, J. Opt. Soc. America 41, 377 (1951)
3. E. Eckerm, Z. Techn. Physik 7, 300 (1926).
4. L. Monk, Nucleonics 10, 52 (1952).
5. K. Sun and M. Kreide, Glass Ind. 33, 514 (1952).

34

MASS-SPECTROMETRIC AND SPECTROSCOPIC STUDIES
OF HYDROGEN DISCHARGE OF AN ION SOURCE

A. I. Nastyukha, A. R. Striganov, I. I. Afanas'ev,
L. N. Mikhailov, and M. N. Oganov

The production of currents having a maximum relative content of either protons or ions of molecular hydrogen, from hydrogen ion sources, is of significant interest for a number of physical problems. Preliminary mass-spectrometric studies of ions emerging from the slit source of the 1.5 m cyclotron of the Academy of Sciences of the USSR have shown that ion currents of the order of 60 ma, containing 95% protons or 80% molecular hydrogen ions, can be obtained from an area 20×2 mm [1]. Later, by employing optical-spectroscopic techniques, a successful attempt was made to trace not only the ratio of H^+ to H_2^+ ions in the ion source, but at the same time to monitor variations in the relative content of neutral H and H_2 particles in the plasma of the discharge. An ion source with its associated electrical supplies are diagrammed in Fig. 1. A three-prism glass Zeiss spectrograph, with camera objective of focal length 840 mm, was used in investigating the optical spectrum of the hydrogen. The reciprocal linear dispersion of this instrument in the region of 6500 A was 38 A/mm.

Light from the ion source emerges from a rectangular opening 15 mm high and 2 mm wide, oriented along the discharge channel. The first line of the Balmer series (6562.79 A) was used in studying the emission of

monatomic hydrogen. The half-sum of the intensities of lines 6031.90 A and 6018.29 A were used as measures of the emission of molecular hydrogen. Spectral-line intensity may be used to advantage to estimate the concentration of neutral particles. It should however be borne in mind that this intensity relates to the number of excited particles at a given energy level [2]. Under conditions of constant excitation, variation in the relative intensity of the spectral lines of monatomic and molecular hydrogen may be used to monitor variations in the relative concentration of neutral particles N_H / N_{H_2}. When the conditions of excitation are varied, the relative intensity J_H / J_{H_2} characterizes the ratio $N_H \sigma_H / N_{H} \sigma_{H_2}$, where σ_H and σ_{H_2} are the effective excitation cross sections for H and H_2. Since the value of σ_H varies only slightly over the range of electron energies pertinent to the investigation [3], the variation in the relative intensity J_H / J_{H_2} will in this case reflect the variation occurring in the relative concentration of neutral particles in the hydrogen discharge.

During the experimentation, a sharp difference between the yields of H^+ and H_2^+ ions from the source, de-
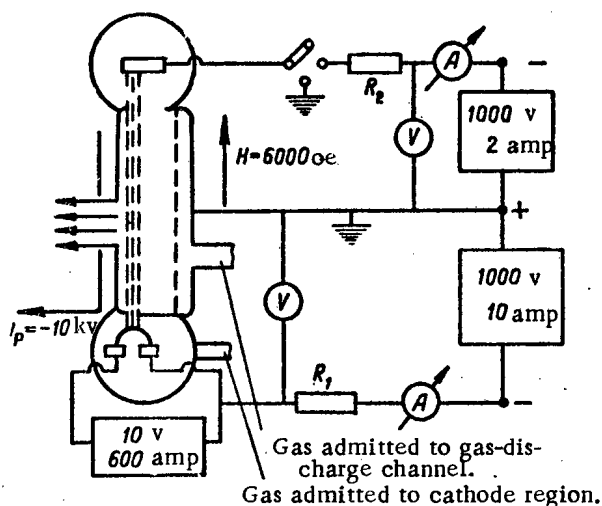
Fig. 1. Diagram of ion source.
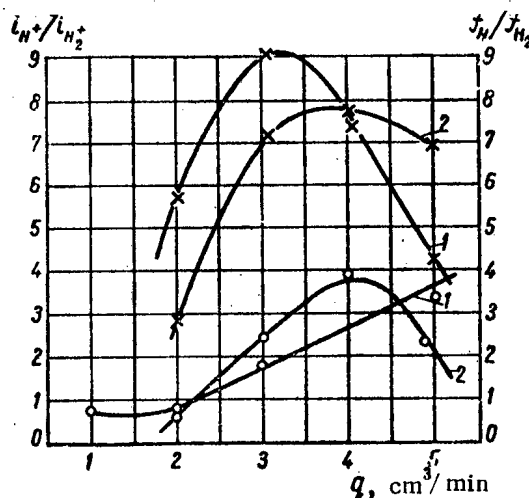
Fig. 2. Ratios of ion currents 1 and of line intensities 2 plotted against rate of gas influx q, at $I_p = 3$ amp, $U_p = 160$ v.
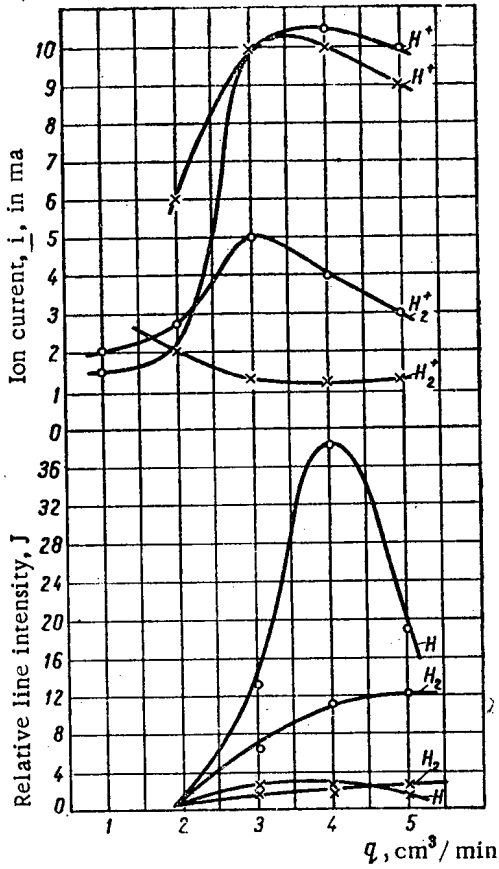
Fig. 3. Variation in the absolute values of ion currents and spectral-line intensities as a function of gas influx, at $I_p = 3$ amp, $U_p = 160$ v.

pending on the point at which the gas was admitted, was disclosed. Figure 2 shows the ratios of ion currents $i_{H^+}/i_{H_2^+}$ and line intensities J_H/J_{H_2} plotted as functions of gas influx where two different methods were used for introducing the gas. The points plotted in all cases correspond to admittance of gas to the cathode region (hollow circles), while curves with crosses correspond to admittance of gas into the gas-discharge channel. The shape of the curves of relative intensity J_H/J_{H_2} characterizing the dissociation process show that dissociation is greater when the gas is admitted to the gas-discharge channel. To shed light on the behavior of curves $i_{H^+}/i_{H_2^+}$ and J_H/J_{H_2}, the absolute values of the ion currents $i_{H^+}/i_{H_2^+}$ and spectral-line intensities J_H and J_{H_2} are plotted in Fig. 3 as functions of gas influx. For greater clarity, the intensity of the lines in the first spectrum is assigned a value of unity, and the intensity of lines in subsequent spectra is referred to it. Plotted in Fig. 4, for comparison purposes, are curves expressing the relation of ratios $i_{H^+}/i_{H_2^+}$ and J_H/J_{H_2} to the discharge current when the gas is admitted to the gas-discharge channel or to the cathode region, as the case may be, at the point of peak difference between the yields of H^+ and H_2^+ ions.

In the case where gas is admitted to the gas-discharge channel, the curve for the line-intensities ratio shows that the relative concentration of monatomic hydrogen increase quite steeply as discharge current rises. Likewise, the relative concentration of H^+ and H_2^+ ions as a function of discharge current also shows this behavior.

When the gas is admitted to the cathode region, dissociation of hydrogen molecules and the relative concentration of protons at first decline in response to increased discharge current, and then later rise. The variation in
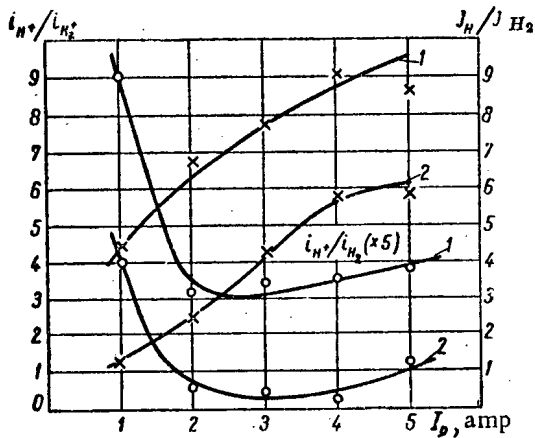
Fig. 4. Ratios of ion currents 1 and line intensities 2 versus discharge current, for the case where gas is admitted to the discharge channel ($q = 4$ cm³/min , $U_p = 180$ v), and where gas is admitted to the cathode region ($q = 2$ cm³ / min, $U_p = 160$ v).
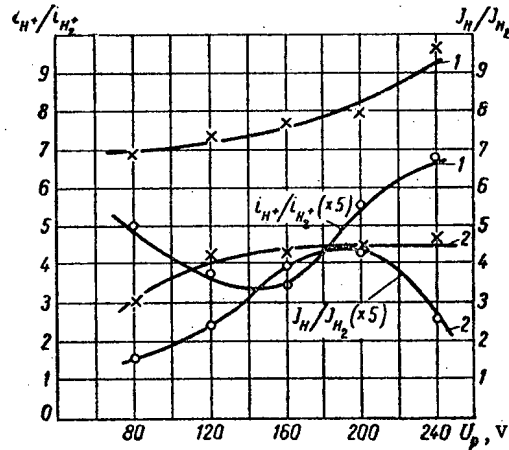
Fig. 5. Dependence of ratio of ion currents and line intensities on discharge voltage, when gas is admitted to discharge channel ($q = 4$ cm³/min , $I_p = 2$ amp) and when gas is admitted to cathode region ($q = 2$ cm³ / min, $I_p = 2$ amp).

36

the absolute values of the spectral line intensities and ion currents demonstrates that the minimum in Fig. 4 is due to a sharp drop in the concentration of monatomic hydrogen, resulting in a relatively high yield of molecular hydrogen ions. Note that a decline in H and H⁺ with increased discharge current is characteristic for the case when gas is admitted to the cathode region. The reasons for this effect are obscure.

Figure 5 shows the dependence of the ratios mentioned on discharge voltage. Curves giving the ratios of the intensities of spectral lines are similar in shape to the ion-current curves; the curve of relative intensity for gas admitted to the discharge channel reaches saturation at about 200 v, while the curve for the ion currents continues upward.

In the case where gas is admitted to the cathode region, the curve of relative intensity of spectral lines shifts by about 40 v in the direction of lower voltages. This is an indication that the most complete dissociation sets in earlier in the plasma than does ionization, as the voltage increases. Spectral-line intensities and absolute ion-current values show that the variation in the degree of dissociation of molecular hydrogen and in the relative concentration of protons as a function of discharge voltage are associated with the increase or decrease in the concentration of monatomic hydrogen in the plasma.

The experimental material reviewed here shows that the degree of dissociation in the ion source, as likewise the proton yield and yield of molecular hydrogen ions, are affected by the point of admittance of the gas. An important role is assigned to such discharge constants as gas influx rate, discharge voltage, and discharge current [4]. The similar behavior of the curves characterizing the dissociation and ionization processes accompanying variations in the discharge constants bears evidence that the process of proton formation has a two-stage character: dissociation of H_2 takes place first, followed by ionization of the hydrogen atoms. The large proton yield in the case where gas is admitted to the gas-discharge channel is explained by the fact that a larger number of molecules engages in interaction with the electrons in that case than when gas is admitted to the cathode region. Another possibility is that, when the gas is admitted to the discharge channel, the gas particles interact with slower electrons; the process of dissociation of the molecules would be more effective in that case [5].

LITERATURE CITED

1. I. I. Afanas'ev, L. F. Kondrashov, L. N. Mikhailov, and A. I. Nastyukha, Pribory i Tekh Eksp., 6, 25 (1959).
2. S. E. Frish, Uspekhi Fiz. Nauk 11, 641 (1957).
3. L. Ornstein and H. Linderman, Z. Phys. 80, 526 (1933)
4. R. Livingston and R. Jones, Rev. Scient. Instrum. 25, 552 (1954).
5. A. Kruithof and L. Ornstein, Physica 2, 611 (1935).

NEW ISOTOPES OF HOLMIUM AND ERBIUM

N. S. Dneprovskii

The conversion-electron spectra of isotopes of the erbium fraction, formed upon bombardment of tantalum by protons of 660 Mev energy on the Dubna synchrocyclotron, were investigated.

The spectra were studied on a BPP-1 magnetic betaspectrograph with a focusing angle of $\pi\sqrt{2}$ [1]. When a source 1×30 mm was used, with solid angle 0.4% of 4π, the resolution of the instrument at the K-661.6 line of Ba^{137} was 0.2-0.25%. The magnetic field in the spectrometer was measured by means of a special magnetometer, thus ensuring efficient performance and making it possible to study conversion lines with a half-life of 15 min or longer. An accuracy of 0.1-0.3% was achieved in determining the energy of the conversion lines

A group of lines with half-life $T_{1/2} = 2.4$ hr was discovered from among the host of conversion lines (over 100) belonging to the neutron-deficient isotopes of erbium and holmium [2]. The investigation of these lines made it possible to identify several transitions occurring both in the holmium nucleus (Z = 67) and in dysprosium nucleus (Z = 66) [cf Table].

Upon isolation of the daughter holmium isotope from the erbium fraction 2 hr. after the latter was isolated from tantalum, the intensity of lines corresponding to γ transitions of the dysprosium nucleus had dropped one-half within (27 ± 2) min.

From the facts accumulated, we may ascertain the presence of the decay chain

$$\text{Er} \xrightarrow{\;2,4\text{hr}\;} \text{Ho} \xrightarrow{\;27\,\text{min}\;} \text{Dy}.$$
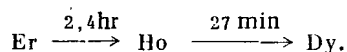
The ratio of energies 98.6 and 218.2 kev and of intensities of the transitions support the inference that these transitions take place between levels $E_1 = 98.6$ kev (2^+) and $E_2 = 316.8$ kev (4^+) of the first rotational band of the even-even dysprosium nucleus. The position of the first excitation level as a function of neutron number [3] suggests that the mass number of the nuclei belonging to the above decay chain is A = 158.

Gamma Transitions in Erbium and Holmium Nuclei.

$h\nu$, kev	$T_{1/2}$, hr	Charge on nucleus undergoing transition	Multiple order
98,6	2,4±0,1	66	$E2$
218,2	2,5±0,1	66	—
320,5	2,4±0,1	66	$E2$ or $M3$
357,1	2,4±0,1	66	—
387,3	2,4±0,1	67	—
945,9	2,5±0,1	—	—
848,5	2,5±0,1	—	—

The values of the constants A and B in the equation for energy levels $E = AI(I + 1) - BI^2(I + 1)^2$, determined according to the position of the first two levels, are equal, respectively, to 16.7 ± 0.35 and 0.042 ± 0.008.

LITERATURE CITED

1. I. M. Bekkerman, B. A. Gumenyuk and I. S. Dneprovskii, The BPP Type Beta Spectrometer (VINITI, Moscow, 1959).
2. I. S. Dneprovskii and G. M. Kolesov, Izv. Akad. Nauk SSSR, Ser. Fiz. 22, 935 (1958).
3. B. S. Dzhelepov and L. K. Peker, Deformed Nuclei in the Nd-Os Region [in Russian] (Dubna, 1958).

38

FISSION CROSS SECTION OF Th229 FOR MONOCHROMATIC NEUTRONS IN THE 0.02 - 0.8 ev REGION

Yu. Ya. Konakhovich and M. I. Pevzner

Until recently, studies of cross sections of fissionable substances had been largely limited to the three most easily available isotopes of greatest practical importance, viz., U^{233}, U^{235}, and Pu^{239}. Analysis of data obtained on the cross sections of fissionable isotopes [1], has revealed some interesting regularities in the distribution of level spacing between levels of fission and neutron widths [2-4].

One feature common to all the fissionable nuclei studies up to now, including Pu^{241} and Am^{241} in addition to those enumerated above, is the large value of the fission cross sections in the thermal region, varying in obedience to the inverse law $1/\sqrt{E}$, and not interpretable in terms of the resonances lying close by to the right. This "$1/\sqrt{E}$ background" is usually attributed to the effect of the "bound" level lying to the left of the neutron zero kinetic energy. The fact that a resonance appears in the energy range 0.2-0.3 ev in the cross sections of all isotopes fissioned by thermal neutrons which have been studied to date merits attention, although there is no difficulty in demonstrating that the statistical probability of such a coincidence is very meager. The number of isotopes investigated must be increased in order to throw some light on the underlying aspects of the behavior of the fission cross sections. However, an obstacle to measuring fission cross sections is the intense α activity of most isotopes fissionable by thermal neutrons, resulting in the effect of pulses triggered by alpha particles being superimposed on the fission counter, while measurements of total cross sections require a large number of different substances, inaccessible at present for most isotopes.

One of the most convenient nuclei for research purposes is the Th^{229} nucleus, an α-active nuclide with a half-life of 7,300 years [5].

The fission cross section spectrum of Th^{229} over the neutron energy range 0.025-0.80 ev was studied, using a crystal neutron spectrometer [6] mounted on the horizontal beam of the IRT reactor. An ionization fission chamber containing the material under study and a "thin" proportional counter loaded with boron trifluoride were placed in series in the path of the monochromatic beam of neutrons. The cross section for the $B^{10}(n,\alpha)$ reaction obeys the law $1/\sqrt{E}$ over a broad range of energies, and the relative values of the fission cross sections may be found from the formula

$$\sigma_f = \text{const}\,\frac{1}{\sqrt{E}}\left(\frac{N_{Th}}{N_B}\right),$$

where N_{Th} and N_B are, respectively, the counting rate of the chamber and proportional counter for monochromatic neutrons, after deducting background. In our arrangement, there was $6 \cdot 10^{-5}$ g Th^{229} obtained by chemical separation from U^{233}, in which it has accumulated as a result of α decay.

The purity of the preparation we used is discussed in an earlier paper [7]. According to the data reported therein, uranium impurities did not exceed several hundredths of a percent. The preparation was coated in oxide form on platinum foil 7 μ thick. The geometry of the layer was close to rectangular, with sides 20 X 26 mm. The amount of Th^{229} present was determined by the total α activity of the layer, with the four α decay steps following decay of Th^{229} accounted for. The foil bearing the preparation was placed on the high-voltage electrode of the plane ionization chamber, which was filled with a mixture of argon and carbon dioxide (8%) to a pressure of 500 mm Hg. Since the cross section of the diffracted beam (8 X 25 mm) was smaller than the dimensions of the layer, the electrodes were placed at a 30° angle to the beam path, favoring effective use of the material. On account of the very low counting rate for fission events, the time required to reach 10% statistical accuracy fell within the range of 50-100 hr for one point. Special measures were therefore utilized to cope with noise, and measurements of effect and background were alternated.

The diagram shows the variation of the fission cross section of Th^{229} over the energy interval 0.02-0.80 ev, with some indication as to the resolution of the instrument. The curve is normalized to the value $\sigma_f = (45 \pm 11)$ barns [1]. This normalization must be regarded as only tentative, since the value of 45 barns apparently has reference to the reactor neutron spectrum, while the variation of the cross section of Th^{229} does not follow the $1/\sqrt{E}$ inverse law in the thermal region. The energy scale of the instrument was calibrated according to the level of iridium at 0.654 ev, by measuring the total cross section. A correction for higher-order reflection
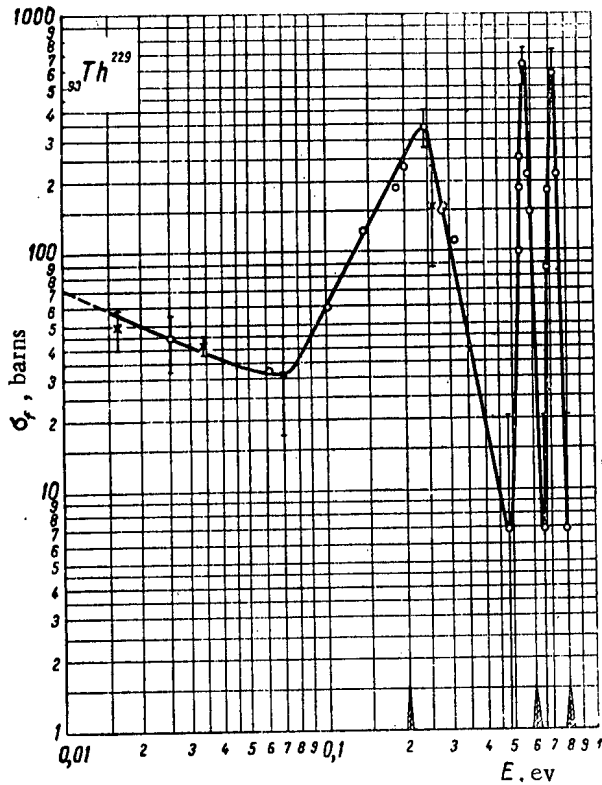
Fission cross section of Th^{229};
O) crystal spectrometer; x) mechanical chopper.

The resonance peaks at 0.563 and 0.727 ev provide an explanation for only a small part of the observed resonance integral.

Measurements were made for control purposes near the resonance peak at 0.240 ev. The chamber counting rate found when the beam was masked by a cadmium layer 0.8 mm thick was equal to the counting rate for an incoherently scattered beam; this attests to the fact that the 0.240 ev resonance is due to first-order reflection neutrons.

In the 0.02-0.26 ev energy region, the fission cross section of Th^{229} was measured by V. F. Gerasimov, at our request. The same fission chamber and target were used, with monochromatic neutrons selected out by a mechanical monochromator. Results of the measurements appear in the diagram.

The authors consider it a welcome obligation to express their gratitude to I. V. Kurchatov for the interest kindly manifested in their research [8], to G. N. Yakovlev and S. V. Pirozhkov for preparing a pure thorium specimen, and to Chang Huang-ch'ao for his aid in the measurements.

effects was introduced in the 0.025-0.07 ev region. Three resonance levels are manifest in the cross section, at energies 0.240, 0.563, and 0.727 ev.

The magnitude of the area S under the cross section curve was used to determine the product $\sigma_{f_0} G = 2S/\pi$ for the 0.240 and 0.563 ev levels, which were 34 ± 7.5 and 7 ± 3.3 ev-barns, respectively.

The resonance integral for Th^{229}, $J_{Th} = \int_{0,4}^{\infty} \sigma_f (E) \frac{dE}{E}$, determined from the value of the cadmium ratio R_{Cd} in accord with the familiar formula

$$J_{Th} = \frac{\sigma_{Th} \text{ thermal}}{2} \cdot \frac{R_{Cd}^{B} - 1}{R_{Cd}^{Th} - 1},$$

was 240 barns, since $R_{Cd}^{Th} = 2.34$ and $R_{Cd}^{B} = 15.2$ in the spectrum of the IRT reactor.

LITERATURE CITED

1. Neutron Cross Section. BNL-325 (1958). 2nd ed.
2. C. Porter and R. Thomas, Phys. Rev. 104, 483 (1956).
3. L. Bollinger, R. Cote and G. Thomas, Paper 687, presented by the USA at the Second International Confer. on the Peaceful Uses of Atomic Energy. (Geneva, 1958).
4. I.I. Gurevich and M. I. Pevzner, Zhur. Éksp. i Teor. Fiz. 31, 162 (1956).
5. I. P. Seliknov, Atomic Nuclei and Nuclear Transmutations. [in Russian] (Gostekhizdat, Moscow, 1951).
6. Yu. Ya. Konakhovich and I. S. Panasyuk, Pribory i Tekh Eksp., 3, 26 (1959).
7. V. I. Lebedev and V. I. Kalashikova, Zhur. Eksp. i Teor.Fiz. 35, 535 (1958).
8. I. V. Kurchatov, Nuclear Radiations in Science and Engineering [in Russian] (Moscow, 1958).

MEAN NUMBER OF PROMPT NEUTRONS PER SPONTANEOUS FISSION OF U²³⁸

É. K. Gerling and Yu. A. Shukolyukov

To find $\bar{\nu}_{238}$, the mean number of neutrons per single act of spontaneous fission of U^{238}, knowledge of two quantities, determined independently of each other, is required: the number of prompt neutrons emitted by 1 g of uranium in unit time Δn, and the number of spontaneous fissions in 1 g of uranium in unit time ΔN_{238}. These quantities are related by the simple formula

$$\bar{\nu}_{239} = \frac{\Delta n}{\Delta N_{233}}.$$

When the number of neutrons accompanying spontaneous fission in natural uranium is measured, the most reliable result is found to be the one reported in [1]: $(1.65 \pm 0.09) \cdot 10^{-2}$ neutrons per sec per g of U (cf [2]).

The generally accepted value for the spontaneous fission half-life of U^{238} is $8.0 \cdot 10^{15}$ years [3]. The corresponding value of ΔN_{238} is 24.8 fission events per hr per gram of U [1]. Calculation of $\bar{\nu}_{238}$ based on data reported in [2, 3] yields 2.4 neutrons per spontaneous fission of U^{238}; this value has been accepted as the most trustworthy [1,4].

By employing the new geochemical method for determining the spontaneous fission half-life of U^{238}, we obtained a value of $(5.8 \pm 0.5) \cdot 10^{15}$ years [5] which, upon comparison with data reported by other authors in recent years [6-9], strongly suggests that the results in [3] were too high, and that the true value for the half-life of U^{238} is $5.8 \cdot 10^{15}$ years. We then have $\Delta N_{238} = 34$ fission events per hr per g of U, while the mean number of neutrons per act of spontaneous fission of U^{238} will be 1.7, instead of the previously accepted value of 2.4.

As demonstrated in an earlier paper [10], the mean number of prompt neutrons may be calculated from the energy balance of the fission reaction. Results computed for Pu^{236}, Pu^{238}, Pu^{240}, Pu^{242}, Cm^{242}, Cm^{244}, Cf^{244}, and Cf^{252} are found to correspond to empirical data. U^{238} is an exception, calculations giving $\bar{\nu}_{238} = 1.6$. When this last value is compared to the one we found, there is evidence for practically complete agreement.

It is apparent that the value $(5.8 \pm 0.5) \cdot 10^{15}$ years should be accepted for the half-life of U^{238} resulting from spontaneous fission, while the mean number of neutrons per fission event should be assigned the value of 1.7.

LITERATURE CITED

1. D. Littler, Proc. Phys. Soc. 65A , 203 (1952).
2. K. A. Petrzhak, Physics of the Fission of Atomic Nuclei, Supplement No. 1 to Atomnaya Énergiya (1957).
3. E. Segrè, Phys. Rev. 86, 21 (1952).
4. J. Fraser, Proc. of the Symposium on the Phys. of Fission (Chalk River, Ontario, 1956) p. 238.
5. É. K. Gerling, Yu. A. Shukolyukov and B. A. Makarochkin, Radiokhimiya 1, 223 (1959).
6. P. Kuroda and R. Edwards, J. Chem. Phys. 22, 1940 (1954).
7. P. Kuroda and R. Edwards, J. Inorg. and Nucl. Chem. 3, 345 (1957).
8. G. Seaborg, The Transuranium Elements (New York, 1958).
9. B. D. Kuz'minov, L. S. Kutsaeva, V. G. Nesterov, L. I. Prokhorova, and G. N. Smirenkin, Zhur. Éksp. i Teor. Fiz. 37, 406 (1959).
10. B. D. Kuz'minov and G. N. Smirenkin, Zhur. Éksp. i Teor. Fiz. 34, 503 (1958).

THE EFFECT OF BORON-CONTAINING LAYERS ON THE YIELD
OF SECONDARY GAMMA RADIATION

D. L. Broder, A. P. Kondrashov,
A. A. Kutuzov, and A. I. Lashuk

In most cases, the weight and size of biological reactor shielding are decided in terms of hard secondary γ radiation originating in the reactor vessel and in the first shielding layers, as a result of neutron capture. The quest for methods of reducing this γ-ray flux is therefore an extremely timely and urgent problem.

The most intense secondary γ radiation arises in response to radiative capture of thermal neutrons and of comparatively low-energy neutrons, formed as a result of slowing down in the lighter shielding materials. Absorption of these neutrons in a boron-containing layer reduces the amount of neutron capture in structural materials, particularly in steel which emits gammas at high energies [1, 2]. When neutrons are captured in boron, soft gammas of low penetrating power and $\sim$0.5 Mev energy are generated, and shielding problems are much easier to handle.

The present communication deals with an investigation of the effect introduced by a layer of boron carbide sandwiched between steel and plexiglas to simulate water, upon the rate of production of gamma photons in steel. The geometry of the experiment is indicated in Fig. 1. Two different grades of steel were investigated: St-3 and 1Kh18N9T stainless. A prism of transverse dimensions 710 × 710 mm was made from the steel-plexiglas sandwich.
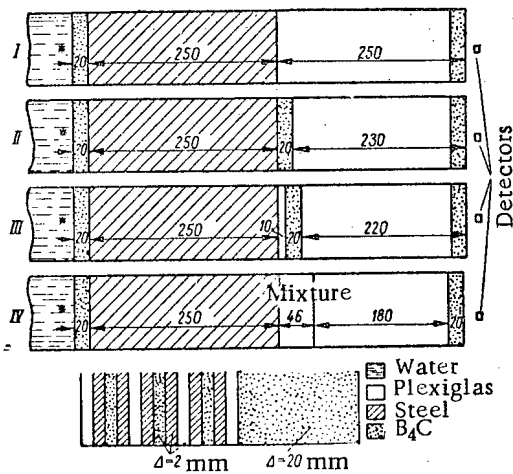
A Po-α-Be source yielding $2 \cdot 10^7$ neutrons/sec was placed in a water shielding arrangement in front of the steel prism. Channels with plugs to hold indicators were made in the steel—plexiglas prism. Boron-containing filters for absorption of thermal and epithermal neutrons emerging from the water (or plexiglas) and impinging on the steel were inserted between the steel and plexiglas. Filters of three distinct types were employed (see variants II, III, IV in Fig. 1).
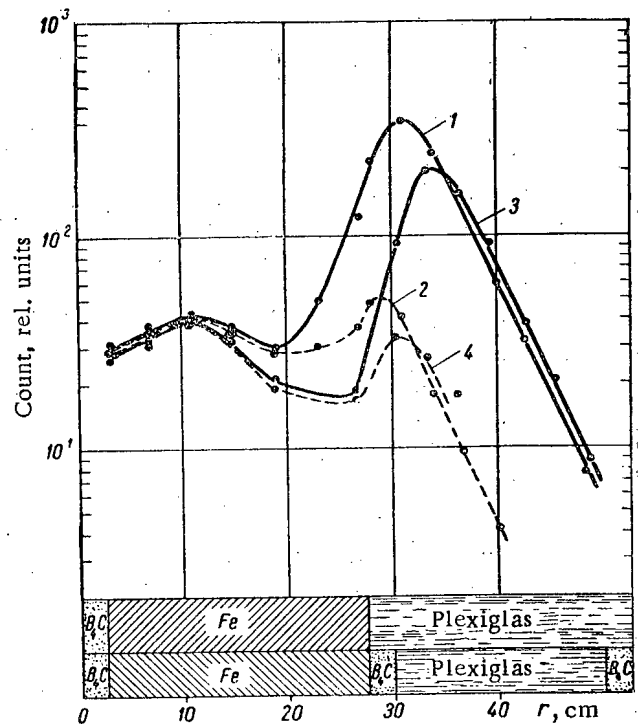
Fig. 2. Spatial distribution of neutrons in the St-3 plus plexiglas prism: 1) Measurements by indium (B_4C layer absent); 2) measurements by indium in cadmium (B_4C layer absent); 3) measurements by indium (B_4C layer 20 mm thick and 1.1 g/cm³ density sandwiched in between steel and plexiglas); 4) measurements, indium in cadmium (B_4C layer 20 mm thick, density 1.1 g/cm³, sandwiched in between steel and plexiglas).

Fig. 1. Geometry of the experiment.
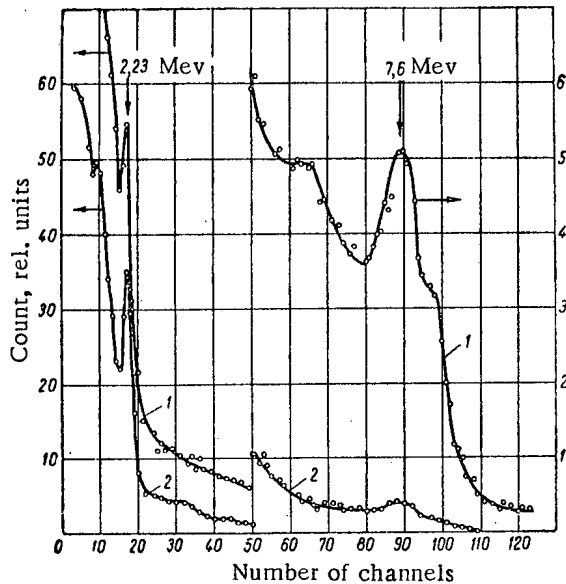
Fig. 3. Spectrum of γ quanta formed in the St-3 prism: 1) No B_4C layer present; 2) B_4C layer 20 mm thick, density 1.1 g/cm^3, sandwiched in between steel and plexiglas.

Fig. 4. Gamma spectrum formed in the prism of 1Kh18N9T stainless steel: 1) No B_4C layer present; 2, 4) B_4C layer sandwiched between steel and plexiglas (variant II in Fig. 1) or layer composed of mixture of plexiglas, St-3 steel, and B_4C (variant IV in Fig. 1); 3) B_4C layer sandwiched between steel and plexiglas (variant III in Fig. 1).

The spatial distributions of thermal and resonance neutrons were measured, as well as the spectra of gammas formed in the steel and plexiglas in response to neutron capture. The neutron distributions were determined by means of round indium foils 20 mm in diameter, contained within cadmium cases (or without the latter). The spectrum of the gamma quanta was measured with a single crystal NaI (Tl) scintillation γ spectrometer 40 mm in height and 40 mm in diameter. An 11% resolution was obtained for the Zn^{65} line. A 128-channel pulse-height analyzer with ferrite-core memory was used for analysis of the pulses. Positioning of the scintillation crystal during the measurements is indicated in Fig. 1.

Figure 2 shows the spatial distribution of neutrons measured in the St-3 plus plexiglas prism, both with and without a B_4C layer sandwiched in. Figures 3 and 4 give the measured gamma spectra reported herein (here also, with a B_4C layer present, and in its absence).

The spectrum of capture γ radiation shown in Fig. 3 contains γ lines at energies 2.2 and 7.6 Mev, corresponding to the absorption of neutrons by hydrogen and iron.

Insertion of a boron carbide layer between the steel and plexiglas has the effect of reducing γ-radiation intensity at 7.6 Mev by a factor of 13.4. The spectrum of gammas emitted from 1Kh18N9T stainless steel has another set of γ lines, in addition to those mentioned, forming as a result this time of capture of neutrons in

chromium and nickel, which contribute to the composition of this steel. The absorption of thermal and epithermal neutrons by the boron carbide layer, 20 mm thick, reduces the gamma flux at 7.6 Mev, emanating from 1Kh18N9T stainless steel by 7.8-fold.

The reduction in the yield of capture γ radiation from St-3 steel when a boron carbide layer is sandwiched between the steel and plexiglas was computed theoretically. The measured meutron distributions (cf. Fig. 2) was used in the calculations. The spectrum of neutrons thermalized in steel, used in this calculation, was determined in the age approximation for a semiinfinite steel slug with an absolutely "black" medium at the boundary. Corrections were introduced for self-shielding on the part of the indicators at the 1.44 ev resonance. The computed decrease in intensity of yield of secondary gammas in steel was 9.5, which is in excellent agreement with the results of the direct measurements of γ spectra.

The authors would like to express their heartfelt acknowledgment to N. A. Alishin, V. S. Borisov, G. V. Rykov, and E. V. Shestopalov for their kind assistance in the technical work.

LITERATURE CITED

1. Reactor Physics Constants. ANL-5800 (1958).
2. T. Rockwell, Reactor Shielding Design Manual (Van Nostrand, New York, 1956).

43

CRITICAL HEAT FLOWS IN THE FORCED FLOW OF LIQUIDS IN CHANNELS

A. A. Ivashkevich

In the design of nuclear reactors in which heat removal is effected by means of a boiling fluid, the value of the critical heat flow q_{cr} at which nucleate boiling will be replaced by film boiling must be known. The purpose of the present note is to generalize on experimental data obtained in different investigations, and to derive an equation for determining q_{cr}.

Reference [1] provides a system of criteria for characterizing the boiling process of a liquid under conditions of natural convection. After transformation and discarding of secondary criteria, this system takes the form:

$$\frac{u^2 \gamma''}{g d_0 (\gamma' - \gamma'')} \; ; \; \frac{w d_0}{v'} \; ; \; \frac{\gamma'}{\gamma''} \; ; \; \frac{i' - i_c}{r} \; , \qquad (1)$$

where $\underline{w}$ and $\underline{u}$ are the velocities of the liquid and vapor; $\underline{g}$ is the acceleration due to gravity; v' and $\underline{r}$ are the kinematical viscosity and heat of vaporization of the liquid; γ' and γ'' are specific weights of the liquid and vapor; i' and i_c are the enthalpy of the liquid at t_{sat} (temperature of saturation) and the enthalpy in the center of the heat flow. As the determining criterion, we may take the quantity

$$d_0 = \sqrt{\frac{\sigma}{\gamma' - \gamma''}} \, ,$$

proportional to the collapse diameter of the bubble; σ is the surface tension of the liquid. The system of criteria derived in [2] may also be used to derive the system in [1].

In the boiling of a liquid in channels with forced flow, system (1) must satisfy the criteria characterizing the channel geometry. By expressing $u = q_{cr}/r\gamma''$ [2] and substituting the expression for d_0 into system (1), we get

$$\left. \begin{aligned} K_{cr} &= \frac{q_{cr}}{r^* \sqrt{g \gamma''} \sqrt[4]{\sigma (\gamma' - \gamma'')}} \; ; \\ Re_1 &= \frac{w \sqrt{\sigma}}{v' \sqrt{\gamma' - \gamma''}} \; ; \quad K_2 = \frac{i - i_c}{r} \; ; \\ K_3 &= \frac{l_1 \sqrt{\gamma' - \gamma''}}{\sqrt{\sigma}} \; ; \quad K_4 = \frac{l_2}{d_h} \; ; \\ K_5 &= \frac{d_h \sqrt{\gamma' - \gamma''}}{\sqrt{\sigma}} \; , \end{aligned} \right\} \qquad (2)$$

where l_1 is the distance from the beginning of the heated interval to the cross section in question; l_2 is the distance from the channel cross section at which x=0 (if x >

> 0 at the channel entrance, l_2 is measured from the beginning of the heated interval) to the cross section in question; $\underline{x}$ is the vapor content of the flow; d_h is the hydraulic diameter of the channel.

On the basis of treatment of the experimental data obtained from references [3-14], an equation was derived for q_{cr} in the case of forced flow of liquid in channels:

$$K_{cr} = 1.9 \cdot 10^{-5} Re \{1 + 1.8 \cdot 10^{-6} [K_3 (1 + K_2)^{-2} + K_4] Re\}^{-1}, \qquad (3)$$

where

$$Re = \frac{w \sqrt{\sigma}}{v' \sqrt{\gamma' - \gamma''}} \quad \text{at} \quad \frac{d_h \sqrt{\gamma' - \gamma''}}{2 \sqrt{\sigma}} \geqslant 1;$$

$$Re = \frac{w d_h}{2 v'} \quad \text{at} \quad \frac{d_h \sqrt{\gamma' - \gamma''}}{2 \sqrt{\sigma}} \leqslant 1;$$

$$r^* = r \left(1 + A \cdot \frac{i' - i_c}{r} \right) \quad \text{for} \quad t_{liquid} < t_{sat};$$

$$A = 1 + 0.065 \left(\frac{\gamma'}{\gamma''} \right)^{0.8}; \quad r^* = r (1 - x) \quad \text{for} \quad x \geqslant 0;$$

t_{liquid} is the temperature of the center of the liquid flow.

Also confirmed is Eq.(3) by data obtained in experiments with ethyl alcohol, Dowtherm A, liquid carbon dioxide, nitrogen, and hydrogen; q_{cr} values obtained from Eq. (3) refer to the cross section for which the determining criteria are taken. The physical parameters of the liquid and vapor used in Eq. (3) are determined at t_{sat}.

Equation (3) is written in the general form both for surface boiling, when the temperature of the center of the liquid flow $t_{liquid} < t_{sat}$, and for boiling of the vapor-liquid mixture, when the vapor content of the flow x > 0; for particular cases, it may be simplified. For example, for $t_{liquid} < t_{sat}$, we naturally have $K_4 = 0$, and for x ≥ 0, $K_2 = 0$. From the experiments described in references [3-14], we find that the stabilization of the velocity profile and vapor content sets in at $K_3 = 50$ and $K_4 = 125$, so that, for $K_3 > 50$ or $K_4 > 125$, the values $K_3 = 50$ or $K_4 = 125$ must be substituted in Eq. (3).

Figures 1-3 represent experimental data from several investigations [3-14] with a criterial treatment of the

44
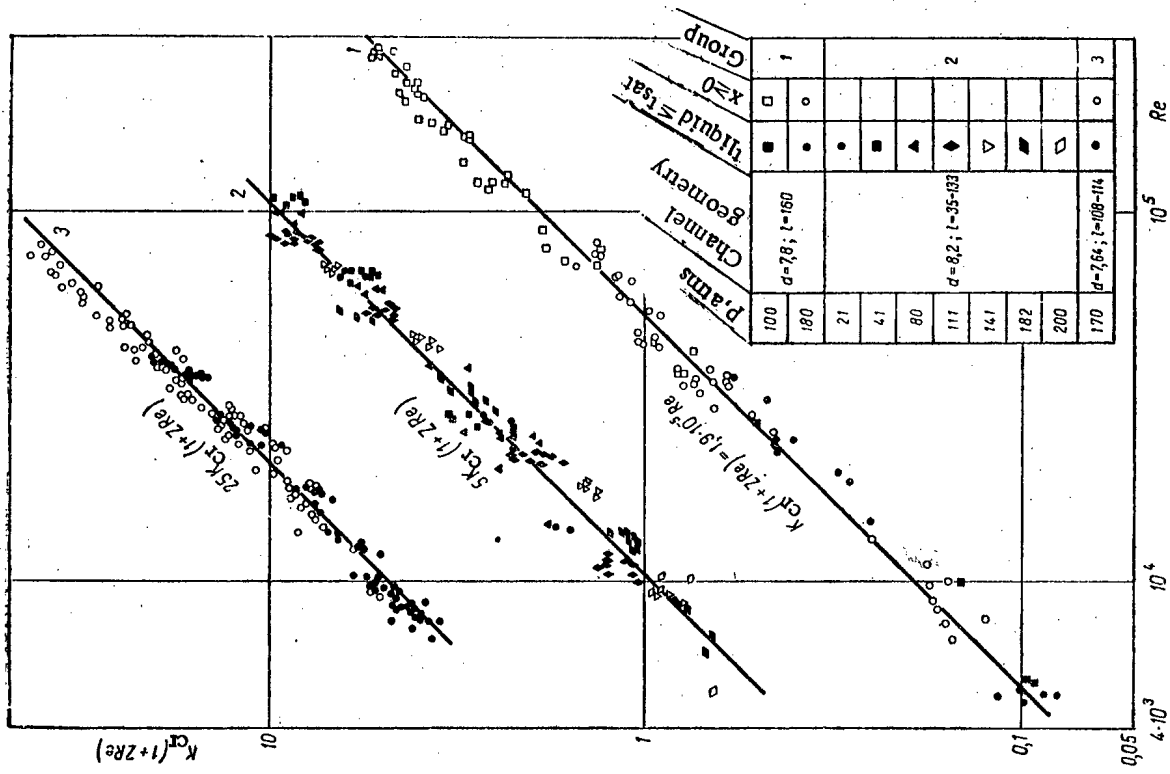
Fig. 2. Comparison of experimental data with Eq. (3): points of groups 1, 2, and 3 are taken from references [6, 7, 5], resp.
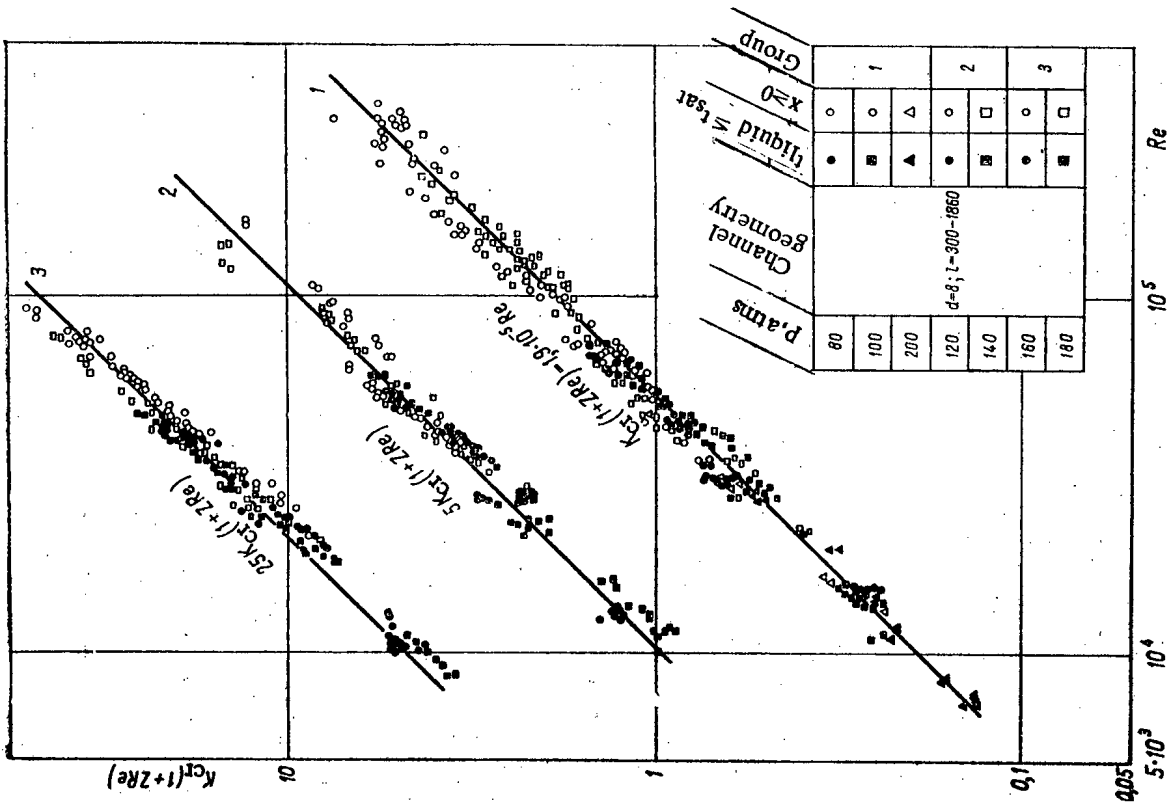
Fig. 1. Comparison of experimental data in [4] and Eq. (3).

45

data in the form of $K_{cr}(1+Z\,Re)$ as a function of the function of Re, where $Z = 1.8 \cdot 10^{-6}\,[K_3(1+K_2)^{-2}+K_4]$. For convenience, the experimental points are broken up into groups, with the ordinate scale expanded 5 and 25 times. Straight lines are drawn on the basis of Eq. (3). Points obtained in experiments where water is boiled with a nucleus heated to below boiling point are designated as $t_{liquid} < t_{sat}$, and points obtained when boiling a vapor-water mixture are designated as $x > 0$; $\underline{d}$ is the channel diameter; δ is the slit width; l is the heated channel length.

As is clear from Figs. 1-3, the data from different investigations, in criterial treatment, show agreement, since the initial data in [3] and in [11, 12], [4], and [5, 6] coincide; this is explained by the fact that com-

parison is usually effected while ignoring channel length. The spread of experimental points relative to the straight lines drawn from Eq. (3) is nonsystematic, and is less than ± 25-30% for the majority of points. This spread may be explained by the limited accuracy of the experiments and the simplifications assumed: the flow velocity $\underline{w}$ was determined as the rate of flow divided by the channel area and by the specific weight, for average temperature or vapor content due to mixing; i_c is determined as the average value due to mixing.

Equation (3) has been checked by the experimental data reported in 12 investigations carried out with boiling of water with the center heated to below the boiling point, and with a vapor-water mixture in channels of round, rectangular and annular cross sections over a broad

Point	P atms	Channel geometry	$t_{liquid} \leq t_{sat}$	$x \geq 0$	Group
1	1	d=20; l=60		o	
		d=30; l=80		⊡	
	182			◊	1
2	200	d=30; l=201		△	
	209			▽	
3	204-220	d=29; l=300	■	□	
4	2-6	δ=6,6; l=292	▲		
5	1-11	d=4,77×12,6; l=76	▼		
	35		◆		
6	70	d=6,35; l=635	■		2
	140		●		
	42			◊	
7	70	d=7,8; l=590		□	
	140			o	
8	1	δ=2,5-5,6; l=55	●		
		δ=0,5-2,5; l=55	■		3
	2-22	δ=2; l=55	▲		
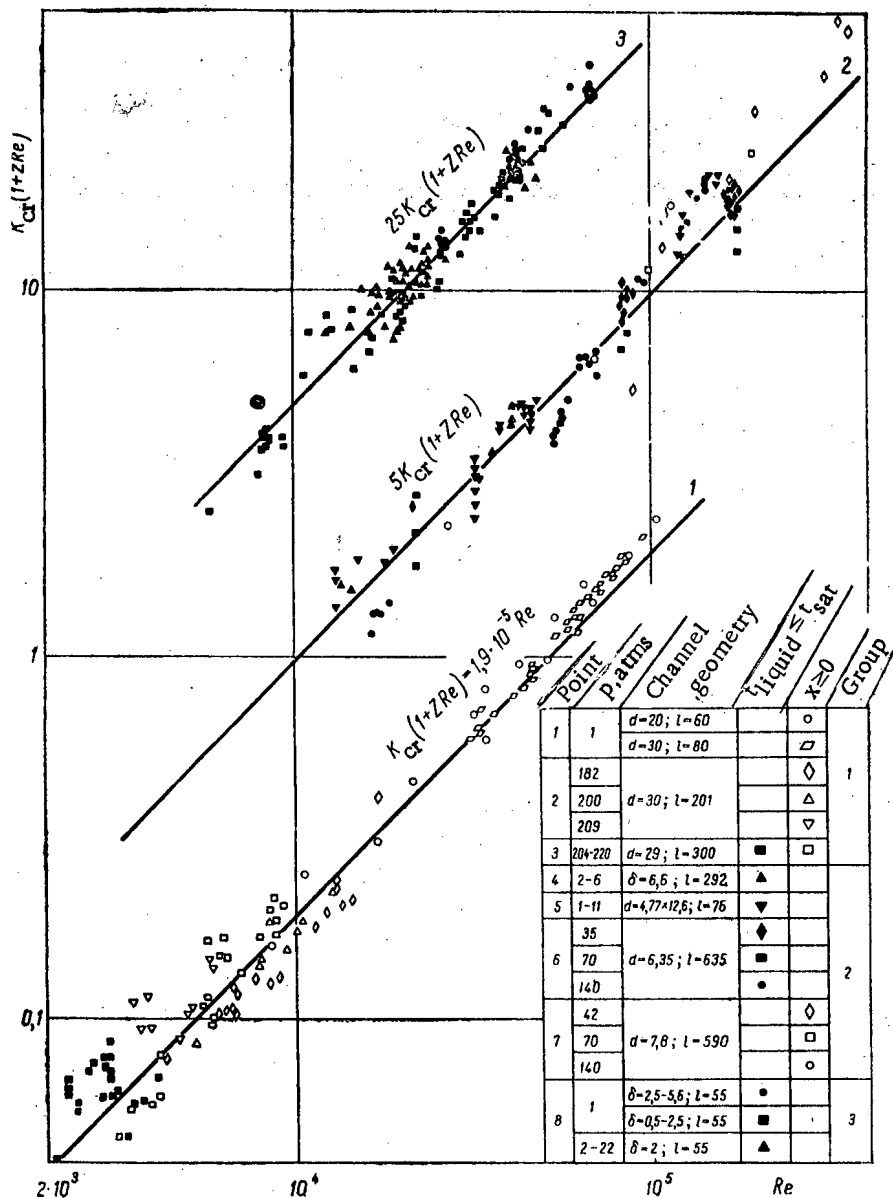
Fig. 3. Comparison of experimental data with Eq. (3), points 1-8 are taken from references [10, 8, 9, 11, 12, 13, 14, 3], resp.

46

range of parameter values: $p = 1\text{-}220$ atm; $w = 0.3\text{-}24$ m/sec; $t_{sat} - t_{liquid} = 0\text{-}160°C$; $x = 0\text{-}0.7$; $d_h = 1\text{-}30$ mm; $l = 35\text{-}1800$ mm, i.e., in the following range of variation of criteria: $Re = 2\cdot10^3\text{-}4\cdot10^5$; $K_2 = 0\text{-}0.8$; $K_3 = 20\text{-}2000$; $K_4 = 1\text{-}220$; $K_5 = 0.4\text{-}48$.

Equation (3) is recommended for determining q_{cr} in forced flow of a liquid in channels with the center heated to below the boiling point, and in the case of a vapor-water mixture over the indicated range of parameter variation.

LITERATURE CITED

1. G. N. Kruzhilin, Izvest. Akad. Nauk SSSR Ser. Tekh., 7, 967 (1948); 5, 701 (1949).
2. S. S. Kutateladze and M. A. Styrikovich, Hydraulics of Gas and Liquid Systems [in Russian] (Gosénergoizdat, Moscow, 1958).
3. V. S. Chirkin and V. P. Yurkin, Zhur. Tekh. Fiz. 26, 1942 (1956).
4. V. I. Subbotin et al., Symposium Studies of Heat Rejection to Steam and Water Boiling in Tubes at High Pressures [in Russian] (Atomizdat, Moscow, 1958) pp. 95, 120.
5. V. E. Doroshchuk and F. P. Frid, Symposium Studies of Heat Rejection to Steam and Water Boiling in Tubes at High Pressures [in Russian] (Atomizdat, Moscow, 1958) p. 71.
6. Z. L. Miropol'skii and M. E. Shitsman, Symposium Studies of Heat Rejection to Steam and Water Boiling in Tubes at High Pressures [in Russian] (Atomizdat, Moscow, 1958) p. 24.
7. I. T. Alad'ev, L. D. Dodonov, and V. S. Udalov, Atomnaya Énerg. 6, 74 (1959).[*]
8. M. A. Styrikovich, Symposium Fluid Dynamics and Heat Transfer in Boiling in High-Pressure Boilers [in Russian] (Akademizdat, Moscow, 1955)
9. M. A. Styrikovich, M. E. Shitsman, and Z. L. Miropol'skii, Teploénergetika, 12, 32 (1955).
10. M. A. Styrikovich, Symposium Generation of Steam at Superhigh Parameters [in Russian] (Gosénergoizdat, Moscow, 1950).
11. W. McAdams, W. Kennel, C. Minden, R. Carl, P. Picornell, and J. Dew, Industr. and Engng. Chem. 41, 1945 (1949).
12. F. Gunther, Trans. ASME 73, 115 (1951).
13. H. Buchberg, F. Romie, R. Lipcis, and M. Greenfield, Heat Transfer and Fluid Mechanics Institute (Stanford, California, June, 1951).
14. S. Mak-Lain, Lectures on Reactor Design Techniques, [in Russian] (Sudpromgiz, Moscow, 1957).

---

[*] Original Russian pagination. See C. B. translation.

INVESTIGATION OF HEAT TRANSFER IN THE TURBULENT FLOW OF LIQUID METALS IN TUBES

M. Kh. Ibragimov, V. I. Subbotin, and P. A. Ushakov

Experiments were carried out on two different pieces of apparatus. On one setup mercury was used, on the other lead and a eutectic lead—bismuth alloy (43.5% Pb + 56.5% Bi).

Experiments with Mercury. Before being put into the apparatus, P-3 type mercury (99.9% pure) was passed through a chamois filter. The experimental apparatus was a "tube-in-tube" type heat exchanger made from 1Kh18N9T steel. The mercury flowed inside a tube with diameter of 17 $\times$ 12.5 mm. The heat given off in the pump and loop was carried off from the mercury by water flowing in an annular space 4.5 mm wide. Heat exchange over a length of 760 mm between the mercury and water was realized on the counterflow principle, with the mercury moving from the bottom upward. Before entry into the working part of the tube, allowance was made for a hydrodynamic stabilization interval, equal to 40 diameters.

To reduce heat losses over the parts of the tube prior to the heat exchanger and after it, compensation heaters were mounted on those parts. The temperature of the heat-exchange surface between the mercury and water at the inlet and outlet were measured by thermocouples. The power of the heat exchanger was determined from the mass flow rate and cooling of the mercury and was controlled according to the mass flow rate and heating of the water. The arithmetic mean temperature, calculated from the readings of thermocouples placed at the inlet and outlet of the heat exchanger, was assumed as the mean temperature of the mercury. The mean temperature of the heat-exchange surface was determined by planimetry of the temperature profile over the length of the heat exchanger, taking into account corrections for depth to which the thermocouples were built in.

Experiments with Lead and Lead—Bismuth Alloy. The exposed liquid metal surfaces were protected against oxidation by a cushion of inert gas (argon). Before the experiment, the liquid metal was purified of oxides by hydrogen regeneration of the latter in the feed tank of the apparatus. Chemical analysis showed that the amount of oxygen in the liquid metal remained practically invariant throughout the experiments and was about $1 \cdot 10^{-3}\%$ by weight.

The test part (tube with diameter of 12 $\times$ 9 mm, made from 1Kh18N9T steel) was set up vertically. The inner surface of the tube was reamed out. For measuring the temperature of the tube wall, a resistance thermometer made from 0.07 mm platinum wire, 1800 mm long and imbedded 118 mm, was used. The distance from the point where heating began to the resistance thermometer was 33 diameters.

The temperature of the liquid metal at the inlet to the experimental interval was also measured by a platinum resistance thermometer, the heating of the heat carrier by chromel-alumel thermocouples. The mass flow of the liquid metal was determined from the readings of a magnetic flowmeter, which was calibrated preliminarily by the volumetric method. The heat flow was created by an electric heater element. The length of the heat exchange interval was 520 mm. Heat losses were compensated for by an external heater interlocked with a thermometer.

Experimental Results. The mean heat-transfer coefficients for mercury were determined over a heat-exchange interval equal to 60 diameters. Here the preliminary hydrodynamic stabilization interval was equal to 40 diameters. The data obtained in the experiments with lead and lead—bismuth alloy refer to an interval of the tube removed from the heat source at a distance of 33 diameters, from the tube inlet at a distance of 41 diameters. On the basis of [1-3] it may be assumed that the results obtained characterize the heat exchange in the stabilized zone. The limits of variation of some of the quantities during the course of the tests are shown in the accompanying table.

In processing the experimental data, the physical parameters of the liquid metals were taken from data in [4], the thermal conductivity of the 1Kh18N9T steel from data in [5]. The results of the experiments, processed after similarity criteria, are illustrated in the figure. In the same graph are plotted curves calculated from an empirical formula given in [1]:

$$\text{Nu} = 4.5 + 0.014 \, \text{Pe}^{0.8} \qquad (1)$$

and according to Lyon's semi-empirical formula [6]

$$\text{Nu} = 7 + 0.025 \, \text{Pe}^{0.8} . \qquad (2)$$

48

Variations in the quantities during the tests.

Parameters	Mercury	Lead	Eutectic lead–bismuth alloy
Temperature, °C	24—48	400—420	250—340
Heating, °C	1—13	1,5—3	1—22
Temperature drop, °C	3—14	2—3,2	1,4—5,3
Liquid metal flow velocity. m/sec	0,4—4	1,5—3,5	0,2—5,6
Heat-transfer rate, kcal/$m^2 \cdot$ hr	(20—100)$\cdot 10^3$	42$\cdot 10^3$	(11—52)$\cdot 10^3$
Heat-transfer coefficient, kcal/$m^2 \cdot$ hr $\cdot$ °C	(4—15)$\cdot 10^3$	(13—23)$\cdot 10^3$	(6,6—24)$\cdot 10^3$
Prandtl number, Pr$\cdot 10^3$	22—27	20	20—27
Reynolds number, Re$\cdot 10^{-3}$	40—400	65—160	8—290
Peclet number, Pe$\cdot 10^{-3}$	1—10	1,3—3,2	0,2—5,8
Nusselt number, Nu	7—27	8,6—15	6—19
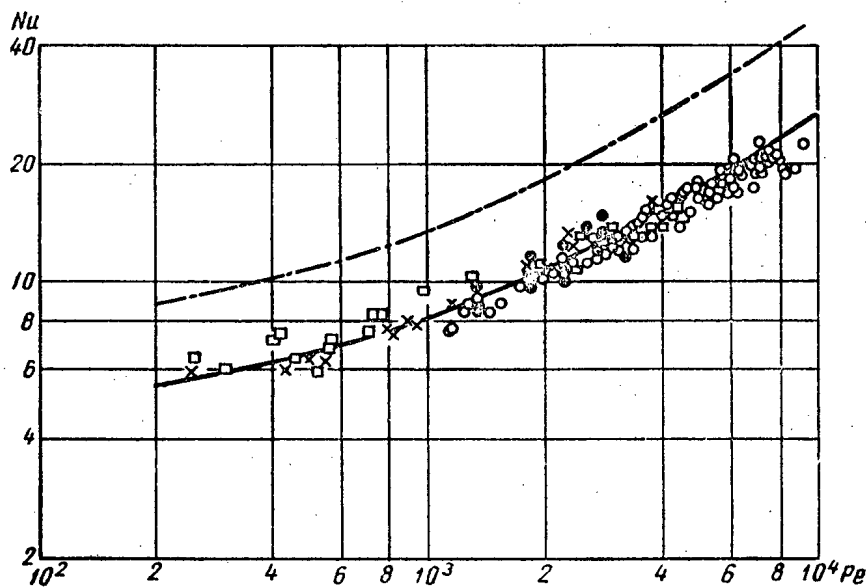
Results obtained after similarity criteria: O) Mercury; ●) lead; □) eutectic lead-bismuth alloy; X) eutectic lead-bismuth alloy, with addition of 0.1% Mg ; ——) according to[1] Nu = 4.5 + 0.014 Pe$^{0.8}$; —·——) according to Lyon's formula Nu = 7 + 0.025 Pe$^{0.8}$.

The experimental data that we obtained for heavy liquid metals are satisfactorily approximated by Eq. (1). An addition of 0.1% magnesium to the eutectic lead — bismuth alloy led to no significant change in the heat-transfer coefficient. At the same time, the experimental points are distributed far below the values calculated according to Eq. (2), with which the data obtained in the absence of a thermal contact resistance are found to agree [3, 7, 8].

The experiments whose results appear in the present paper were conducted under the usual industrial-experimental conditions. During the course of the tests the liquid metals were not purified of oxides, and the heat-exchange surface was not wetted. It may be assumed that under these conditions there existed a thermal contact resistance, which led to the difference between the experimental data and Eq. (2). Our later experiments, in which the temperature field in the flow of heavy liquid metal was determined, called for this assumption. The heat-exchange coefficients found by extrapolation of the temperature profile to the wall agreed with the values calculated according to Eq. (2).

Taking part in the experiments and setting up of the experimental equipment were Kh. A. Khachaturov, A. A. Sholokhov, V. I. Petrovichev, E. V. Nomfilov, and O. V. Remizov.

49

LITERATURE CITED

1. M. A. Mikheev, V. A. Baum, K. D. Voskresenskii, and O. S. Fedynskii, Collection: Reactor Design and Theory of Reactors [in Russian](Izd. AN SSSR, 1955) p. 139.
2. V. M. Borishanskii and S. S. Kutateladze, Zhur. Tekh. Fiz. 28, 836 (1958).
3. P. L. Kirillov, V. I. Subbotin, M. Ya. Suvorov, and M. F. Troyanov, Atomnaya Energiya 6, 382 (1959).*
4. S. S. Kutateladze, V. M. Borishanskii, I. I. Novikov, and O. S. Fedynskii, Liquid-Metal Heat Transfer Media [in Russian](Atomizdat, Moscow, 1958).
5. B. E. Neimark, Teploénergetika, 3, 3 (1955).
6. R. Lyon, Chem. Engng. Progr. 47, 25 (1951).
7. S. Isakoff and T. Drew, General Discussion on Heat Transfer, London Conference (1951) p. 405.
8. H. Brown, B. Amstead, and B. Short, Trans. ASME 79, 279 (1957).

*Original Russian pagination. See C. B. translation.

DETERMINATION OF MELTING POINTS OF BINARY MIXTURES OF URANIUM OXIDES WITH OTHER OXIDES IN AIR

S. G. Tresvyatskii and V. I. Kushakovskii

In connection with the increased interest in uranium oxides and their reaction with other oxides, the authors determined the melting points of a series of mixtures in air.

Starting materials and preparations of mixtures. The following were used as starting materials: . . . .

UO_2, BeO, MgO, $CaCO_3$, $BaCO_3$, Al_2O_3, La_2O_3, SiO_2, TiO_2, ZrO_2, ThO_2, CeO_2, H_3PO_4, V_2O_5, Ta_2O_5, Bi_2O_3, Cr_2O_3, $(NH_4)_2MoO_4$, H_2WO_4, Fe_2O_3, $MnCO_3$.
Most of the compounds used were classified, according to their degree of purity, as pure, analytically pure, and chemically pure. The degree of purity of Ta_2O_5, prepared by the oxidation of tantalum, and of V_2O_5 was unknown. The mixtures were prepared by mixing the samples thoroughly in a mortar for one hour. The compositions of the mixtures corresponded to equimolar ratios of the oxides used. Additional compositions with molar ratios of 1 : 2 and 2 : 1 were prepared for mixtures of uranium dioxide and magnesium, calcium, strontium, and barium oxides.   To oxidize the uranium dioxide the mixtures were fired in air in porcelain crucibles at 800°C. Briquettes (25 mm diameter) were molded from the oxidized mixtures and fired at 800-900°C. The briquettes were ground after firing and the powders obtained again molded into briquettes, which were fired at 1000-1100°C. In the next processing cycle the firing temperature was raised to 1200-1300°C. At temperatures above 1000°C the briquettes were fired in platinum crucibles or on a platinum plate. The cycles of grinding, molding, and firing at 1300°C were repeated until the briquettes were strong and showed no signs of cracking or contracting after firing. The mixtures obtained after grinding of the briquettes thus obtained, were used for further investigation.

Determination of melting points of mixtures. The melting points of the mixtures were determined by the cone deformation method.* The upper section of the cone was heated in an electric arc, passing between carbon electrodes. The temperature was measured with a microoptical pyrometer. The accuracy of the melting point determination was ±30-50°C for samples melting with the formation of a drop, and ±50-100°C for samples sweating on the surface and forming drops with difficulty. The melting points of the mixtures and the nature of the melting are given in the table.

---

* With the exception of those mixtures which melted during the preliminary firing. (P.P. Budnikov and S.G. Tresvyatskii, Coll: Physicochemical Basis of Ceramics) [in Russian] (Promstroiizdat, Moscow, 1959) pp. 301-315).

Melting Points of Binary Mixtures of Uranium Oxides with Other Oxides in Air.

Composition, mol. %		U/Me ratio according to chemical analysis*	Melting point °C	Nature of melting
In charge				
UO_3	other oxides			
50	50 BeO	1/1,5	2200± 50	Melts with difficulty, almost no drop
67	33 MgO	1/0,56	1900± 50	Drop forms with difficulty
50	50 MgO	1/1,12	1750± 50	Melts with drop formation
33	67 MgO	1/1,53	1850± 30	The same
70	30 CaO	1/0,404	2000± 50	" "
50	50 CaO	1/1	2000± 50	" "
30	70 CaO	1/2,35	2200±100	No drop forms, sweats on surface
67	33 SrO	1/0,4	2000± 50	The same
50	50 SrO	1/0,93	2100± 50	" "
33	67 SrO	1/2,37	2200± 50	Melts with drop formation
67	33 BaO	1/0,54	1700± 30	The same
50	50 BaO	1/1,03	1700± 50	" "
33	67 BaO	1/1,9	1680± 50	Drop forms with greater difficulty than in previous composition
50	50 Al_2O_3	—	1940± 30	Melts with drop formation
50	50 La_2O_3	1/1,6	2350± 10	Drop forms with difficulty
50	50 SiO_2	1/1	1770± 30	Sweats on surface
50	50 TiO_2	—	1480± 30	Melts readily
50	50 ZrO_2	—	2600± 50	Melts with difficulty, almost no drop
50	50 ThO_2	—	Does not melt	—
50	50 CeO_2	—	2700± 150	Melts very little, sweats near electrodes
50	50 P_2O_5	—	1200±1350	Sample melts during preliminary firing
50	50 V_2O_5	—	<800	The same
50	50 MoO_3	—	900—1000	" "
50	50 WO_3	—	1100—1200	" "
50	50 Ta_2O_5	—	1850± 30	Melts readily
50	50 Bi_2O_3	—	1800± 50	Sweats slightly, evaporates considerably on heating
50	50 PbO_2	—	1850± 50	The same
50	50 SnO_2	—	—	Cone does not melt in arc, considerable evaporation observed
50	50 Cr_2O_3	—	2050± 100	Drop forms with difficulty
50	50 Fe_2O_3	—	1370± 30	Melts readily
50	50 MnO_2	—	1650± 30	" "
100	None	—	2700—2750±100	Melts with difficulty

*The change in chemical composition was practically insignificant in those cases when no analysis was carried out, with the exception of mixtures with bismuth, lead, and tin oxides.

THE DISTRIBUTION OF IRON IN MICROVOLUMES OF ZIRCONIUM ALLOYS

P. L. Gruzin, G. G. Ryabova and G. B. Fedorov

The principal factor limiting the use of zirconium in nuclear power reactors is its loss of strength and corrosion resistance at high temperatures. It is known that the presence of hundredths or thousandths of one percent of admixtures of nitrogen, carbon, aluminum, titanium and other elements in zirconium [1, 2] markedly reduces its resistance to corrosion in hot water or steam. The harmful effect of these admixtures can be neutralized by the presence of tin , iron, nickel, chromium and certain other [1, 3] admixtures of alloying elements which have a favorable action. With a specific combination of admixtures, zirconium iodide smelted in an arc furnace can, therefore, possess a sufficient corrosion resistance in water and steam at elevated temperatures and pressures. The mechanism of the influence of admixtures and alloying elements on the corrosion resistance of zirconium has been insufficiently investigated; the investigation of the distribution of admixtures (for example, carbon [4]) and alloying elements (for example, tin [5]) in zirconium by the autoradiograph method can be of real value for its determination.

Iron is one of the elements which improve the corrosion resistance of zirconium. Alloys of zirconium and tin obtain a maximum corrosion resistance only with additions of iron, nickel and chromium or one of these elements [3]. In some cases small admixtures of iron improve the corrosion resistance of zirconium iodide [2, 6], particularly in superheated steam [2, 3]. Iron has a negligible effect on the strength properties of zirconium.

The distribution of iron in an alloy of zirconium with 0.15 wt.% of iron and in an alloy of the Zircalloy type (also with a zirconium iodide basis) of the following composition (in wt.%): tin 1.1, iron 0.1, chromium 0.1, and nickel 0.05, were investigated by the contact autoradiograph method. The radioactive isotope of iron Fe^{59} was added to the alloys in the form of a metallic powder when they were smelted in an arc furnace in an argon atmosphere. An NIKFI film of the MR type was used to obtain the autoradiograms. The Fe^{59} isotope has a γ radiation with an energy of 1.295 Mev and β radiation with a maximum energy of 0.46 Mev.

To ensure the necessary resolving power, the x-ray pictures were obtained from samples with a thickness of the order of several dozen microns. The intensity of the radiation of the section was 5-10 thousand counts/min·cm^2.The exposure was selected by experiment.

The investigation showed that the distribution of iron in a cast zirconium alloy and after various types of thermal-mechanical treatment remains uneven. In a cast alloy (Fig. 1) the major part of the iron is concentrated at the edges of the blocks formed as a result of the $\beta \rightarrow \alpha$ phase conversion, while part remains in solid solution, unable to separate out from the latter because of the rapid cooling of the fused system. The distribution of iron in cast Zircalloy-2 has a similar character.

Cold 5-10% deformation gives almost the same picture of the distribution of iron as in cast alloys. Annealing of cold-deformed alloys leads to displacement of iron from the solid solution to the boundaries of the α-phase. Hot forging of alloys in air at 850-750°C results in marked disintegration of the structure but the unevenness of the distribution of iron is retained. Thermal treatment of cast and hot-forged alloys was carried out in quartz tubes evacuated to $\sim 10^{-4}$ mm Hg.

In the case of hardening of alloys from different temperatures from the β-region the distribution of iron in both alloys was similar to the distribution in cast alloys. Such distribution is due to the fact that at high temperatures (in the β-region) iron remains in the solid solution [7]. Rapid cooling leads only to partial separation of iron at the boundaries formed as a result of $\beta \rightarrow \alpha$ conversion. Slow cooling of alloys in a furnace from temperatures of the β-region leads to more complete separation of iron from solid solution at the boundaries and sub-boundaries of the α-phase (Fig. 2a and b).

Figure 3 shows the microstructure and autoradiogram of zirconium-iron cast alloy (not hot-forged) annealed at 800°C, i.e.,the eutectoid temperature of zirconium-iron alloys [7]. During annealing, the iron separated out almost completely from the solution as the intermetallide $ZrFe_2$, located at the boundaries and within the grains of the α-phase of zirconium.

Annealing of zirconium-iron alloys in the α-region at 600°C (20 hours) and 500°C (40 hours) after chilling from 1200 and 900°C,respectively, showed that the unevenness of the iron distribution was retained.

Rapid cooling from temperature of the β-region retains part of the iron in the α-solid solution, the other

53

part is distributed at the sub-boundaries of the α-phase. Slow cooling from high temperatures and annealing in the α-region assists more complete separation of iron at the boundaries of the grains and blocks of the α-phase.

In Zircalloy-2, redistribution of iron takes place more slowly than in pure zirconium. This is probably due to the presence of chromium and nickel in the alloy, which — judging from preliminary data — are distributed similarly to iron. It can be assumed that the reason

×70   ×56
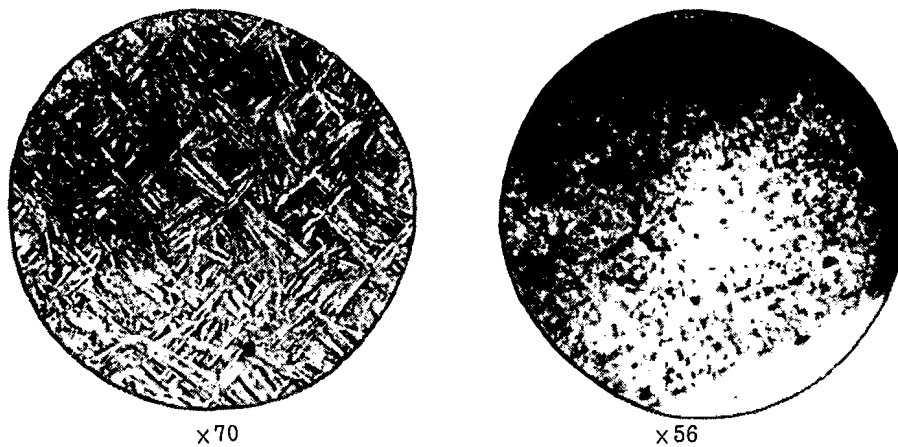
Fig. 1. Microstructure (left) and autoradiogram (right) of cast zirconium alloy with 0.15 wt.% Fe.

a

×70   ×63

b

×70   ×56
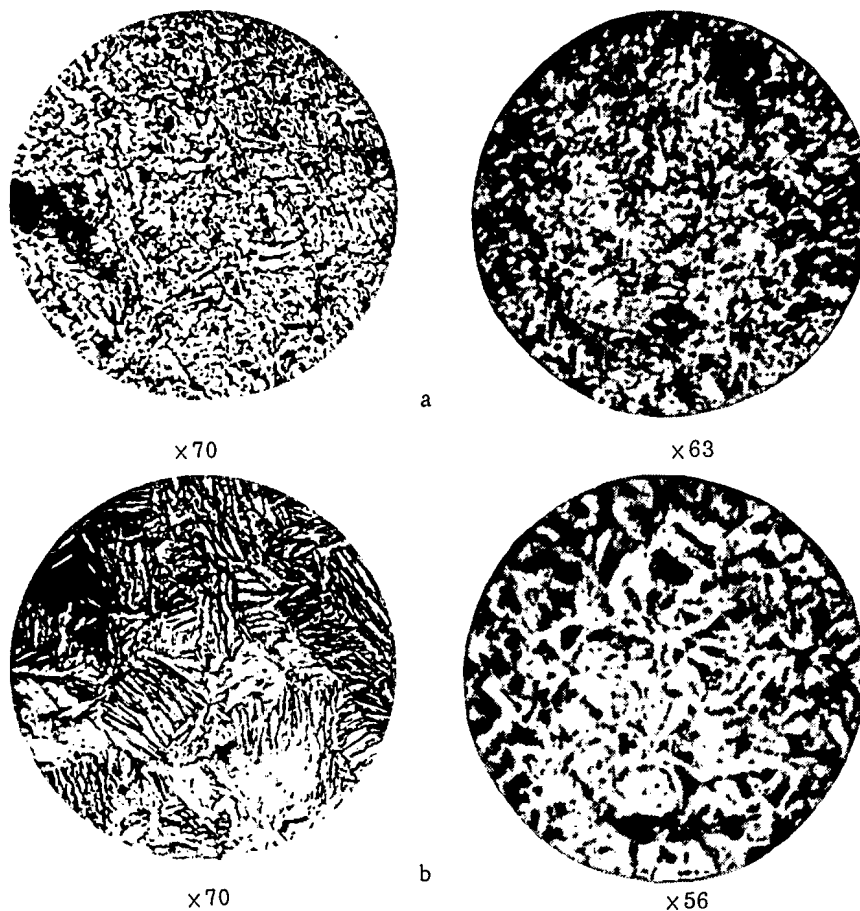
Fig. 2. Microstructure (left) and autoradiogram (right) of alloys after annealing in the β-region (1000°C) for 3 hours and slow cooling: a) Zirconium-iron alloy; b) alloy of the Zircalloy-2 type.

54

×70   ×63
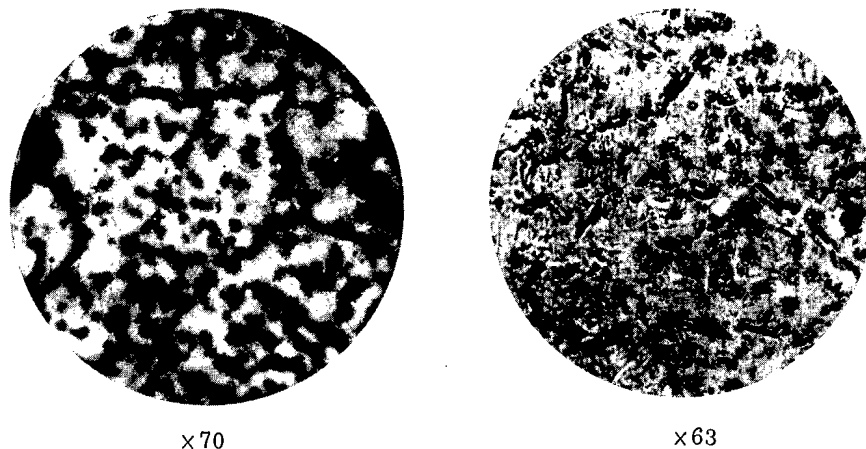
Fig. 3. Microstructure (left) and autoradiogram (right) of zirconium-
iron alloy after annealing at 800°C for 3 hours.

alloys of the Zircalloy group have a higher corrosion re-
sistance than zirconium-tin binary alloys is as follows:
tin, being distributed uniformly in zirconium, increases
the corrosion resistance of the solid solution, forming the
main alloy. Iron, chromium and nickel, which are con-
centrated at the boundaries of the grains and blocks,
evidently delay boundary corrosion.

LITERATURE CITED

1. B. Lustman and F. Kerze, The Metallurgy of Zirco-
nium (McGraw-Hill, London, 1955) p. 608.
2. Documents of the Atomic Energy Commission USA
[Russian translation] (IL, Moscow, 1956) p. 318.
3. D. Thomas, Reports to the International Conference
on the Peaceful Uses of Atomic Energy (Geneva,
1955) [Russian translation] (Leningrad, Gozkhimiz-
dat, 1958) Vol. 9, p. 497.
4. P. L. Gruzin, V. S. Emel'yanov, G. G. Ryabova, and
G. B. Fedorov, Proc. Second International Conference
on the Peaceful Uses of Atomic Energy (Geneva,
1958) "The preparation and use of isotopes," [in
Russian] (Moscow, Atomizdat, 1959) Vol. 6, p. 189.
5. Yu. F. Babikova, P. L. Gruzin, and G. G. Ryabova,
Investigation of the Distribution and Electrodiffusion
of Tin in Zirconium Alloys. Second Symposium of
the Work of the Department of Metallurgy and Metal-
lography of MIFI [in Russian] (Atomizdat, Moscow,
1960) (in press).
6. R. S. Ambartsumyan, A. A. Kiselev et al., Proc.
Second International Conference on the Peaceful
Uses of Atomic Energy (Geneva, 1958) "Nuclear
fuel and reactor materials," (Moscow, Atomizdat,
1959) Vol. 3, p. 486.
7. E. Hayes, A. Roberson, and W. O'Brien, Trans. Amer.
Soc. Metals 43, 888 (1951).

55

REACTIONS OF NITROGEN DISSOLVED IN WATER, UNDER THE ACTION OF IONIZING RADIATIONS

M. T. Dmitriev and S. Ya. Pshezhetskii

The kinetics and mechanism of the reaction of nitrogen with oxygen under the effect of electrons and γ radiation were investigated in [1, 2]. It was also of interest to investigate reactions of nitrogen with water and its radiolysis products inder the action of radiation. Comparison of these results would make it possible to obtain certain data essential for determining the reactivity of nitrogen under irradiation conditions. These processes are important for the operation of nuclear reactors in which water containing dissolved gases is used as a heat carrier or neutron moderator. This paper gives certain characteristic results.

Nitrogen dissolved in water is oxidized by ionizing radiations to nitrate and nitrite, and forms ammonia. Thus, after irradiation chemically active solutions are obtained. The formation of nitrate and nitrite was established [3, 4] when γ radiation acted on aqueous solutions of potassium nitrate and nitrite. It was shown [5] that at a pressure of 1 atm the radiation reaction is due mainly to the absorption of energy in the gaseous phase. In the present work Co^{60} γ radiation and fast electrons were used.

From the accelerator the electron beam with a mean energy of 0.2 Mev passed through aluminum foil of thickness 15μ and a 1.5 cm layer of air; it then fell on an aluminum membrane of thickness 10μ closely covering the vessel containing the solution. To eliminate reactions in the gaseous phase above the solution the membrane was brought into intimate contact with the surface of the water. The gas residue was removed by pressure from the outer side of the membrane. The absorbed energy of the electrons was determined in a calorimeter with distilled water by comparison with a dc heater. The sensitivity of the calorimeter was 2.10^{-2} deg/min· w.

Co^{60} with an activity of 1.4 and 20 kC was used as the γ-ray source. Irradiation was carried out in sealed glass or metal ampoules (of stainless steel). The gases were dissolved under pressure in the bidistillate.

During irradiation the ion concentration in the solutions was determined by the conductivity. After irradiation the content of nitrate, nitrite and ammonium ions was determined calorimetrically. The nitrate ions were determined by reaction with disulfophenolic acid and ammonia, the nitrite ions by reaction with α-napthylamine and sulfanilic acid. The ammonium ions were determined by reacting with potassium mercuric iodide in alkali, with the formation of ammonium mercuric iodide. The minimum amounts of acid or ammonia
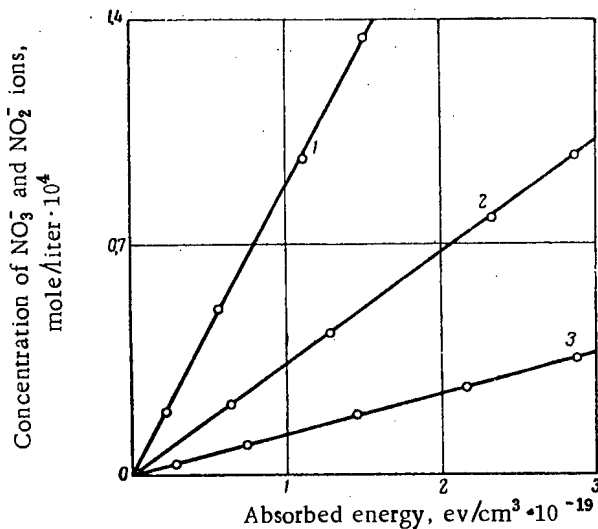

Fig. 1. Relation between the concentration of nitrate and nitrite ions and the absorbed γ-radiant energy. Air pressure (in atm) : 1) 100; 2) 20; 3) 1.
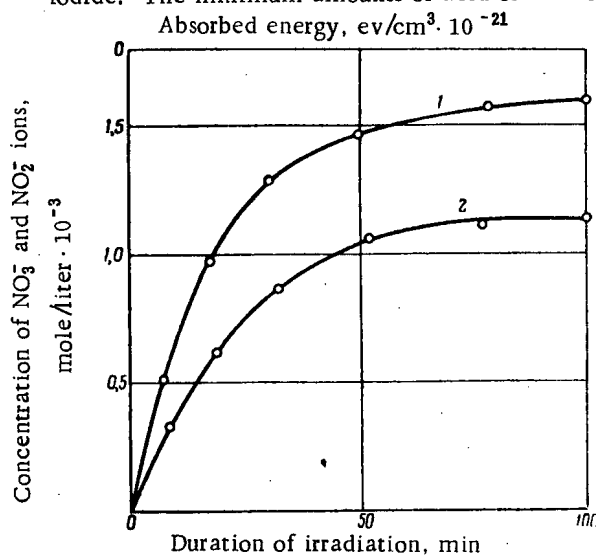
Fig. 2. Relation between the concentration of nitrate and nitrite ions and the duration of irradiation by electrons with an energy of 200 kev (gas pressure 1 atm): 1) Nitrogen; 2) air.

56

TABLE 1. Relation Between the Reaction Velocity and the Duration of Irradiation (air pressure above the solution 1 atm, radiation intensity $1.8 \cdot 10^{17}$ ev/cm^3 ·sec)

Duration of irradiation, hr	Concentration of nitrate and nitrite, 10^{-17} mole/cm^3	Reaction velocity, 10^{-14} mole/cm^3·sec	Velocity constant of the first order, 10^4 sec^{-1}
0,22	1,05	1,20	1,51
0,67	2,95	0,89	1,48
1,55	6,52	0,37	1,51
2,23	6,98	0,15	1,53
2,67	8,60	0,054	1,53
2,88	8,85	0,014	1,56

TABLE 2. Relation Between the Ratio of the Nitrate and Nitrite Concentrations and the Absorbed Energy

Absorbed energy, ev/cm^3	Ratio of the nitrate and nitrite concentrations			
	Nitrogen, atm			Air, 1 atm
	1	2	50	
10^{18}	3,3	2,7	1,5	0,7
10^{20}	1,8	1,5	0,9	0,4
10^{22}	0,5	0,4	0,3	0,1

TABLE 3. Relation Between the Yield of Ammonium Ions and the Total Nitrate and Nitrite Ions and the Absorbed Energy

Absorbed energy, ev/cm^3	Relative yield of ammonium ions		
	Nitrogen, atm		Air, 1 atm
	1	100	
10^{18}	1,6	1,2	1,3
10^{20}	1,1	0,9	0,8
10^{22}	0,9	0,8	0,3

TABLE 4. Relation Between the Relative Yield of Nitrite and Ammonia and the Nitrogen Pressure Above the Solution (absorbed energy $2.2 \cdot 10^{19}$ ev/cm^3)

Pressure, atm	$[NO_2^-]/[NO_3^-]$	$[NH_4^+]/[NO_2^-]+[NO_3^-]$
1	3,3	1,55
10	2,8	1,52
50	1,5	1,35
100	1,2	1,22
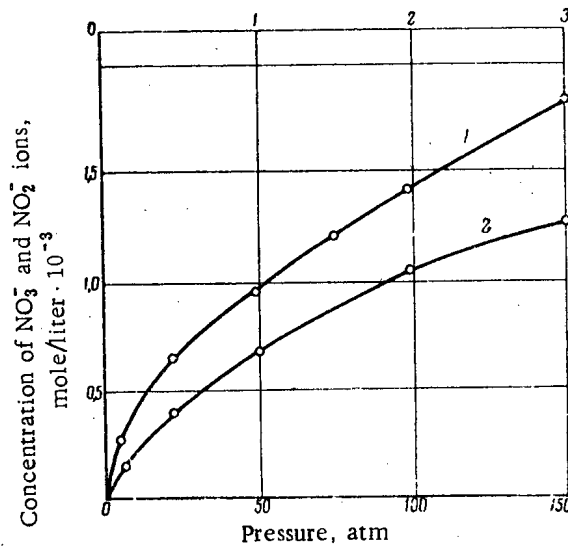
Fig. 3. Relation between the concentration of nitrate and nitrite formed by the action of γ radiation and the gas pressure; radiation intensity $1.79 \cdot 10^{14}$ ev/sec · cm^3 , exposure 50 hr (1- nitrogen; 2- air).

TABLE 5. Energy Yield of Reactions of Dissolved Nitrogen with Water

Pressure above the solution, atm	Gas composition, %	Nitrate yield, mole/100 ev	Nitrite yield, mole/100 ev	Ammonia yield mole/100 ev	Yield of combined nitrogen, atom/100 ev
1	100 N$_2$	0,016	0,054	0,108	0,18
1	80 N$_2$+20 O$_2$	0,032	0,021	0,085	0,14
1	50 N$_2$+50 O$_2$	0,028	0,008	0,052	0,09
10	80 N$_2$+20 O$_2$	0,068	0,057	0,205	0,33
50	100 N$_2$	0,138	0,216	0,472	0,83
100	100 N$_2$	0,238	0,283	0,730	1,25
150	80 N$_2$+20 O$_2$	0,296	0,171	0,615	1,08
150	100 N$_2$	0,267	0,342	0,760	1,37

57

which could be reliably determined by these methods was $\sim 10^{-3}$ mg.

The relation (Fig. 1) is shown between the amount of nitrate and nitrite formed at various gas pressures and the absorbed radiant energy. The amount of reaction products formed depends on the pressure above the solution. At low degrees of conversion it is proportional to the absorbed energy. The amount of combined nitrogen is proportional to the absorbed radiant energy up to 10^{19}-10^{20} ev/cm^3. At large amounts of absorbed energy no proportionality is observed. This is illustrated by data obtained during irradiation with fast electrons (Fig. 2). If gas is passed through the solution during the course of the experiment the reaction velocity remains constant, but the concentration of combined nitrogen increases proportionally to the amount of absorbed energy. The energy yield does not vary. The reaction obeys an equation of the first order with respect to nitrogen. From Table 1 it is seen that the value of the velocity constant does not change.

At a pressure of up to 1 atm the reaction velocity is directly proportional to the gas pressure above the solution. But at a pressure above 1 atm the proportionality between the reaction velocity and the pressure is disturbed, as may be seen from Fig. 3.

Table 2 gives the relation between the ratio of the concentrations of nitrate and nitrite ions and the absorbed energy. With an increase in the latter the proportion of nitrate increases.

Table 3 gives data on the relation between the ratio of ammonia yield/nitrate + nitrite yield and the absorbed energy. With an increase in the amount of absorbed energy the relative yield of ammonia decreases.

In addition to the amount of absorbed energy, other factors influence the yield of various products.

Table 4 gives data from which it follows that the relative yield of the reaction products varies with an increase in the pressure above the solution.

Table 5 gives certain values of the initial yields of the reaction products during conversion up to 10%.

Thus, under the effect of ionizing radiations nitrogen dissolved in water is combined in the form of nitrate, nitrite and ammonia. The relative yield of each of the products depends on the composition of the dissolved gas and the amount of absorbed energy. The energy yield is 0.09-0.18 atoms of combined nitrogen at a pressure of 1 atm and 1-1.4 atoms at 150 atm per 100 ev of absorbed radiant energy.

The probable mechanism of the process will be examined in the next paper.

LITERATURE CITED

1. S. Ya. Pshezhetskii and M. T. Dmitriev, Doklady Akad. Nauk SSSR 103, 647 (1955); Atomnaya Énerg. 3, 350 (1957).*

2. M. T. Dmitriev and S. Ya. Pshezhetskii, Proc. All-Union Conference on Radiation Chemistry [in Russian] (Izd. AN SSSR, Moscow, 1958) p. 26; Zhur. Fiz. Khim. 32, 2418 (1958); Zhur. Fiz. Khim. 33, 463 (1959); Symposium: The Action of Ionizing Radiations on Inorganic and Organic Systems [in Russian] (Izd. AN SSSR, Moscow, 1958) pp. 145 and 171.

3. M. A. Proskurnin, V. D. Orekhov, and E. V. Barelko, Session of the Academy of Sciences of the USSR on the Peaceful Uses of Atomic Energy (Meeting of the Chem. Sci. Section) [in Russian] (Izd. AN SSSR, Moscow, 1955) p. 41.

4. V. D. Orekhov, A. I. Chernova, and M. A. Proskurnin, Symposium of Work on Radiation Chemistry [in Russian] (Izd. AN SSSR, Moscow, 1955) p. 91.

5. J. Wright, J. Linacre, W. Marsh, and T. Bates, Conference on the Peaceful Uses of Atomic Energy, Paper 445 (New York, 1956) Vol. 7, p. 560.

*Original Russian pagination. See C. B. translation.

58

METHOD OF CALCULATING DOSAGE FIELD
OF POWERFUL ISOTOPIC UNITS

N. I. Leshchinskii

The calculation of the dosage fields of radiators for powerful isotopic units is connected with considerable mathematical difficulties resulting from the complexity of the formulas for the calculations [1-6]. These calculations can be speeded up considerably and simplified by the use of the method presented below.

To determine dose rate P from a point source in an infinite homogeneous medium,

$$P = \frac{KM}{R^2} e^{-\mu x} B(h\nu, \mu x, Z), \qquad (1)$$

where M is the activity of the radiation source; R is the distance from the radiation source to the point at which the dose rate is determined; K is a coefficient taking into account the dimensions of the quantities and total γ constant of the radiation source in the formula. Use of this formula, however, is difficult, since the absorption $e^{-\mu x}$ and the age factor B depend on the linear absorption coefficient of radiation in the substance μ, the thickness of the absorbing layer x, the energy of the radiation $h\nu$ and the effective atomic number of the medium Z.

Analysis of the product $e^{-\mu x} B(h\nu, \mu x, Z)$ indicates that for large thicknesses of the absorbing media it may be approximated by an equation of the form $f(x) = e^{-\mu x} B(h\nu, \mu x, Z) = ax^2 + bx + c$ and for small thicknesses, by

an equation of the form $f(x) e^{-\mu x} B(h\nu, \mu x, Z) = bx + 1$. The results of the approximation and the values of the coefficients are shown in the table.

The approximation permits formula (1) to be represented in the form

$$P = \frac{KM}{R^2} (ax^2 + bx + c) \quad \text{for large thicknesses} \qquad (2)$$

$$P = \frac{KM}{R^2} (bx + 1) \quad \text{for small thicknesses.} \qquad (3)$$

Formulas (2) and (3) are used for determining the dose rate from an elementary source which is part of an extended or volume source of radiation. Using these formulas for a linear source of activity M and length L at a distance R between the point at which the dose rate is to be determined and the linear source, and with an absorbing layer thickness x_1, one finds that the dose rate P_1 is

$$P_1 = \frac{KM}{LR} \left[\int_0^{\varphi_1} \left(\frac{ax_1^2}{\cos^2 \varphi} + \frac{bx_1}{\cos \varphi} + c \right) d\varphi + \int_0^{\varphi_2} \left(\frac{ax_1^2}{\cos^2 \varphi} + \frac{bx_1}{\cos \varphi} + c \right) d\varphi \right], \qquad (4)$$

where

$$\varphi_1 = \text{arctg} \frac{y_1}{R}; \quad \varphi_2 = \text{arctg} \frac{L - y_1}{R}.$$

TABLE. Values of f_∞ and Sizes of the Largest Errors in the Calculation of the Dose Rate

Material	Thickness of absorbing layer x, cm	Co^{60} radiation		Cs^{137} radiation	
		from the formula $f(x)$	greatest error, %	from the formula $f(x)$	greatest error, %
Air	0—100	1 ($b=0$)	0,5	1 ($b=0$)	0,5
	0—10	1 ($b=0$)	0,0	1 ($b=0$)	0,0
Water (biological objects)	2—70	$1,55 \cdot 10^{-4} x^2 - 0,025x + 1,0755$	3,0	—	—
	7—70	—	—	$2 \cdot 10^{-4} x^2 - 0,03x + 1,1665$	4,4
Aluminum	0—10	$-0,0135 + 1$	1,8	$-0,0135 + 1$	1,8
	0—10	$-0,05x + 1$	1,7	$-0,046x + 1$	1,9
	0—5	$-0,055x + 1$	1,4	$-0,042x + 1$	0,7
	0—2	$-0,056x + 1$	0,9	$-0,041x + 1$	0,0
Steel	0—5	$-0,1345x + 1$	3,0	—	—
	0—3	$-0,141x + 1$	0,7	$-0,1663x + 1$	3,1
	0—2	$-0,1415x + 1$	0,4	$-0,1545x + 1$	1,7
Cobalt	0—2	$-0,149x + 1$	1,0	$-0,160x + 1$	2,0

59
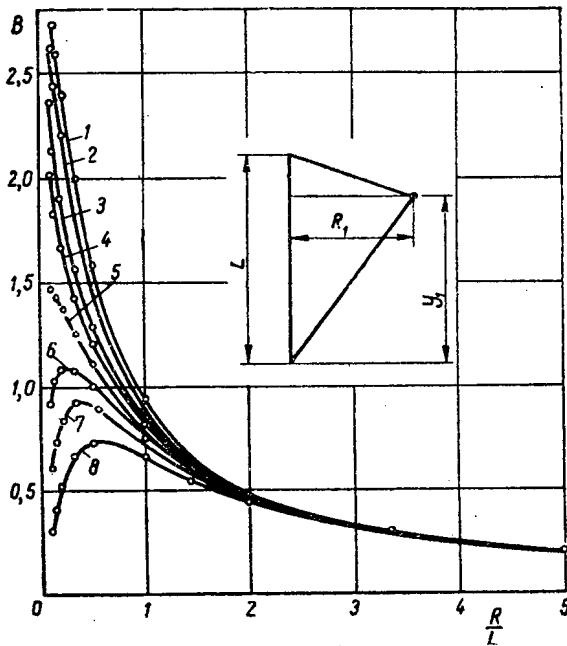
Fig. 1. Dependence of the coefficient $B = \mathrm{arctg}\ y_1/R + \mathrm{arctg}\ (L-y_1)/R$ on R/L for the following values of y_1: 1) $1L/2$; 2) $3L/4$; 3) $7L/8$; 4) $15L/16$; 5) $4L/4$; 6) $17L/16$; 7) $9L/8$; 8) $5L/4$.
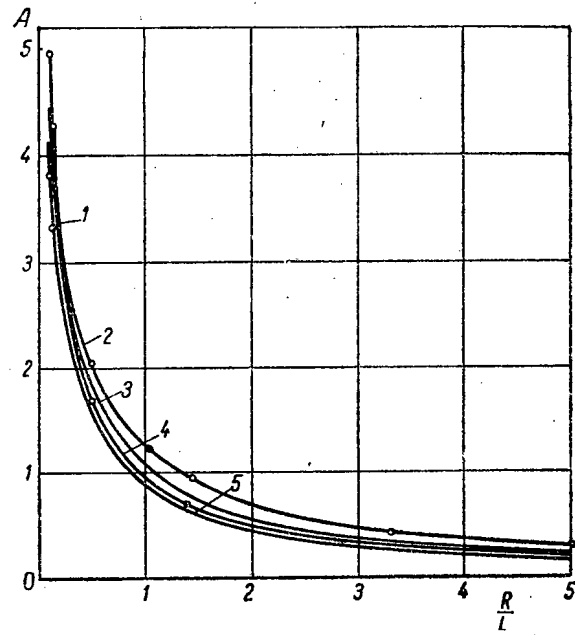
Fig. 2. Dependence of the coefficient $A = \ln\ \times$

$$\times \left[\mathrm{tg}\left(\frac{\pi}{4} + \frac{\mathrm{arctg}\ \frac{y_1}{R}}{2} \right) \mathrm{tg}\left(\frac{\pi}{4} + \frac{\mathrm{arctg}\ \frac{L-y_1}{R}}{2} \right) \right]$$

on R/L for the following values of y_1: 1) $1\,L/2$; 2) $5\,L/4$; 3) $9L/8$; 4) $3L/4$ and $1L/2$; 5) $7L/8$.

Integrating and inserting the values of φ_1 and φ_2, we obtain

$$P_1 = \frac{KM}{LR}\left(ax_1^2 \frac{L}{R} + bx_1 A + cB \right),\qquad (5)$$

where

$$A = \ln\left[\mathrm{tg}\left(\frac{\pi}{4} + \frac{\mathrm{arctg}\frac{y_1}{R}}{2} \right) \mathrm{tg}\ \times \right.$$

$$\left. \times \left(\frac{\pi}{4} + \frac{\mathrm{arctg}\frac{L-y_1}{R}}{2} \right) \right];$$

$$B = \mathrm{arctg}\frac{y_1}{R} + \mathrm{arctg}\frac{L-y_1}{R}\ .$$

The quantity B characterizes the dose rate from a linear source of radiation without taking into account the absorption and the age factor; the quantity A characterizes the influence of thin layers of absorbing media; and $ax_1^2 L/R$, the influence of thick layers. The values of the quantities B and A are shown in Figs. 1 and 2.

For the calculation of the absorption of the radiation in a multi-layer medium, the following expression holds:

$$P = \frac{KM}{LR}\ \frac{\left(a_1 x_1^2 \frac{L}{R} + b_1 x_1 A + c_1 B \right)\left(a_2 x_2^2 \frac{L}{R} + b_2 x_2 A + c_2 B \right) \cdots \left(a_n x_n^2 \frac{L}{R} + b_n x_n A + c_n B \right)}{B^{n-1}},\qquad (6)$$

where n is the amount of absorbing layers.

For the calculation of the dose field of a linear source along whose length the activity is not uniformly distributed, the linear source can be replaced by equivalent point sources, and the dose can be determined from the formula

$$P = K \sum_{i=1}^{i=n} \frac{M_i}{R_i^2}\ (a_i x_i^2 + b_i x_i + c_i).\qquad (7)$$

Comparison of the results of the calculations with experimental data [1, 4, 5] showed that the disparity does not exceed 10%. Such accuracy may be considered sufficient, since it is within the accuracy of direct measurements.

In designing radiators of any configuration, the radiators can be represented as consisting of linear or point sources, and the dose rate can be determined as the arithmetic sum of the dose rates from each of the radiation sources.

LITERATURE CITED

1. A. V. Bibergal', M. M. Korotkov, and T. G. Ratner, Atomnaya Énerg. 7, 244 (1959).*
2. E. E. Kovalev, V. P. Popov, and L. N. Smirennyi, Atomnaya Énerg. 2, 181 (1957).*

*Original Russian pagination. See C. B. translation.

60

3. U. Ya. Margulis and A. V. Khrustalev, Atomnaya Energ. 3, 338 (1957).*

4. Shielding Atomic Reactors. Atomic Energy Commission Reports, USA [Russian translation] (Il, Moscow, 1958).

5. G. White, Phys. Rev. 80, 154 (1950).

6. B. Manowitz, O. Kuhl, D. Richman, and L. Galanter, Report No. 1069 Presented by the USA at the Second International Conference on the Peaceful Uses of Atomic Energy (Geneva, 1958).

*Original Russian pagination. See C. B. translation.

61

INTEGRATING DETECTOR OF PENETRATING RADIATION

O. A. Myazdrikov

The electret state of a dielectric, according to the theory of Gross [1, 2], is due to the presence in its volume of bound and real charges of density $\rho_{f(z)} = -\operatorname{div} P_{(z)}$ and $\rho_{(z)}$. Surface densities $\tau_f = \pm P_n$ and τ_r correspond to these charges.

Since the methods of measurement of the surface charge densities based on the principle of electrostatic induction give the total value of this density, we can take $\tau_f + \tau_r = \pm P_n'$, the normal component of the equivalent electric moment of a unit volume of dielectric.

In considering the influence on the electret state of the dielectric (frozen polarization) of one or another form of penetrating radiation in order to explain the law of time variation of the surface density, we shall start from a model of the detector shown in Fig. 1. We assume that the electret is placed on a grounded base, and above its upper surface, which bears a charge density τ, is an enclosed volume of a gaseous medium of height Z_G at a pressure P_G. Of course, a change of τ in the irradiation process will occur, owing to the absorption of energy in both the gas volume V_G and in the dielectric volume V_D. The field intensity in the gaseous region, according to the condenser model suggested in [2], is determined by the expression

$$E = \frac{4\pi\tau Z_D}{\varepsilon_D Z_G + Z_D}, \qquad (1)$$

where ε_D is the dielectric constant of the dielectric. The quantity E reaches a numerical value of hundreds of volts and higher and, consequently, the ions produced in the gas volume give rise to a saturated ion current. The influence of the gas volume is taken into account by the density of the leakage current in the gas volume j_G.

Since the electret charge is bound, the neutralization of the ions is not possible, and the field of the latter decreases the value of τ.

The energy absorption in the dielectric volume leads to a more complicated process: the formation of space
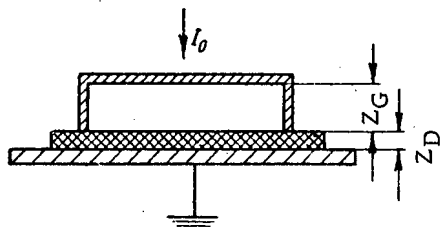
charges and hole—electron pairs, i.e., pseudo-dipoles. Ionization lies at the basis of these processes, too, and hence their effectiveness depends, in particular, on the form of radiation. In the end result, these processes depend on the change of P_n'. In this connection, the effect on the dielectric volume is taken into account by means of the leakage current density in the dielectric volume j_D.

If I is the radiation intensity, then the general equation for the behavior of the frozen polarization in the irradiation process can be written in the form

$$-\frac{d\tau}{dt} = j_G + j_D = k_1 \int_{V_G} \operatorname{div} I\, dV + k_2 \int_{V_D} \operatorname{div} I\, dV. \qquad (2)$$

For complete electron equilibrium and a saturated condition in the region V_G for the γ-radiation field, formula (2) takes the form

$$-\frac{d\tau}{dt} = cZ_G P_\gamma \frac{P_G}{P_0} \pm k\mu_{0f}\mu_D \frac{Z_D J}{Z_G}, \qquad (3)$$

where c is the electric roentgen equivalent; P_γ is the γ-ray dose, μ_D is the linear absorption coefficient of the dielectric (for $h\nu > 1$ Mev, it is determined mainly by Compton scattering); μ_{0f} is the pseudo-dipole moment; P_0 is the atmospheric pressure. The first term of formula (3) expresses the value of the ion current passing through 1 cm² of gas volume of height Z_G. The meaning of the second term is somewhat more complicated. As is known, the scattering angles φ and θ, for the case of Compton scattering are related by the expression

$$\operatorname{ctg} \frac{\varphi}{2} = (1+\alpha)\operatorname{tg}\theta, \qquad (4)$$

i.e., in each act of scattering the recoil electron undergoes a displacement of positive sign in the direction of the primary γ quanta flux m_z.

Assuming that there is a small probability of recombination of the holes and electrons resulting from their capture by trapping centers, we may state that each act of scattering leads to the creation of a long-lived electron—hole pair (pseudo-dipole), where, according to formula (4), these pseudo-dipoles are oriented. If we neglect the reverse emission of recoil electrons from the trapping centers, if we assume that their concentration in these centers is considerably less than the concentration of the centers themselves, and if we take into account the attenuation law in differential form, then the meaning of the second term of formula (3) becomes obvious. For this, it is sufficient to sum the number of flop-overs in a dielectric column per 1 cm²/sec and

Fig. 1. Model of the detector.

multiply the result by μ_{0f}. The coefficient $\underline{k}$ takes into account the processes of pseudo-dipole multiplication, since the recoil electron energy is large.

The production mechanism of pseudo-dipoles permits the interpretation of the experimentally observed polarization of a dielectric by radiation [3, 4]. A numerical estimate indicates that $j_G \gg j_D$, even when the space-charge field of the dielectric produced by electrons knocked out of the walls bounding the volume V_G is taken into account. Therefore,

$$-\frac{d\tau}{dt} = cZ_G P_\gamma \frac{P_g}{P_0} . \qquad (5)$$

If the electret consists of organic dielectrics and contains hydrogen, then the process of interaction of the electret structure with a neutron flux will depend on the recoil proton. In this case, formula (2) takes the form

$$-\frac{d\tau}{dt} = FZ_D P_{n0}, \qquad (6)$$

where P_{n0} is the neutron flux density; F is a function whose numerical value is determined by the percentage content of hydrogen nuclei.
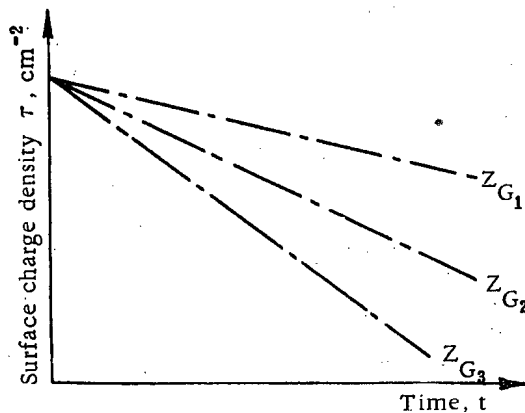
Fig. 2. Dosimetric characteristic for γ radiation ($Z_{G_1} > Z_{G_2} > Z_{G_3}$).

Integrating expression (5), we have

$$D = \frac{\Delta\tau}{cZ_G} \frac{P_0}{P_G} , \qquad (7)$$

i.e., the change in the surface density $\Delta\tau$ is a measure of the recorded dose D. Similar conclusions may be reached in the case of neutron fluxes.

The results of the experimental investigation of formula (7) for γ radiation is shown in Fig. 2 for three different values of Z_G.

Thus the change in the frozen polarization can serve as a measure of the recorded dose, and the electret itself is an integrating radiation detector [5]. The sensitivity of this detector for γ and neutron fluxes, determined respectively by the expression

$$S_\gamma = cZ_G \frac{P_g}{P_0} \qquad (8)$$

and

$$S_{n0} = FZ_D, \qquad (9)$$

can be adjusted within sufficiently wide limits, owing to the terms on the right-hand side of formulas (8) and (9).

LITERATURE CITED

1. B. Gross, Phys. Rev. 66, 26 (1944); J. Chem. Phys. 17, 886 (1949).
2. W. Swann, J. Franklin Inst. 250, 219 (1950); J. Franklin Inst. 256, 167 (1953).
3. O. A. Myazdrikov, "Method of Preparation of Electrets," Author's Abstract No. 120273 [in Russian] (November, 1957).
4. P. Böning, J. Deutsch. Elektr, 12, 138 (1958).
5. P. S. Gaponov, O. A. Myazdrikov, and Yu. V. Sinel'-nikov, "Special Dosimeter for Radioactive or Other Penetrating Radiation," Author's Abstract No. 115132 [in Russian] (December, 1957).

MEASUREMENT OF Co^{60} γ -RAY DOSE CLOSE TO THE BOUNDARY BETWEEN TWO BODIES

V. I. Kukhtevich, B. P. Shemetenko, and B. I. Sinitsyn

In the present work, the passage of Co^{60} γ rays through water (Medium I) close to a plane boundary with a second medium (Medium II) was investigated. Air, lead, nickel, and aluminum were used as Medium II. The source-to-detector distance ρ was varied from 0.7 to 5.0 mean free paths of γ rays in water, and the height of the source and detector $\underline{h}$ was from 0.05 to 2.0 mean free paths. A diagram of the experiment is shown in Fig. 1. The measurements were carried out in a water tank of dimension 2.0 × 2.2 × 1.6 m. Lead, nickel, and aluminum plates of area 90 × 150 cm and thickness equal to 2.5 mean free paths of Co^{60} γ rays in each of the materials of Medium II were placed at the bottom of the tank. The measurements at the boundary between water and air were carried out in a water tank with an open surface. A scintillation γ dosimeter with an anthracene crystal [1] was used as the γ-ray detector. The Co^{60} source was made in the form of a sphere of 0.5 cm diameter; the source activity was 0.153 ± 0.005 curie.

The purpose of the measurements was to determine the dose rate $D_1(\rho, h)$ in water close to the boundary between the two media. The influence of the boundary

on the passage of rays can be characterized by the coefficient L from the ratio $D_0(\rho, h_\infty)/D_1(\rho, h) = L$, where $D_0(\rho, h_\infty)$ is the dose rate in a medium of infinite extent measured at the same distance ρ used for the determination of $D_1(\rho, h)$.

The results of the measurements are shown in Fig. 3, where the values of the coefficients L are given for different distances ρ and heights $\underline{h}$. The errors in the determination of the coefficient L did not exceed 3%. The obtained results are compared with data [2], in which the dissipation energy of γ rays of initial energy 1.28 Mev
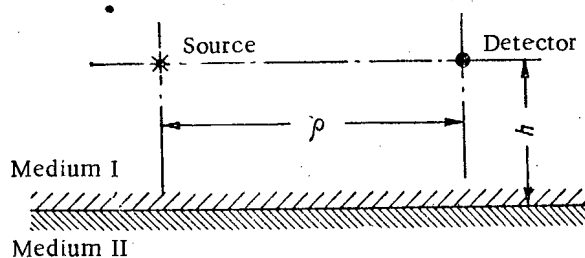
Fig. 1. Diagram of the experiment.
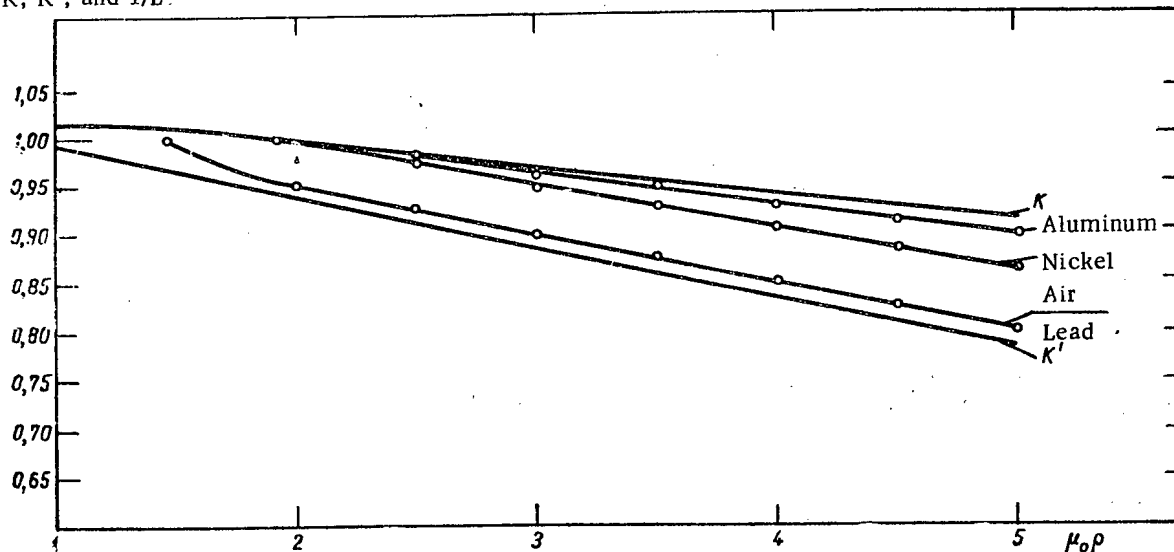
Fig. 2. Comparison of the experimental values of the coefficient 1/L (as a function of the distance between the source and detector for $\mu_0 h = 0.5$ for different materials of Medium II) with the theoretical coefficient K and K' of [2].

in Medium I (with Z close to that of H_2O) at the plane boundary with a second medium (Medium II) was calculated by a Monte Carlo method for two extreme cases: 1) Medium II has the same atomic number as Medium I,

but is several times more dense; then the influence of the boundary of separation is taken into account by the correction coefficient K dependent on source—detector distance and the height of the source and detector above the
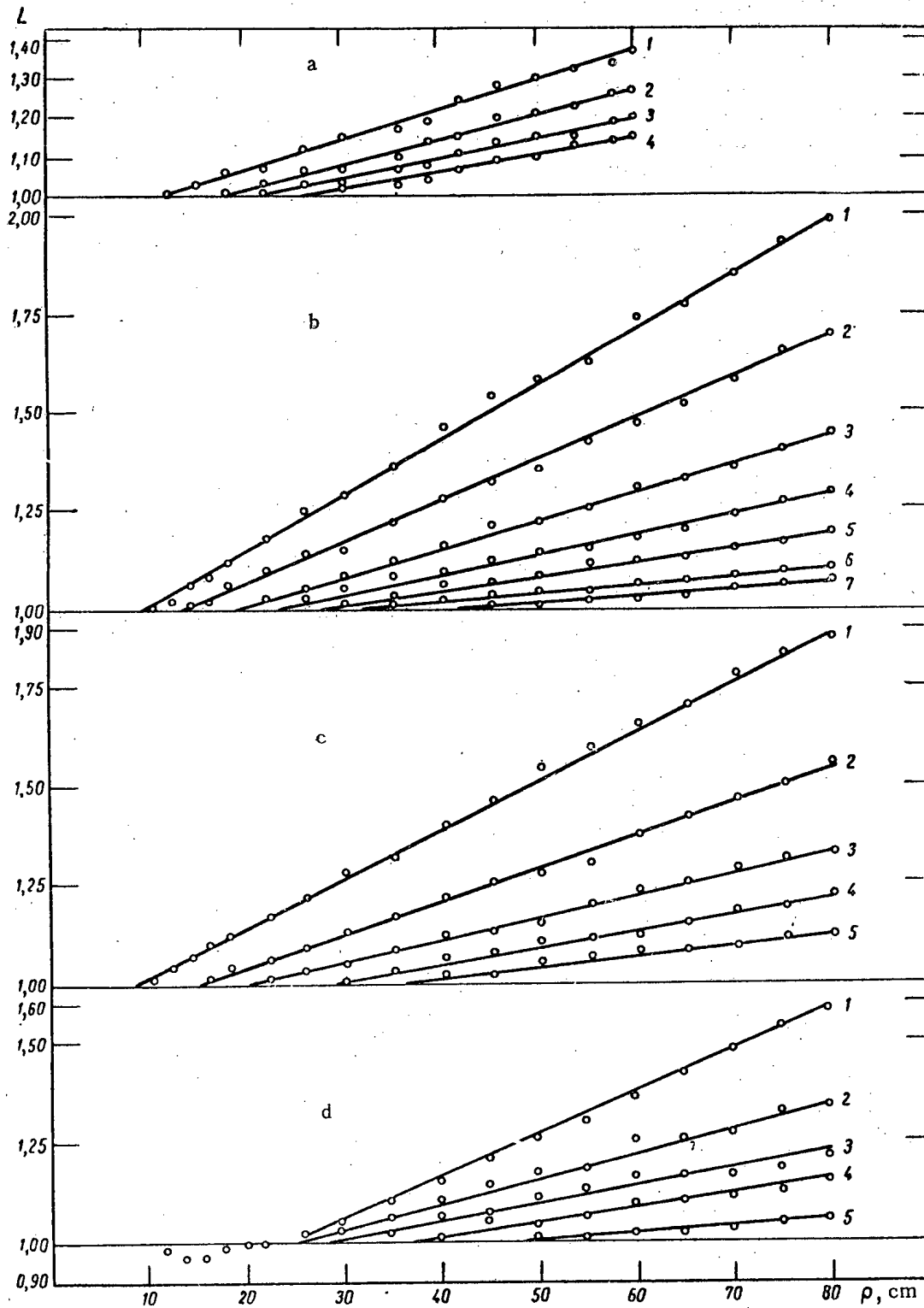
Fig. 3. Dependence of the experimental values of the coefficient L on ρ and h for Medium II:
a) Air (h in cm: 1–2.8; 2–4.8; 3–6.8; 4–8.8); b) lead (h in cm: 1–0.8; 2–2.1; 3–4.4; 4–6.4; 5–10.4; 6–16.4; 7–20.4); c) nickel (h in cm: 1–0.8; 2–2.4; 3–4.4; 4–6.4; 5–10.4); d) aluminum (h in cm: 1–0.8; 2–2.2; 3–4.2; 4–6.2; 5–10.2).

65

level of the boundary of separation; 2) Medium II represents a vacuum or material with a very low albedo; in this case the correction factor is denoted by K'. Coefficients K and K' are the inverse values of the quantity L which we defined earlier, i.e., $K = 1/L$.

The results of the comparison for $\mu_0 h = 0.5$ are shown in Fig. 2. The values of $1/L$ were obtained by interpolation of the experimental data. The values of the quantity $1/L$ for the media water—air and water—lead coincide, and within the limits of error of calculation and experiment, are in agreement with the values of K'. The experimental point $1/L$ for $\mu_0 \rho = 1.5$ was obtained by linear extrapolation of this quantity to unity. Strictly speaking, such an operation is not entirely just-

ified, since the quantity L tends asymptotically to unity. The correction factors $1/L$ for the media water—nickel and water—aluminum lie between the values of K and K', as is also the case for the calculations of the author of [2].

The authors thank S. G. Tsypin for discussion of the results of the measurements.

LITERATURE CITED

1. V. I. Kukhtevich, S. G. Tsypin, and B. P. Shemetenko, Atomnaya Énerg. 5, 638 (1958).*
2. M. Berger, J. Appl. Phys. 28, 1502 (1957).

*Original Russian pagination. See C. B. translation.

ON THE EFFICIENCY OF GAS-DISCHARGE COUNTERS

V. P. Bovin

Translated from Atomnaya Énergiya, Vol. 8, No. 1, pp. 68-70, January, 1960
Original article submitted February 13, 1959

The efficiency* of gas-discharge counters has been investigated by a number of authors [1-6]. The formulas and experimental curves obtained clearly explain the main physical processes occurring during the recording of γ radiation, but they cannot be used for practical purposes, since they do not reflect the peculiarities of the design of modern counters and the conditions of their use.

We determined the variation of efficiency with the radiation energy in gas-discharge counters of various types produced by domestic industry. These counters differed from one another regarding the material and the design of the cathode and the filling gas. Counters of the MS and VS type, filled with an argon-alcohol mixture have, respectively, copper and tungsten cathodes deposited on the interior of a glass envelope of wall thickness 1 mm. Counters of the GS type have a graphite cathode and halogen counters of the STS type, a steel cathode.

Figure 1 shows the averaged experimental characteristics of five counters of each type. For the individual counters of each type, there was observed a spread in the efficiency within the limits of 10-20%, but the shape of the characteristics remained unchanged. The great-est spread in parameters was observed for counters of the VS and STS type, and also for all counters filled with an argon-alcohol mixture after 10^6-10^7 pulses had been recorded.

Analysis of the curves shown in Fig. 1 indicates that, in the quantitative measurements, counters of the MS and GS type have better characteristics, but they have a high operating potential (1300-1350 volts). Counters of the VS type have the highest integral efficiency owing to the high coefficient of photoabsorption of γ rays in the tungsten cathode. The maximum observed on the curve is explained by the fact that, for a given region, the efficiency is determined primarily by the product $R\tau$, where R is the range of photoelectrons in the cathode material of the counter and τ is the absorption coefficient for γ rays. The product $R\tau$ has a maximum in the energy region close to the K jump of the photoabsorption coefficient.

---

*By efficiency of γ-ray receivers, we will mean the ratio of the number of recorded γ quanta to the total number of γ quanta of a given energy entering the radiation receiver volume during the same time.
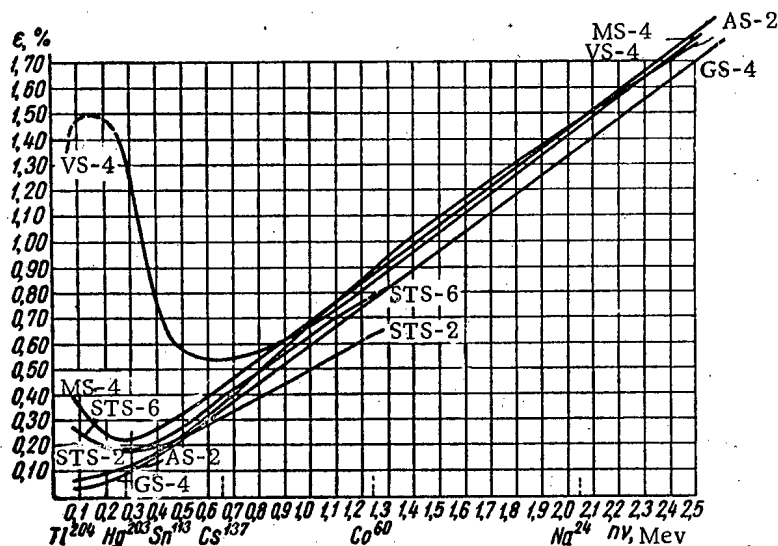
Fig. 1. Dependence of the efficiency of gas-discharge counters of various types on the radiation energy.

The shape of the curves for counters of the STS type in the energy region above 1.5 Mev has not yet been sufficiently investigated.

When gas-discharge counters are used, they are, as a rule, placed in aluminum or steel sheaths of thickness 1-3 mm, and sometimes are specially shielded by lead filters of different thicknesses for equalizing their spectral efficiency or are shielded from soft, scattered radia-

tion. The use of filters and shields has a basic influence on the efficiency of γ-ray registration.

Figure 2 shows the experimentally obtained dependence of the efficiency on the radiation energy for counters of type STS-6, STS-2, MS-4, and VS-4 placed inside cylindrical filters of various materials (aluminum, iron, lead). In the given case, the efficiency was determined to a considerable degree by the interaction be-
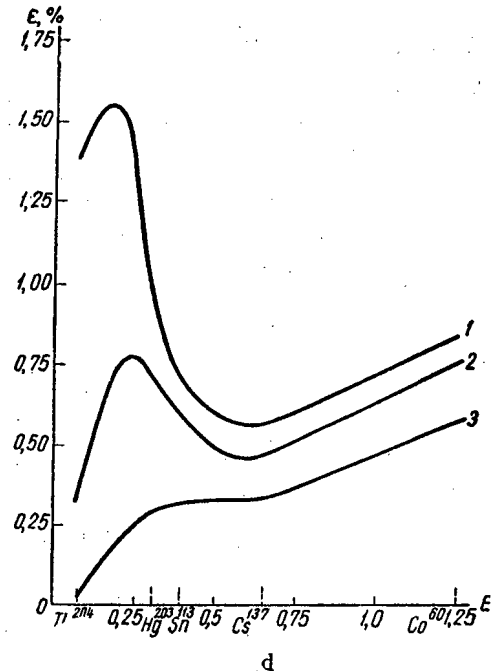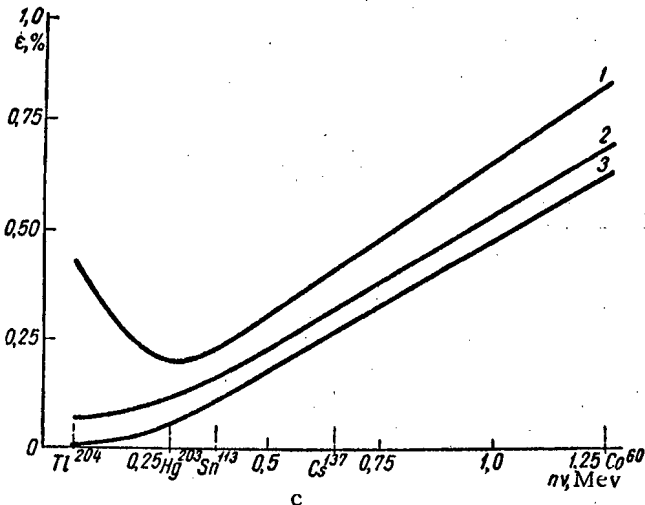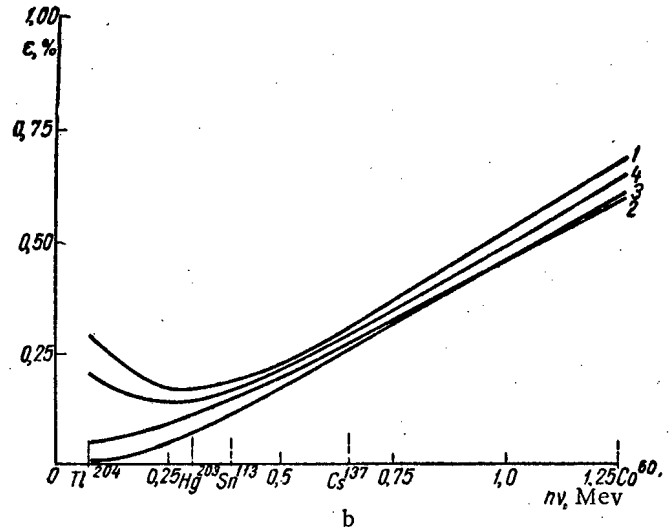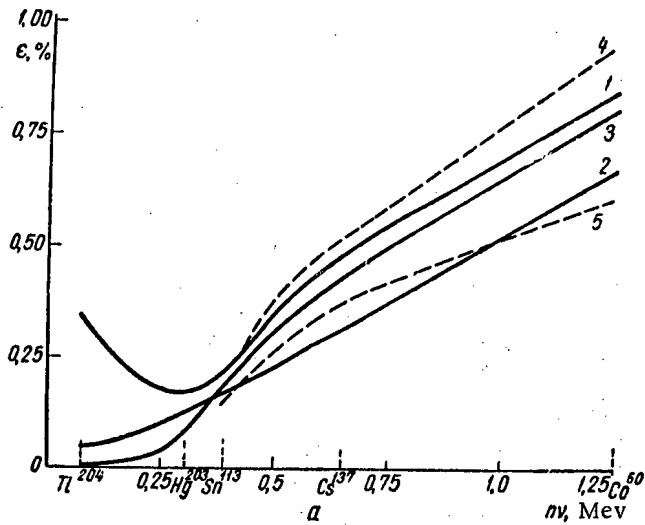
Fig. 2. Dependence of the efficiency of counters with various filters on the radiation energy: a) STS-6 counter [(1) without filter; (2) with iron filter of thickness 3 mm around counter; (3) with lead filter of thickness 2 mm around counter; (4) with lead filter of thickness 2 mm behind counter; (5) with lead filter of thickness 2 mm between counter and radiation source]; b) STS-2 counter [(1) without filter; (2) with iron filter of thickness 3 mm around counter; (3) with lead filter of thickness 2 mm around counter; (4) with aluminum filter of thickness 2 mm around counter];c) MS-4 counter [(1) without filter; (2) with iron filter of thickness 3 mm around counter; (3) with lead filter of thickness 2 mm around counter]; d) VS-4 counter [(1) withour filter; (2) with iron filter of thickness 3 mm around counter; (3) with lead filter of thickness 2 mm around counter].

tween the wall material of the counter and scattered γ radiation, Compton electrons, and photoelectrons produced in the filter.

The influence of secondary electrons can be traced via the characteristics of the β counter STS-6 with a fine steel cathode (Fig. 2a). A lead filter of density 2.3 g/cm^2 gave almost no change in the efficiency of registration for energies of 0.3-1.5 Mev, since it produces a large quantity of secondary electrons which are recorded by the counter. The strong absorption of soft radiation in lead affects the low-energy region of γ quanta, and the efficiency sharply decreases. The glass envelope used in counters intended for recording γ radiation shields the cathode material from the action of secondary electrons, and therefore the above phenomena are not observed in these counters.

In iron filters, the predominant process in this energy region is Compton scattering. The soft, scattered radiation is recorded by counters whose efficiency increases with the atomic number of the cathode material; this is very clearly seen from the characteristics of the counter type VS-4 with an iron filter of density 2.4 g/cm^2 (Fig. 2d). This is also confirmed by the fact that the efficiency of registration drops sharply after a

thin filter of thickness 0.1 mm is placed between the counter and the iron filter.

Aluminum filters of small thickness (2-3 mm) introduce practically no change in the dependence of the efficiency on the radiation (Fig. 2b).

The best filters for gas-discharge counters with glass envelopes are lead shields, since they cause the forms of the efficiency characteristics of counters of various types to approach one another.

During work with thin-walled counters, it is necessary to use combinations of filters: iron-lead or aluminum-lead, where the metal with the smaller atomic number should be placed closer to the counter.

LITERATURE CITED

1. H. Baeyer, Z. Physik. 95, 417 (1935)
2. G. Droste, Z. Physik. 100, 529 (1936)
3. G. Sizoo and D. Coumou, Physik. 3, 921 (1936)
4. H. Jukawa and S. Sakata, Sci. Papers Inst. Chem. Physik. Res. 31, 187 (1937)
5. E. Norling, Arch. Math. Astr. Och. Fisik. 27a, 27 (1941)
6. H. Bradt, P. Gugelot, O. Huber, H. Medikus, P. Preiswerk, and P. Scherer, Helv. Physik. Acta. 19, 77 (1946).

69

AIRBORNE RADIOMETER-ANALYZER

V. V. Matveev and A. D. Sokolov

Airborne radiometric searches for deposits of useful minerals are being utilized more frequently in geophysical work. Even with the great achievements in applying aeroradiometry to this type of search, the possibility of further development and perfection of the present methods still exists. As our initial goal, we must refine the method of airborne determination of the qualitative composition of radioactive ores.

Though the idea has long been [1] used in other geophysical methods [2, 3], aeronautically this method has, up to the present time, hardly been used; this is explained basically by the absence of appropriate airborne instruments.

In the present paper we describe a highly sensitive scintillation airborne threshold γ spectrometer to be used in determining the intensity and relative hardness of the earth's γ radiation.

The radiometer-analyzer consists of a scintillation counter which sends signals to a two-channel threshold amplitude pulse analyzer (see block diagram, Fig. 1).
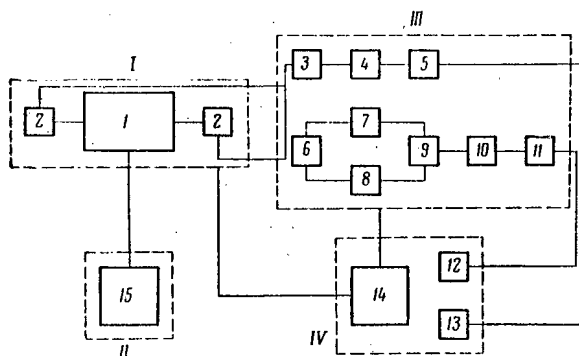
Fig. 1. Block diagram of the device: I) counting head [(1) scintillation counter; (2) cathode repeaters]; II) high-voltage supply for the FÉU; III) electronic circuit [(3, 6) cathode repeaters; (4,7,8) amplitude discriminators; (5,11) measurers of counting speed; (9) anticoincidence circuit; (10) forming monovibrator]; IV) automatic indicating and voltage supply circuit [(12, 13) recording galvanometers; (14) voltage transformer and rectifier; (15) high-voltage battery].

The counting head of the device (the schematic cross section shown in Fig. 2) consists of a hermetically sealed aluminum cylinder (20 cm in diameter and 60 cm long) containing a liquid scintillator 2, and two photoelectric multipliers 5 of the type FÉU-24 or FÉU-19M.

A series of experiments using specially constructed apparatus [4] was performed in order to prepare the liquid scintillator which would have the optimum parameters for a counter with the given geometry (transparency to its own radiation, conversion effectiveness, radiation spectrum, etc.).

A solution of paraterphenol in toluene was used as the scintillator, and this, as is known,is one of the best liquid scintillators. Experiments in the choice of optimum concentration of paraterphenol in toluene were based on the fact (this follows from [5]) that conclusions obtained from studies of liquid scintillators with small volumes may be applied to scintillators with large volumes (if in the process there are no basic changes in the spectral distribution of the scintillator light and the conditions of light reception at the photocathode of the multiplier are preserved). As a result of the studies we obtained a value of 4g/liter as the optimum concentration of paraterphenol in toluene; this is in good agreement with the data given [6, 7].

To the above solution we added napthaphenyloxazole (αNPO) (of a concentration of 20 mg/ liter). This increased the sensitivity of the device by approximately 10%.

It is well known that scintillators are subject to oxygen poisoning. It has been shown [8] that this poisoning is reversible and that the properties of the scintillator may be restored if inert gases are passed through the solution. The mean oxygen extinguishing factor is approximately 20%. Actually, after chemically pure argon was passed through the solution, the conversion efficiency of the scintillator was increased by 10%. In addition, the argon atmosphere which was created in the reservoir 1 (See Fig. 2) served to protect the scintillator from possible poisoning during the further use of the device.

The voltage supply circuit for the photoelectric multiplier consists of a high-voltage sectioned battery which is located outside of the counting head of the de-

70
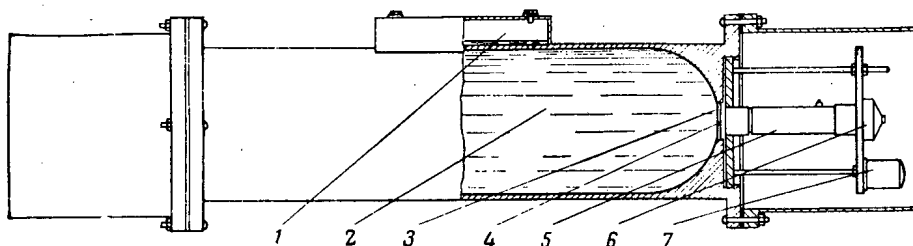
Fig. 2. Schematic cross section of the counting head of the device: 1) reservoir; 2) liquid scintillator; 3) packing, 4) window; 5) FEU; 6) high-voltage divider; 7) cathode repeater.
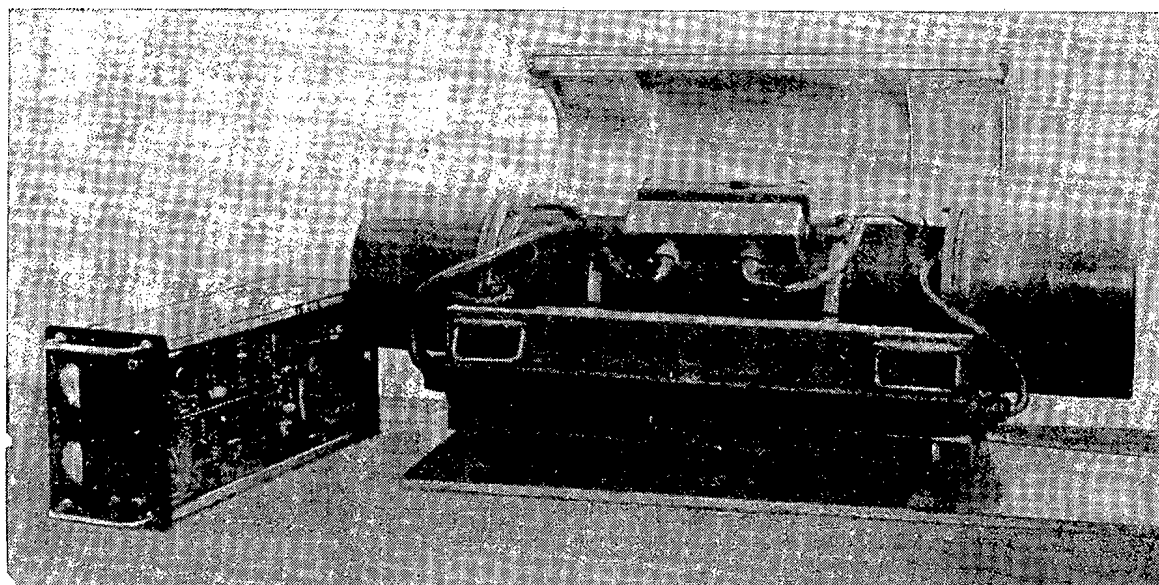
Fig. 3. Exterior view of the electronic circuit and the counting head of the device.

vice. This method of voltage supply simplifies the device significantly and increases the multiplier stability.

It is necessary to note that the method of feeding the photoelectric multiplier from a sectioned battery has the disadvantage that the total voltage and the potential distribution between the electrodes of the photoelectric multiplier is fixed. However, it was shown [4, 9] that for FEU-19M we can choose a mode of operation for which the signal-to-noise ratio is high and the operation is linear.

The electronic circuit of the radiometer-analyzer is shown in the block diagram of the device, Fig. 1.

In order to ensure operation within the necessary energy limits, switches are provided which permit us to change the limits of both channels over a wide energy range: from 50 to 500 kev in the channel for the total count and from 1.5 to 2.5 Mev in the channel for the separate count.

The limits of the discriminators in the channel for the separate count are chosen in such a manner that only the intensity of the hard γ radiation which has an energy exceeding a given energy is registered. Cosmic radiation with an energy exceeding 3 Mev is excluded with the aid of an anticoincidence circuit. Such a decrease in the background noise noticeably improves the accuracy obtained in determining the nature of the layers of radioactive ores.

The parameters of the airborne radiometer-analyzer are as follows: device sensitivity using the FEU-19M in the total count channel is 500 ± 50 impulses/sec for 1 mC/hr of radium radiation; the coefficients characterizing the relative hardness of the γ radiation are equal respectively (in percent deviation from the indications shown in the total count channel) to 4 for thorium radiation and to 2 for radium radiation. The exterior view of the electronic circuit of the device and counting head with the cover of the thermostat raised is shown in Fig. 3.

Trials of the device in 1956 and its use in 1957 have shown that its high sensitivity and the possibility of the

71

threshold spectrometry of γ radiation distinguish the device and permit us to hope that the radiometer-analyzer will be useful in aeronautic searches for minerals.

LITERATURE CITED

1. W. Bothe and H. Kolhorster, Z. Naturwiss. 16, 1045 (1928).
2. G. R. Gol'bek, V. V. Matveev, and R. S. Shlyapnik-ov, Proceedings of the International Conference on the Peaceful Uses of Atomic Energy (Geneva, 1955) [in Russian](Gosénergoizdat, Moscow-Leningrad,1958) Vol. 8, p.278.
3. G. R. Gol'bek, V. V. Matveev, and R. S. Shlyapnik-ov, Atomnaya Énerg. 3, 247 (1957)*
4. V. V. Matveev, G. K. Popkov and D. Sokolov, Pribor. i Tekh. Éksp. 5, 40 (1959).
5. F. Hayes et al., Nucleonics 14, 42 (1956).
6. P. Swank, Annual Rev. Nucl. Sci. 4, 11 (1954).
7. F. Broons, Progr. Nucl. Phys. 5, 252 (1956).
8. R. Pringl et al., Phys. Rev. 92, 1582 (1953).
9. I. Ya. Breido, B. M. Glukhovskoi, and L. G. Leitei-zen, Radiotekh. i Élektron. 11, 1344 (1956).

*Original Russian pagination. See C. B. translation.

INVESTIGATION OF THE PRODUCTION OF AN ELECTROMOTIVE FORCE IN A SYSTEM OF SEMICONDUCTORS WITH URANIUM DURING IRRADIATION IN A REACTOR

Yu. K. Gus'kov, A. V. Zvonarev, and V. P. Klychkova

It is known that under the action of ionizing radiation on a system of p-type and n-type semiconductors in the presence of a contact field an electromotive force is produced in the system. Information on this question, available in the literature, refers primarily to irradiation by light, x rays, γ rays, β and α particles [1]. A system of p-type and n-type semiconductors irradiated by uranium fission fragments was investigated. Some compounds of uranium (for example, U_3O_8), as is known [2], are semiconductors. If a system of semiconductors with uranium is irradiated by a neutron flux, then the fission of uranium leads to the formation of uranium fission fragments. These fission fragments, apart from ionization, produce a large radiation disturbance in the irradiated materials and thus strongly change the electric properties of the latter [3, 4]; therefore, the system of semiconductors with uranium should consist of substances whose electric properties are not affected very much by radiation. Such substances may be semiconductors with a large number of initial lattice defects, for example, polycrystalline semiconductors or single crystals with a large number of impurities.

In the investigated systems, crystalline oxide semiconductors were used. Uranous-uranic oxide U_3O_8, which

has a large work function, was used as the p-type semiconductor in all experiments, and the oxides BaO, TiO_2, MgO, and Al_2O_3, which have small work functions [5], were used as the n-type semiconductors. As materials for the electrodes we used gold or copper for the p-type semiconductors and magnesium or titanium for the n-type semiconductors. The samples of U_3O_8—BaO and U_3O_8—TiO_2 were prepared by successive thermal sputtering of a system of layers of semiconductors and electrodes on a base in vacuo by the method described in [6]. In the samples of U_3O_8—Al_2O_3, the Al_2O_3 layers were prepared by metallization on a titanium base; then U_3O_8 and a gold or copper electrode were sputtered in vacuo on the Al_2O_3 layer. In the U_3O_8—MgO samples, it was impossible to obtain the MgO layers by sputtering in vacuo and metallization; therefore, we used a ceramic plate of MgO of thickness 0.5 mm as the MgO layer. A magnesium electrode was sputtered on one side of this plate and a layer of U_3O_8 and a gold or copper electrode on the other. The area of the working surface of the samples was 6 and 2.8 cm^2, the thickness of the layers of U_3O_8, BaO, TiO_2 was 5-20μ and of Al_2O_3, 100-200μ.

The prepared samples were fixed in holders with clamped bronze electrodes. In order to control the temperature of the sample surfaces, a copper—constantan thermocouple was soldered to one of the electrodes. The holders with the samples were placed in aluminum cylindrical containers and irradiated in the experimental, cooled channel of the reactor of the atomic-electric power plant, where the density of the neutron flux and γ rays was 10^{10}-10^{13} $cm^{-2} sec^{-1}$ depending on the power level of the
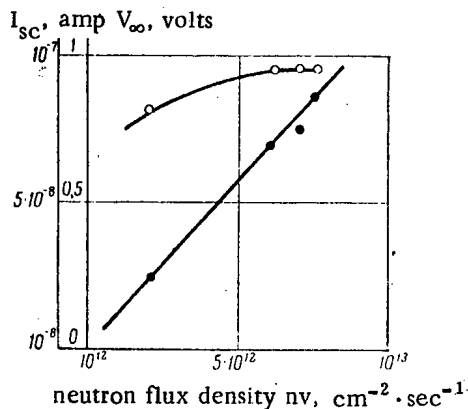
Fig. 1. Dependence of the voltage $V_\infty(O)$ and current $I_{sc}(\bullet)$ of the U_3O_8-MgO sample on the neutron flux density nv.
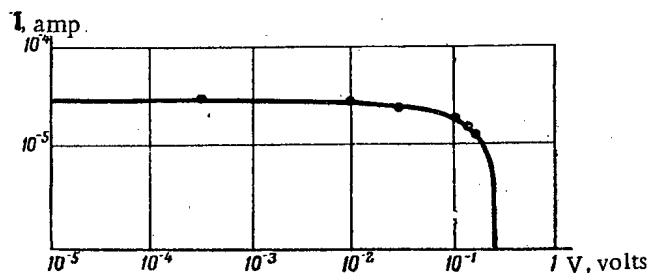
Fig. 2. Load characteristic of the U_3O_8-MgO sample.

73
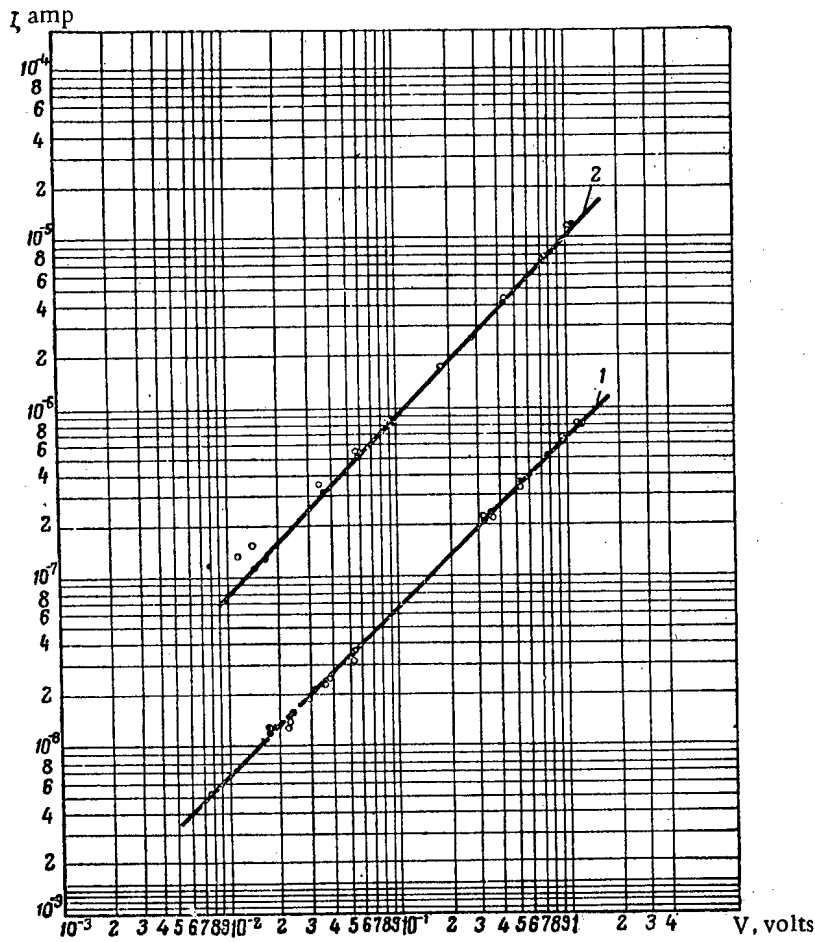
Fig. 3. Volt-ampere characteristics of the U_3O_8-Al_2O_3 sample before (Curve 1) and after (Curve 2) irradiation in the reactor: ●) negative voltage on titanium electrode; ○) positive voltage on titanium electrode.
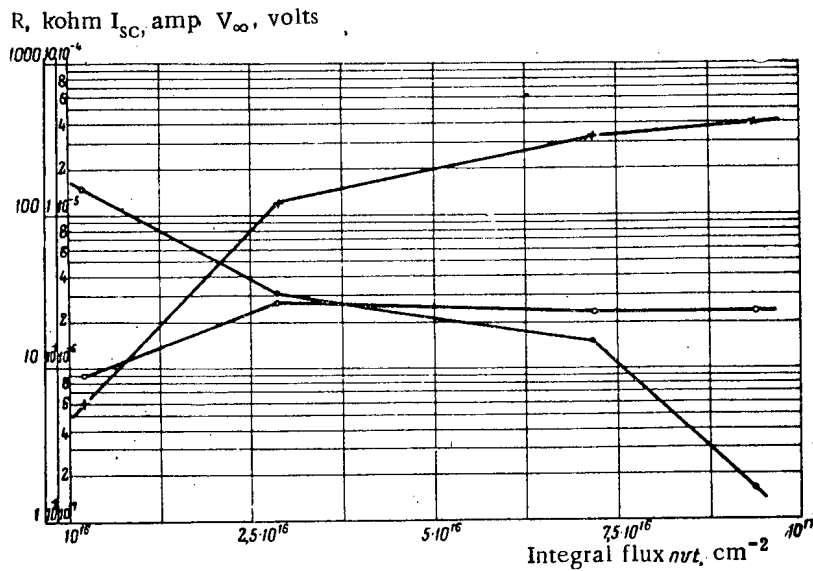
Fig. 4. Dependence of I_{sc} (×), V_∞(○), and R(●) for the U_3O_8-MgO sample on the integral irradiation flux nvt at a constant neutron flux of $8 \times 10^{12} cm^{-2} sec^{-1}$.

reactor. The sample temperature during irradiation was ~120°C.

During the irradiation, the following characteristics were studied for each sample: the no-load voltage V_{∞}, the short-circuit current I_{sc}, the load characteristic, sample surface temperature, and the sample resistance R at 1.4 volts in the forward and inverse directions. The volt-ampere characteristics for the samples were taken before and after irradiation in the reactor.

During the irradiation in the reactor, an electromotive force was observed to arise in all the samples. With an increase in the neutron flux density nv the voltage V_{∞} and current I_{SC} increased. The character of the dependence of the voltage V_{∞} and current I_{SC} on the flux density for the U_3O_8-MgO sample is shown in Fig. 1. It is seen from the graph that V_{∞} reaches saturation at $nv \approx 6 \times 10^{12}$ cm^{-2} sec^{-1}, and I_{SC} increases linearly with an increase in the neutron flux density. The load characteristic of the U_3O_8-MgO sample is shown in Fig 2; it is similar to the characteristic of a barrier-layer photocell. The neutron flux density in this case was 8×10^{12} cm^{-2} sec^{-1}.

Figure 3 shows typical volt-ampere characteristics of the U_3O_8-Al$_2$O$_3$ sample before and after irradiation by an integral neutron flux of 5×10^{17} cm^{-2}. From this figure it is seen that, first, the sample resistance, after irradiation, decreases by an order of magnitude and, second, after irradiation, for small voltages (0.01-0.1 volt) a barrier-layer effect, which was absent before irradiation, was observed. A rather marked rectification effect was observed in samples during irradiation; the rectification factor here reached 2-10 at a voltage of 1.4 volts.

The behavior of the U_3O_8-MgO samples as a function of the integral irradiation flux is shown in Fig. 4. Upon irradiation all characteristics varied greatly. The sample resistance before irradiation was 10 megohm; after irradiation, it fell to 2 kohm, as a result of which I_{sc} increased sharply; with an increase in the irradiation flux, V_{∞} also increased. At an integral irradiation flux of ~10^{17} cm^{-2}, there was observed a tendency towards stabilization of the effect. After the end of the irradiation of the sample in the reactor, the resistance of the sample increased to 1 megohm.

In order to explain the role of uranium fission fragments in the production of the electromotive force a special experiment was set up. Several samples were given a predose in a γ-ray flux before being irradiated in the reactor. In this case, the effect in the samples was 3 orders less than in the case of irradiation by the same neutron flux. This is in agreement with the amount of specific ionization produced by γ rays and the uranium fission fragments. Double samples of U_3O_8-Al$_2$O$_3$ were prepared in which uranium with 10% enriched U^{235} was deposited on one half of the sample and natural uranium on the other half. During irradiation, the 10% enriched sample gave an effect 15 times as great as the sample with natural uranium. The results of these experiments indicate that the electromotive force produced in the samples is due to the uranium fission fragments.

In addition to the above-mentioned semiconductors, oxides and sulfides of beryllium, nickel, molybdenum, tungsten, zinc, and copper were examined qualitatively. In all samples, there was observed the production of an electromotive force, but the best combination of semiconductors proved to be the combination of samples of U_3O_8-MgO.

Our calculations indicate that in the U_3O_8-MgO samples 0.01% of the fission fragment energy is converted into electric energy. This low efficiency is apparently explained by the small lifetimes of the current carriers and the poor ratio of the diffusion length of the current carriers to the thickness of the semiconductor layers in the samples. From an analysis of the obtained results it is possible to conclude that the production of an electromotive force in the samples depends basically on the barrier-layer effect, although volume and thermal electromotive force play a certain role.

LITERATURE CITED

1. E. G. Linder, P. Rappaport, and G. G. Lofersky, Proceedings of the International Conference on the Peaceful Uses of Atomic Energy (Geneva, 1955) [Russian translation] (Izd. AN SSSR, 1958) Vol. 15, p. 340.
2. A. V. Ioffe, Zhur. Tekh. Phys. 18, 1488 (1948).
3. G. Kinchin and R. Pease, Reports Prog. Phys. 18, No. 1 (1955).
4. J. Glen, Advances in Physics 4, 381 (1955).
5. B. M. Tsarev, Contact Potentials [in Russian] (Gostekhizdat, 1955) 2nd ed.
6. Yu. K. Gus'kov et al., Pribor. i Tekh. Éksp. 1, 143 (1960).

INTERNATIONAL SYMPOSIUM ON THE METROLOGY OF RADIOACTIVE ISOTOPES

K. K. Aglintsev and V. V. Bochkarev

An International Symposium on the Metrology of Radioisotopes, organized under the auspices of the International Atomic Energy Agency, was convened in Vienna on October 14-16, 1959. About 100 scientists from 27 countries, including about 20 representatives of various international bodies (CERN, Euratom, International Standardization Organization, IAEA) participated. The symposium was opened by the assistant general director of the IAEA, H. Laboulier. A total of 37 reports and papers were read at the various sessions of the symposium, with lively discussions ensuing.

Seven nations, Great Britain, Canada, USSR, USA, France, West Germany, and Sweden, presented review papers summarizing the officially adopted methods for the metrology of radioactive isotopes in their countries. In these reviews, information was made available on the organization of standardization work, and on the methods and facilities used in the standardization of isotopes and neutron sources.

Some of the papers contained descriptions of the techniques used in fabricating the specimens and measuring their activity, and some data on the manufacture of standard emitters were made available.

Canada manufactures (at the Ottawa laboratory) up to 100 radium preparations annually, contained in platinum-iridium needles.

The number of standard emitters manufactured in France during the years 1957, 1958, and 1959, were, in the form of solutions,9, 118, and 129 specimens, respectively, and 1, 111, and 177 specimens in the form of solid sources.

Standard emitters with the long-lived isotopes Co^{60} and Sr^{90} have been manufactured in West Germany, and 1960 plans call for the manufacture of emitters with the short-lived isotopes Na^{24}, P^{32}, and Au^{198}.

Great Britain is producing a large quantity of standard emitters: the National Physics Laboratory prepared 142 standard emitters in 1958, with Na^{24}, P^{32}, Co^{60}, Sr^{90} + Y^{90}, I^{131}, and Au^{198} (specific activities varying from 1 μC/g to 1 mC/g); the Harwell Nuclear Research Center has put out about 500 sources with 60 different isotopes in 1958; the Radiochemical Center at Amersham produced about 800 emitters during the first nine months of 1959, including 100 α-, 200 γ-, and 500 β-emitters (of the last, 100 liquid and 400 solid sources). The National Bureau of Standards of the USA is making available standard emitters with isotopes H^3, C^{14}, Na^{24}, P^{32}, S^{35}, K^{42}, Co^{60}, Kr^{85}, Sr^{90} + Y^{90}, I^{131}, Cs^{137}, Ta^{182}, Au^{198}, Hg^{203}, Tl^{204}, as well as standard emitters of Po^{210}, U_3O_8, Ra (D+E) solutions and solid preparations of radium.

A survey paper on the methods used in the metrology of radioactive isotopes in the USSR was presented by a group of authors (K. K. Aglintsev, V. V. Bochkarev, V. M. Grablevskii, F. M. Karavaev). The report made a deep impression on the participants at the gathering.

A report on comparisons made of standard radioactive emitters produced in various countries was presented by L. Cavallo and W. Mann (USA). The comparisons, effected during recent years at a number of laboratories, showed that discrepancies in the determination of specific activity were limited: in particular, for the standard emitters (in solution form) of Na^{24} and I^{131}, the error was 3%; for Na^{22} and Au^{198} sources, 5%; for P^{32} and K^{42} sources, 7%. This attests to the reliability of the methods used in standardizing radioactive preparations.

There were 21 papers devoted to original research methods and measurement techniques for measuring the activity of α-, β-, and γ-emitters and emitters decaying by electron capture. H. Robinson from the University of California (USA) described a novel design for a precision alpha counter based on 1 π geometry, which was achieved by means of a special collimating attachment. A report by J. Stein and F. Strelov from the National Physics Laboratory (Union of South Africa) was devoted to the absolute count of α particles in a liquid scintillation 4π α-counter, which was successfully used to determine the half-life of U^{238}.

B. Pate (USA) gave a review of the development of the method used in measuring activity with 4π counters, and pointed out the advantages of such counters over counters with small solid angles, emphasizing the significant influence of β radiation on the results of self-attenuation measurements, especially for emitters with low β-particle energies, and the importance, stemming therefrom of careful manufacture and quality control of specimen thickness and regularity for measurements of specimens on thin organic film.

The problem of the study of self-attenuation of β radiation in the test specimen was dealt with in two reports delivered by Canadian scientists. L. Jaffe and J. Fishman presented ample experimental data on the dependence of self-attenuation on the thickness of the source for different energies in the spectrum ranging from 0.018 Mev (T) to 1.7 Mev (P^{32}). Self-attenuation curves obtained on counters with narrow solid angles and on 4π counters were analyzed, and an estimate was made of the effect of the geometrical shape factor on self-attenuation. P. Campion reported on original research on self-attenuation correction terms, in particular, on new approaches to the extrapolation of self-attenuation curves with the aid of mixed β- and $\beta - \gamma$- sources, developed jointly through the efforts of J. Taylor and J. Merritt. Calculations of corrections for absorption and self-attenuation of β radiation in sources with 4π geometry were also taken up in a report by A. Baptista (Portugal).

Some of the reports discussed problems involved in measuring extremely low-level sources, which are of particularly great importance for some problems encountered in biology, medicine, and geology, in research using labeled atoms, etc. The three basic pathways for increasing the reliability of such measurements were considered, viz: devising improved counters, devising more reliable noise-free electronic networks, and reducing background noise. G. Manoff (USA) reported, in particular, on work involving a study of the effect of cosmic radiation, natural radioactive impurities in the structural materials of the counting equipment and hot-cell materials, etc. on background; the radiochemical purity of reagents was studied, different counting circuits (in an anticoincidence circuit for reduction of background) were considered, and an estimate was made of the relative quality of the circuits for measuring activity levels of the order of 0-10 decay events per min, the feasibility of using specially prepared long-lived standards, i.e., low-activity standard emitters, for this purpose was demonstrated. A number of recommendations were advanced for reducing background, choosing materials with a low content of radioactive substances, etc., by N. Trott (Great Britain). A team of French scientists (W. Gallique, B. Grinberg, and M. Tenard) developed a low-background device consisting of three plane counters which makes it possible to measure the specific activity of liquids containing β emitters in quantities corresponding to the amounts currently accepted as limiting allowable concentrations. This method also makes it possible to detect small radioactive impurities in solutions, e.g., a 0.02% P^{32} impurity in an S^{35} preparation.

A paper by R. Hasstrom (Finland) on improving liquid scintillators for measuring low activity levels and on the use of transistors for fast coincidence counters, and reports by M. Forte and A. Ansani (Italy) on a method of scintillation counting of very low-energy particles (below 1 kev) stimulated much interest.

J. Stein (Union of South Africa) discussed the relative efficiency of a liquid scintillation 4π counter compared to a proportional $4\pi\beta$-counter and a $4\pi\beta\gamma$-coincidence counter, finding that the efficiency drops as the energy of β radiation decreases, with a value of 98.5% reported for Co^{60}.

G. Engelman (France) told of an electrostatic method for measuring the activity of β emitters, making it possible to standardize P^{32} and Sr^{90} preparations to within 2% accuracy.

Three papers were devoted to measurements of radioisotopes in gas form. K. Hogreve (West Germany) discussed the process of absolute measurements of gases from the standpoint of the introduction of various corrective terms (including terms for drift of part of the electrons to the counter walls and absorption of the gas to be measured on the walls) reaching 2-3% accuracy. W. Mann (USA) submitted results of several research efforts with internally filled compensation counters in use at the National Bureau of Standards, particularly on the role of inhomogeneity of the electric field, the dependence of "wall effect" on the pressure of the gass filling the counter, and the effect of pulse discrimination and operating voltage on the plateau slope.

Several techniques for absolute measurements of β-active gases with the aid of special devices and internally filled compensation counters and some methods for absolute and relative measurements of the activity of volatile liquids (including liquid organic preparations) through their vapors were described in a report delivered by V. V. Bochkarev and V. A. Bazhenov (USSR).

The British scientists, R. Allen and S. Curran, delivered reports on methods for measuring isotopes decaying by electron capture. Measurements of low-Z isotopes by means of a $4\pi(x - \gamma)$ coincidence counter and proportional 4π counter under high pressure (up to 40 atm), and of high-Z isotopes with high-pressure counter for x rays and a scintillation 4π counter were described. Several problems concerning the mechanism of the operation of the counting circuit designed to measure isotopes decaying by electron capture were also discussed, particularly the effect of the diameter of the anode lead of the proportional counter on its energy resolution.

Problems concerning calibration of neutron flux and standardization of neutron sources were dealt with in papers presented by J. Thomas (Denmark) and K. Geiger (Canada) calorimetric measurements were discussed by M. Lecoin (France) and A. Brinjolfson (Denmark), a Compton dosimeter for measuring x rays and high-intensity gammas was discussed by B. Gross (Brazil). G. Kainz, K. Scharf, and R. Patselt (Austria) proposed a special device to determine fatigue effects in photomultipliers.

J. Domanus and B. Osuczewski (Poland) advanced a suggestion to redefine the concept of the "gram-equivalent of radium" as a radiological unit, taking into account the absence of any uniquely determined relation between the activity of the source and the dose rate due to the source, since γ emitters usually are not point sources and the dose rate is a factor of self-absorption of radiation within the source.

A report by G. Manoff (USA) on a technique for processing measurement data with the aid of various types of electronic computers was met with interest.

Several other reports bearing on the use of absolute counting techniques for solving such problems as variation in crystal sensitivity upon boring (K. Bechter, West Germany), particle detection in free-neutron decay (T. Novay, USA), detection and determination of the activity of β emitters distributed in specimens, by bremsstrahlung measurements (J. Patmen, Great Britain) were also discussed.

The proceedings of the symposium will be published by the IAEA.

INTERNATIONAL CONFERENCE ON ACCELERATORS

A. N. Lebedev

An International Conference on High-Energy Accelerators and Scientific Research Equipment, organized by the European center for nuclear research (CERN) with the support of the International Union of Pure and Applied Physics, met in Geneva, September 14-19, 1959. About 350 physicists and engineers from 29 countries participated in the conference.

The basic task confronting the conference was to get a picture of the progress made in theoretical and experimental research on the development of new acceleration techniques, leading to greatly increased energies and particle beam intensities. The conference also discussed ways of perfecting already existing facilities or those in the process of construction.

The conference was opened with a report given by a well-known specialist in the field of high-energy physics, the leader of the project working on the design of the huge 45 Bev linear accelerator, W. Panovsky (Stanford U., USA). This report discussed phenomena in the field of elementary particles which must be studied, in Panovsky's view, by means of high-energy accelerators, as well as the requirements set by the needs of the physical experiments on the energy and intensity specifications for the new accelerators.

Reports by Johns (Univ. of Mich., USA) and O'Neill (Princeton, USA) presented the requirements for associated equipment and particle beam parameters, as well as the features of the experimental work to be pursued in colliding-beam facilities. These questions are currently being much discussed. O'Neill gave a review of the work done at Stanford University on storage rings of various geometries incorporating injection from linear and cyclic accelerators. According to O'Neill, the installation of a storage magnet with colliding beams in the Stanford linear accelerator will be completed sometime in 1960. The system for introducing particles with a quick-acting magnetic shutter (operating time

$10^{-8} - 10^{-9}$ sec) already installed and tested in the Stanford facility was found highly interesting. The mechanism for trapping 500-Mev electrons in the storage system is closely related to the radiation effects accompanying the motion of relativistic electrons, and leading to intense damping of transverse oscillations. Since it was not possible to simulate these effects at low energies, the full-scale facility was built from the start. It must be particularly noted that O'Neill expects to produce an extremely high vacuum (10^{-9}–10^{-10} mm Hg). This vacuum will make it possible to extend the beam lifetime in the accelerating chamber to several hours, and will consequently provide the high circulating current values required.

The task of setting up a colliding-beam system has another solution which is not related to the need to have a separate injector-accelerator. This involves a symmetrical fixed-field ring synchrocyclotron suggested about three years ago by both A. A. Kolomenskii (USSR) and Okawa (Midwestern Universities Research Association). Facilities of this type make it possible to effect simultaneous acceleration and storage of two colliding beams of identical particles. As reported at the conference, this trend is being pursued currently by MURA (papers delivered by Cole and Simon), the Physics Institute of the USSR Academy of Sciences (papers by Kolomenskii and Lebedev), and CERN (paper by Penz).

The fundamental approach common to the three teams is, in addition to theoretical research, the development of electron ring synchrocyclotrons of relatively low energy; e.g., a colliding-beam machine accelerating to 38 Mev has already been built (but not commissioned) in the USA, and is designed primarily for research in techniques. CERN is engaged in the design of a similar accelerator and is aiming at 100 Mev, the idea being to use the machine for physics research. Both groups are in addition considering building a stacked-

beam ring synchrocyclotron as one of the possible ways of obtaining a stabilized Budker beam. Reports presented by American scientists informed us that work is in progress on a 10-15 Bev proton accelerator, which is apparently to consist of radial sectors with a spiral-modulated field.

Soviet papers on the same topic told of theoretical and simulated research carried out at the Physics Institute of the Academy of Sciences in connection with the development of electron ring synchrocyclotrons.

A large part of the conference reports was devoted to acceleration involving the use of plasma, four of the eight reports in this area being authored by Soviet scientists. Work on so-called plasma betatrons, in which electrons stripped from a discharge ignited at the beginning of the acceleration cycle in a chamber are accelerated, has been moving apace in several countries in recent years. CERN, for instance, is building five such machines, four of which are already in operation (report by Meusonnier). Measurements have shown that the value of the current of accelerated electrons in all these machines is extremely low, in every case several orders of magnitude lower than what was expected. At the present time, research is being pursued to probe into the reasons underlying such large losses.

Another interesting machine of the same type is the so-called "megatron," a plasma betatron designed by the Stevens Institute of Technology (USA), which has not yet been put into operation. It is designed to accelerate to 150 Mev, with the current of the order of 1000 amp. Its most striking feature is the very high value of the magnetic field strength (as high as 100 koe) and its correspondingly small size.

Two reports on plasma method were made by Okawa (Japan), speaking in the name of two collaborating groups. The first report gave an account of the theory and development of the plasma betatron, in which the magnetic field bears a strong resemblance to that in a stellarator. The second report told of a small linear accelerator designed to accelerate plasma bunches by the pressure of radio waves propagated in waveguides. This last technique is based on the idea of coherent acceleration as set forth by V. I. Veksler.

Several modifications of this basic idea were also discussed in papers presented by Soviet scientists Veksler and Tsytovich, on some problems dealing with the shock mechanism of acceleration in the case of collision of rings with relativistic current; Askar'yan, Levin, and Rabinovich delivered a paper on the stability of some plasma formations.

As was previously the case, a great deal of interest persists abroad in the idea of a stabilized electron beam as advanced by Budker. Emphasizing the difficulties lying in the way of realizing this idea in practice, Finkelstein (Stevens Institute, USA) told of theoretical research performed on the stability of a stabilized beam, and in particular,related the view that, from

this standpoint, the most promising approach is the use of an external strong-focusing guide magnetic field.

Of several new methods proposed for acceleration, we might single out the stochastic mode of operation, in which interest has grown measurably during the recent years, although the idea of the stochatron had been voiced by Burshtein, Veksler, and Kolomenskii as long ago as 1948. Some of the general problems relating to stochastic modes of acceleration were dealt with in the report by Kolomenskii and Lebedev, in which a number of considerations were voiced on the choice of the spectrum of accelerating voltages, and other topics. A report on the first working machine embodying these principles was made by Keller (CERN), who told of experiments with a small 4.7 Mev proton stochatron. With the aid of simple techniques for creating a "noise" voltage on the dees, the authors successfully obtained an intensity of the same order as in the synchrocyclotron mode of operation. In addition, Keller told of the possibility of employing the stochastic mode of acceleration to increase the intensity obtainable on the large CERN synchrocyclotron. This same group of topics should include the theoretical investigations by Robinson (Cambridge, USA) on an accelerator with simultaneously operating accelerating voltages of different frequencies.

An interesting project for designing an ironless strong-focusing synchrotron was related by Christophilos (Berkeley, USA). An interesting feature of the magnet is that it is to be cooled to a temperature of 80°K or even below. The report gave the machine parameters and some structural considerations regarding a 24 Bev machine of that type.

Some other reports by Soviet and foreign scientists were devoted to cyclotrons with spatial variation of the magnetic field. Of those, a report by Zamolodchikov and Dmitrievskii (Joint Institute for Nuclear Research, Dubna) on a spiral-sector field machine now in operation excited particular interest, since it is the first operating machine of this type.

Papers devoted to limitations and perturbing factors in accelerators were read at a special session.

Reports by Simon (MURA, USA), Orlov and Tarasov (Physics Institute of the Armenian Academy of Sciences, and Institute of Theoretical and Experimental Physics of the USSR Academy of Sciences), Robuche and Bariber (CERN) gave further developments in the nonlinear theory of betatron oscillations; in particular, the last-mentioned paper reported on investigations into particle losses in passing through a nonlinear resonance.

Simon's report further dealt with a theoretical analysis of the instabilities arising in a circulating charged beam, similar to the discussion in Kolomenskii's and Lebedev's report. These effects may be highly important in storage systems, imposing additional limitations on the parameters of the system.

79

In a report by Vladimirskii and Kapchinskii (Institute of Theoretical and Experimental Physics, USSR Academy of Sciences), a detailed exposition of the theory of particle motion in a proton linear accelerator was given, with the space charge effect taken into account. This problem has assumed an important practical stature at the present conjuncture, in view of the need for higher currents from linear accelerators, particularly for injection into large cyclic accelerators.

Large electron accelerators did not get much attention at the conference. It could be gathered from the report by Robinson (Cambridge, USA) that the concept formulated on radiation effects as a result of the work of Soviet and foreign authors is held to be valid at the present time. Most of the papers on electron synchrotrons were devoted to theoretical analyses of individual effects: choice of damping systems, calculations of losses with attenuation accounted for, etc., (papers by Orlov and Kheifets, Orlov, Kheifets, and Tarasov, USSR).

Of the experimental papers, we note the report by Sands (Cal Tech, USA) in which the quantitative agreement between the experimental data obtained from the 1.2 Bev electron synchrotron and the theoretical calculation of particle losses due to quantum fluctuations in radiation is pointed out.

As the session devoted to the state of the art in the design of high-energy accelerators, 10 short reports were heard on machines being designed or built in various countries. Plans for large synchrotrons were presented in a report by Livingston on the Cambridge 6 Bev accelerator, and another by Entschke on the 6 Bev Hamburg accelerator, which is still in the drafting stage.

Several weak-focusing proton synchrotrons are being built in various countries at present, the largest of them being the 7 Bev Harwell machine, the 12.5 Bev ANL machine, and the 3 Bev machine at Princeton.

Several papers dealt with the construction of strong-focusing proton synchrotrons. Thus, Green (Brookhaven, USA) told of a 30 Bev accelerator on which pre-operational work has been in progress for one-half year; Walton (ORNL, USA) told of a 12 Bev machine, and Vladimirskii (Institute of Theoretical and Experimental Physics of the USSR Academy of Sciences) gave an account of a 7 Bev accelerator. Neal (Stanford, USA) also stimulated much interest with his report on the design of a linear electron accelerator (10-20 Bev in the first cycle, 20-45 Bev in the second).

No special report was presented on the CERN 25 Bev strong-focusing synchrotron, but it became the subject of any number of unofficial discussions, in view of the fact that a huge success was obtained on that machine while the CERN conference was in session, namely the achievement of the first acceleration cycle on the machine.

The limited scope of this survey unfortunately does not afford us any opportunity to go into the enumerated papers in any detail. Furthermore, space considerations do not permit mention of many interesting papers, such as the contributions of the Khar'kov Physics and Engineering Institute on linear accelerators and plasma techniques, as well as quite a few papers on chambers, counters, and the use of beams in existing accelerators. A detailed account of the proceedings will be contained in the full proceedings of the conference, to be published by CERN in the near future.

The conference demonstrated with full clarity that Soviet science has rendered a sizable contribution to accelerator physics and engineering; this is attested to by the large number of Soviet papers (which comprised some one-third of the entire number, and about half of the papers on topics concerned solely with accelerators). This stands out even more clearly with respect to the new ideas propounded by Soviet scientists, which have provided the groundwork for further work in many countries all over the world.

AT THE INSTITUTE FOR PHYSICAL METHODS OF SEPARATION (GERMAN DEMOCRATIC REPUBLIC)

N. M. Zhavoronkov and K. I. Sakodynskii

Responding to the invitation of the German Academy of Sciences in Berlin, the authors visited Leipzig for several days; in which time we became familiar with the work accomplished at the Institute for Physical Methods of Separation (Director: J. Müllenpfordt), which is the main center for the dissemination of information in work with stable isotopes in the German Democratic Republic (East Germany).

The Institute was organized in 1955. Its basic task is to promote the use of stable isotopes in scientific research and to render assistance to all interested organizations in arranging and performing work using stable isotopes.

The Institute is engaged in intensive work on the systematization of basic information on the uses of stable isotopes in chemistry, biology, medicine, geo-

80

logy, etc., on techniques for handling stable isotopes, on the theory underlying separation processes. Several review articles written by workers at the Institute have appeared in print on these topics.

Despite the fact that the Institute was organized comparatively recently, work of no mean interest has been accomplished in this time. But the chief merit of the Institute is that it is the mainspring behind the development of work with stable isotopes in the entire German Democratic Republic, making available labeled compounds and carrying out isotopic analysis for all interested organizations.

The Institute is made up of six sections: a section on experimental separation by the fractional distillation method (headed by E. Krehl), a section on experimental separation by chemical exchange techniques (headed by K. Vetzel), a section on the theory of separation methods (headed by G. Focht), a theoretical section (headed by G. Voit), an analytical section (headed by G. Birkenfeld), and a section on the use of stable isotopes (headed by H. Hübner).

The tasks of the various separation sections are to produce concentrates of stable isotopes of hydrogen, boron, carbon, nitrogen, and oxygen. The Institute has for this purpose set up facilities for the separation of stable isotopes by the methods of fractional distillation and chemical isotope exchange. The oxygen O^{18} isotope and deuterium are produced by fractionation of water in a packed column; the concentration of O^{18} thus obtained is 4%, and deuterium, 7%. To obtain concentrates of the N^{15} isotope, the method of isotopic exchange between nitrogen oxides and those of nitric acid is resorted to. These techniques yield up to 10% enrichment in N^{15}. Experiments have been performed on obtaining the carbon isotope C^{13} by fractional distillation of carbon tetrachloride. It was shown that carbon tetrachloride of high purity does not decompose when stored in steel equipment.

Plans for the immediate future call for the expansion of production of stable isotopes, through the building of new and larger facilities, including facilities for producing B^{10} concentrates by exchange distillation between BF_3 and its anisole complex.

In the section on experimental separation by fractional distillation techniques, interesting research has also been performed on the effect of surface roughness of the packing material on separation efficiency. Optimum values of surface roughness have been ascertained, increasing packing efficiency by ~20%. In the same section, a proposal has been put forth to use the isobutyl

ester of benzoic acid as a medium for carrying out the droplet technique of isotopic analysis of water.

The work done in the theoretical sections, whose task is to elaborate the theory underlying the separatory processes and to calculate the values of the separation factors by quantum-statistical methods, is also of considerable interest. Work has been completed on calculation of the separation factors in the chemical exchange of several carbon-containing compounds, in the search for systems possessing the highest separation factors. Some interesting research has also been conducted in calculations of the work performed by a nonadiabatic fractionating column. A schedule of work on the uses of stable isotopes and other methods for separating stable isotopes has been drawn up at the Institute.

Over 30 labeled compounds have been synthesized by the section on the uses of stable isotopes. Many of the procedures evolved have already been adopted by industry. Labeled compounds put on sale include, e.g., ammonium nitrate and trimethylamine hydrochloride, labeled with N^{15}, acetic acid labeled with O^{18}, and other compounds.

The section for the uses of stable isotopes is conducting independent research on the uses of stable isotopes, in addition to providing consultations to various organizations. This section is engaged in a study of the process of biological transport of water in plants, using O^{18}, oxygen exchange between water and glass, exchange between the water of crystallization in sulfates and the water of the solution. Interesting results have been obtained in a study of the mechanism of oxidation of paraffins to fatty acids. Work has also been initiated in the field of the uses of isotope methods in geochemistry.

The analytical section has three mass spectrometers at its disposal. One of them, an MS-1, is specially equipped for carrying out determinations of deuterium content, the second, an MI-1305, is used for determining isotope ratios in solid compounds, while the third serves for conducting mass isotope analyses. Special purpose mass spectrometers are being developed in the analytical section, e.g., a mass spectrometer with a high-frequency filter, and tests are being performed on ion sources of various types. Work on the uses of electronic photomultipliers to determine the intensity of spectral lines is also a center of interest.

The analytical section is performing isotope analysis not only for research being conducted at the Institute itself, but is also engaged in analytical research for all interested organizations in the German Democratic Republic.

BUILDING AND DESIGNING OF ATOMIC-POWERED VESSELS IN WESTERN AND EASTERN COUNTRIES

A. V. Klement'ev

Maritime nuclear power has found its greatest application and development abroad in the area of naval and military shipbuilding, where the tactical and technical possibilities inherent in atomic-powered vessels are paramount and economic performance is a secondary factor.

The use of atomic energy on cargo vessels faces great difficulties of an economic and technical nature. The atomic ships under construction or in the design stage at present do not measure up to conventional cargo ships as do operating costs.

According to data published in the foreign press, capital expenditures for the building of an atomic ship exceed the cost of a conventional vessel by 10-30%. Operational expenses due mainly to high fuel costs and the presence of special auxiliary maintenance facilities run 15-20% higher. However, the increased cargo tonnage capacity and the unhampered sailing range of atomic ships compensates somewhat for the high operating expenses.

It has been established from technical and economic surveys that the use of atomic propulsion plants is most feasible on large ships for long hauls of liquid cargo or bulk cargo. Modern large-tonnage tankers spend 80-90% of their operating time on the high seas, with the weight of the fuel tank alone accounting for 10% of the weight on board, in the case of steam turbine-propelled ships on a long trip. Allowable capital outlays on tankers are therefore at a higher level than on dry-cargo ships, which are in port about half of their operating time.

All of the atomic power units under construction at present for installation in cargo and naval vessels are based on water-moderated, water-cooled reactors.

The most promising power plant approach is the single-loop heat removal system in a block with the gas turbine.

A great emphasis in research and experimental work is laid on designing a more economical and reliable nuclear reactor. Conventional steam turbines are used in the atomic power plants, having proved their usefulness over many years of use.

USA. Paramount attention is given to warships in the development of atomic vessels. Work on atomic-propulsion passenger and cargo ships is pursued with much less intensity. The first vessel of the merchant ship variety to be propelled by atomic energy is the Savannah (cf. Table). The power plant to be installed aboard that ship (similar to the power plant used in the

American atomic submarine Nautilus) will not possess optimum economic and design parameters. On this point, we might mention the long-term program announced in the USA in the beginning of 1957 toward the development of atomic installations for merchant ships. Some machinery manufacturers have been attracted to this program.

In the field of experimental investigation, a good deal of attention is being given to atomic gas-turbine installations, now being studied by several large companies. Under AEC auspices, General Dynamics Corp. is engaged in the design of a land-based prototype of a 20,000 hp maritime atomic power unit. A single-loop system with helium coolant and helium as the working fluid in the gas turbines is used. The prototype is expected to be ready for operation by early 1963. Tests of the setup will determine to what extent a single-loop system with helium coolant will prove feasible for propulsion of sea-going vessels [4].

The problem of installing an atomic propulsion unit on one of the tankers currently under construction is being studied. If the decision is positive, an atomic tanker of 22,500 tons deadweight and capable of 20 knots speed will be launched sometime in 1961 [5].

Great Britain. During the past three to four years Great Britain has been manifesting no mean interest in the use of atomic energy in her merchant and naval fleets.

The British firms Comel Lord and Babcock and Wilcox, Ltd. have drawn up a mutual agreement on research and design projects aiming at the development of an atomic power plant to power a tanker of 65,000 tons deadweight .*

Government scientific research organizations are engaged in the development of other projects for atomic power plants on tankers, in particular 25,000 and 50,000 hp units for tankers of 45,000 and 100,000 tons deadweight, respectively. In contrast to the US, Great Britain gives priority to economic feasibility in its specifications for atomic propulsion plants. As a result of the studies conducted by the British Shipbuilding Association in 1957, it was found that the use of shipboard atomic power plants will not be profitable for some years to come [6].

The problem of creating a submarine atomic-

---

*Deadweight is a term for the total load-carrying capacity of the ship, incl. weight of cargo, passengers with baggage, crew with baggage, fuel, lubricants, water, etc.

82

Essential Data on Ships Under Construction or in Design Stage in Foreign Countries [1-3, 8]

Country	Purpose	Name	Displace-ment, tons	Number of engines, and hp	Cruising speed, knots	Number of reactors, and type	Reactor heat output, Mw	U fuel en-richment,%	Costs, $ millions	Completion date
USA	Cargo-pas-senger	Savannah	22 080	20 000	21,0	water-mod, water-c 1	74	4,4	42,5	End of 1960
	Aircraft car-rier	Enterprise	86 000	4×70 000	35,0	water-mod, water-c 8	—	—	435	End of 1961
	Cruiser	Long Beach	14 000	2×35 000	45,0	water-mod, water-c 2	—	—	150	Mid-1961
	Guided-mis-sile destroyer	Bainbridge	7 900	—	45,0	water-mod, water-c 2	—	—	105	End of 1961
Japan	Passenger	—	26 380	2×20 000	23,5	water-mod, water-c 1	180	1,7	24,2	Design
	Submarine tanker	—	48 200	2×20 000	22,0	water-mod, water-c 1	180	1,7	—	Design
Sweden	Tanker	—	84 000	2×15 000	17,75	water-mod, water-cool-ed with boil-ing in core 1	100	1,0	—	Design

powered tanker is getting a good deal of attention. For example, on the "Cavess" docks of the Mitchell Engineering corporation, tests on various models of undersea atomic vessels are in progress [7].

Japan. In early 1956, a scientific research body was set up under the auspices of the Ministry of Transportation to study atomic shipbuilding possibilities. At the present time, this association includes over 50 scientific organizations and industrial firms throughout the country. A five-year plan elaborated by the association envisages completion of work on the power plant for the first atomic tanker sometime in 1961. In 1957, the body drew up plans for four types of power reactors for tanker propulsion units of 20,000 and 40,000 hp. The schedule of atomic shipbuilding approved by the body is based on the use of reactors acquired from the USA, in the first stage. Enriched uranium will also be imported.

In addition to this association, several firms are involved in atomic ship construction problems. Mitsubishi Heavy Industry has worked out plans for two tankers with atomic power plants, including one undersea tanker; Hitashi Shipbuilding and Engineering is working on a project of an atomic tanker of 65,000 tons deadweight capable of making 17 knots. This firm is also working on projects for atomic submarine tankers and atomic power plants for surface tankers with gas-cooled reactors. Plans for an atomic-powered passenger ship to ply the Japan-South America line have reached completion [8].

France. In late 1957, the Commissariat de l'Énergie Atomique announced a contest for a draft project of an atomic power plant of 20,000 hp to power a tanker of 40,000 tons deadweight. Several Franch companies have developed plans, but practical realization has not been achieved to date [9].

Sweden. The Hetaverken company has completed plans for an atomic tanker of 65,000 tons deadweight (displacement: 84,000 tons), capable of making 17.75 knots. A boiling water reactor has been proposed for the propulsion unit. The authors of the project feel, however, that the vessel will be unable to compete with conventional tankers [10].

Reports of plans for atomic tankers of smaller tonnages have also come to light in Sweden, in particular plans for a tanker of 45,000 tons deadweight with an atomic power plant of 20,000 hp.

LITERATURE CITED

1. Atomic Energy Newsletter 20 2 (1958)
2. Nucleonics, 9, 73 (1959); Motor Ship. 40, 146 (1959).
3. J. Amer. Soc. Naval Engrs. 70 629 (1958); Ship. World 138, 98 (1958).
4. Motor Ship. 39 562 (1959).
5. Marine Engng. 63, 73 (1958).
6. Shipbuild. and Shipp. Rec. 89, 26 (1957).
7. J. marine marchande, No. 2019 (1958).
8. Presentations by Japan at the Second International Conference on the Peaceful Uses of Atomic Energy (Geneva, 1958) Papers 1319 and 1320.
9. Nucl. Power 3 539 (1958).
10. Svensk sjöfarts tidn., 28, 1304 (1958).

BRIEF COMMUNICATIONS

USSR. The VII session of the Learned Council of the Joint Institute for Nuclear Research at Dubna met November 20-25, 1959, at Dubna. Leading specialists in the field of nuclear physics from the 12 member-nations of the Institute took part. Reports were delivered by the Director of the Joint Institute, Corresponding Member of the Academy of Sciences of the USSR, D. I. Blokhintsev, Vice Director Emil Dzhakov (Bulgaria), Prof. Wang Hang-ch'ang (China), and the directors of five laboratories, giving an account of the results of the scientific activity pursued by the staffs un- der their supervision.

USSR. The atomic icebreaker Lenin has been officially incorporated into the Soviet icebreaker fleet by the State Commission. Tests completed on December 5, 1959 showed that all of the mechanisms in the ice-breaker are functioning normally.

The tests were carried out under autumn and winter conditions in the Baltic Sea.

Rumania. Work has been completed at the Physics Institute of the Rumanian Academy of Sciences on a laboratory for work with radioactive isotopes.

NEW LITERATURE

Books, Symposia, Periodicals

Radioactive Methods in Process Control. Proceedings of the scientific-technical conference,Riga. (Izd. AN Latv. SSR , 1959) 295 pp. 12 rubles, 80 kopeks.

The book contains the reports read at the scientific-technical conference on radioactive techniques in the m monitoring and control of manufacturing processes, held at Riga in 1957. The papers deal with theoretical questions and instrument design based on the use of nuclear radiations. Some instruments and facilities used in industry for measuring different kinds of engineering data are described (e.g. level gauges,density gauges,thickness gauges, etc.). Problems which come up in the use of radioactive techniques for automation and controls in the metallurgical, coal, petroleum, and other branches of industry are discussed.

Corrosion and Wear in Water-Cooled Reactors. Edited by DePol [Russian translation] (Sudpromgiz, Leningrad, 1959) 416 pp. 20 rubles, 40 kopeks.

I. NUCLEAR ENERGY PHYSICS
Voprosy Filosofii, No. 9 (1959).

Berestskii, V. B., 117-124. The problem of the structure of "elementary" particles in modern physics.

Cherenkov, P. A., 125-130. Radiation from particles moving faster than the speed of light, and some of the uses of such radiation in experimental physics.
Zhur. Tekh. Fiz., Vol. 29, No. 8(1959).

Akhiezer, A. I., et al., 933-938. Simple waves in magnetohydrodynamics.

Fainberg, Ya. B., Kurilko, V.I., 939-945. The electromagnetic pressure on a charge moving in a magnetic field.

Barsukov, K. A., Kolomenskii, A. A., 954-957. The Doppler effect in an electron plasma with a magnetic field.

Kolomenskii, A. A., 981-991. On a rotating-focusing system for injection of particles into a proton synchrotron.

Lembra, Yu. Ya., 992-994. A note on the design of a regenerative deflector.

Loshak, Zh., 995-1008. Intrinsic functions of betatron oscillations in a ring synchrocyclotron.
Zhur. Tekh. Fiz., Vol. 29, No. 9 (1959).

Ivanov, D. P., et al., 975-977. Study of electron trapping in the magnet air gap of a fixed-field betatron.

Borovik, E. S., Grishin, S. F., 1110-1116. Determination of the composition of residual gases in the operation of a condensation pump.

Grishin, V. K., 1065-1067. Contribution to the design of a fixed-field strong-focusing accelerator.

Ivanov, D. P., et al., 1235-1244. Study of nonstationary current in a betatron.
Zhur. Tekh. Fiz.,Vol. 29, No. 10 (1959).

Fedorchenko, V. D.,et al., 1212-1218. Motion of an electron in a spatially periodic magnetic field.
Zhur. Éksp.i Teor. Fiz., Vol. 37, No. 3 (1959).

Samoilov, I. M., 705-712. On the mechanism of particle acceptance in a betatron.

Klimontovich, Yu. L., 735-744. Relativistic kinetic equations for a plasma. Part I.

Akhiezer, I. A., et al., 756-759. Simple waves in the Chew, Goldberger and Low approximation.

Drukarev, G. F., 847-848. On the Massey parameter in the theory of atomic collisions.

Mikheev, V. L., et al., 859-861. On the spontaneous fission of Am^{241}.

Strutinskii, V. M., 861-863. On the angular anisotropy of gamma photons accompanying fission.
Izvestiya Akad. Nauk SSSR, Seriya Fiz., Vol. 23, No. 8 (1959).

Bulkin, P. S.,et al., 941-947. Study of a self-sustaining pulsed high-frequency discharge in air and its transient behavior.

Levitskii, S. M., Shashurin, I. P., 948-951. Measurement of the charge concentration in a plasma, by the superhigh-frequency probe technique.

Golant, V. E., 952-957. On the appearance of a pulsed superhigh-frequency discharge in inert gases.

Golant, V. E., 958-961. On the relation between the characteristics of a superhigh-frequency current and a constant current in a gas.

Kushnir, R. M., et al., 1007-1011. Study of resonance charge exchange in monatomic gases and vapors of metals.

Mandel'shtam, S. L., Mazing, M. A., 1017-1020. On the broadening and the displacement of spectral lines in the plasma of a gas discharge.

Mitsuk, V. E., et al., 1031-1035. Measurement of the electric field in a superhigh-frequency plasma.
Izvestiya Vyssh. Ucheb. Zaved. Fizika, No. 4 (1959).

Kholev, S. R., 28-37. Equilibrium constants of a powerful shock wave in monatomic gases and hydrogen.

Berzin, A. K., et al., 130-134. Spatial distribution of betatron radiation.

Rodimov, B. N., Medvedeva, T. A., 147-157. The betatron with a guide magnetic field.

Kuz'min, V. N., Kamashev, Yu. M., 158-162. Use of a Hall effect transducer in measuring the dynamics of magnetic fringe fields in pulsed accelerators.

Nauka i Zhizn'. No. 10 (1959).

Kuba, J., 37-40. The Czechoslovak betatron.

Radiotekhnika i Elektronika, Vol. 4, No. 8 (1959).

Kucherenko, E. T., Fedorus, A. G., 1233-1237. The energy distribution of ions extracted from a high-frequency source.

Levitskii, S. M., Shashurin, I. P., 1238-1243. Testing the applicability of the probe technique to measurements of charge concentration in a high-frequency discharge.

Braun, S., 1244-1252. The use of high-frequency electromagnetic fields in plasma research.

Kucherenko, E. T. Nazarenko, O. K., 1253-1256. Features of a discharge with electron oscillations in a magnetic field.

Uspekhi Fiz. Nauk, Vol. 18, No. 3 (1959).

Fedorenko, N. V., 481-511. Ionization in collisions between ions and atoms.

Arkiv fys., Vol. 16, No. 1 (1959)

Eriksson, K., 1-14. Statistical time moments and an asymptotic formula for time and energy distributions of slowing-down neutrons.

Canad. J. Phys., Vol. 37, No. 8 (1959).

Roy, J., and L. Roy, 907-915. Effective neutron capture cross section, thermal capture cross section, and resonance integral of Pr^{143}.

Fickel, H., and R. Tomlinson, 916-925. Yield of light fission fragments in fission of Pu^{239} by thermal neutrons.

Fickel, H. and R. Tomlinson, 926-936. Yields of 21 heavy fragments in fission of Pu^{239} by thermal neutrons.

Nucl. Instrum. and Methods, Vol. 5, No. 2 (1959).

Zaccheroni, E., 78-89. 2.5 Mw high-frequency amplifier for the CERN linear accelerator. .

Kowalewski, V., et al., 90-94. On some properties of a radio-frequency ion source with a longitudinal magnetic field.

Paulin, A., 107-110. Possibility of increasing the energy and intensity of a microtron.

Nucl. Phys., 12, No. 5 (1959).

Johansson, S., 449-464. Spontaneous fission rates.

Nucl. Phys. Vol. 12, No. 6 (1959)

Firk, F., and M. Mokhov, 552-562. Determination of neutron resonance parameters of tungsten, by the transmission method.

Nucleonics, Vol. 17, No. 9 (1959).

Owen, R., 92-95. Pulse-shape discrimination identifies particle types.

Nuovo Cimento, Vol. 13, No. 4 (1959).

Colli, L., et al., 730-760. The (n, p) and (n, np) reactions with neutrons of 14 Mev energy.

Prosperi, D., and S. Sciuti, 767-777. A multipurpose 2π-counter.

Nuovo Cimento, Vol. 13, No. 5 (1959).

Milone, C., and A. Rubbino, 1035-1052. Energy spectrum and angular distribution of photoneutrons from oxygen.

Phys. Rev. Letters, Vol. 3, No. 4 (1959).

Birdsall, C., and A. Lichtenberg, 163-164. Traveling-wave focusing for plasma containment.

Phys. Rev. Letters, Vol. 3, No. 5 (1959).

Diaz, J., 234-235. U^{238} fission upon μ-meson capture.

Progr. Theoret. Phys., Vol. 21, No. 5 (1959).

Fujii, S. et al., 758-759. On the time-variation in thermonuclear fusion systems.

Progr. Theoret. Phys., Vol. 21, No. 6 (1959).

Imoto, M., et al., 939-941. T-Nt diagram for thermonuclear fusion research.

Prog. Theoret. Phys.,Vol. 22, No. 1 (1959).

Hamada, S., 145-146. On magnetohydrodynamic equilibrium.

Research, Vol. 12, No. 8-9 (1959).

Chick, D., and S. Hunt, 340-347. Electrostatic accelerators for nuclear research.

II. NUCLEAR POWER ENGINEERING

Teploénergetika, No. 9 (1959).

Margulova, T. Kh., 27-31. The use of sequential flashing and steam blowdown in the steam-raising units of atomic-fueled electric power stations.

Teploenergetika, No. 10 (1959).

Arsen'ev, Yu. D., 27-34. Choice of optimum vacuum conditions downstream of the turbine in atomic-fueled electric power stations.

Trudy Instituta Energetiki (Akad. Nauk Byelorus SSR) No. 9 (1959).

Ermakov, V. S., 92-115. Study of the temperature field in nuclear reactor fuel elements.

Atompraxis, Vol. 5, No. 9 (1959).

Eversheim, P., 362-367. Problems of nuclear physics and structural materials in reactor design.

Atomwirtschaft, Vol. 4, No. 9 (1959).

Bruni, M., and A. Verde, 368-373. Value of nuclear electric power stations for future electric power needs in Italy.

Schulten R. et al., 377-384. The high-temperature reactor of the Brown-Beveri and Krupp consortium.

Matz, G., 384-387. Fuel elements for high-temperature reactors.

Energia Nucl., Vol. 6, No. 6 (1959).

Silvestri, M., 369-375. A research and development program for heavy water reactors burning natural uranium fuel.

Dalmasso, C., and G. Nardelli, 376-392. The Wigner effect in graphite-moderated nuclear reactors. Part 2. Annealing theory and moderator research.

Zorzoli, G., 393-398. Variations in xenon concentration in reactors.

Industries Atomiques, III, No. 7-8 (1959).

Wertz, J., 55-62. The Belgian BR-3 research center.

Jaderná Energie, Vol. 5, No. 8 (1959).

Smetana, J., 253-255. Nuclear power in the energy budget of the Czechoslovak Republic.

Jaderna Energie, Vol. 5, No. 9 (1959).

Hauer, J., 289-295. New problems in the technology of the production of large-scale nuclear power reactors.

Pluhar, J., Vrtel, J., 296-303. Fuel elements, fuel-element cladding, and structural reactor materials.

Nucl. Power, Vol.4, No. 42 (1959).

Elliott, V., and G. Stathakis, 87-91. The Garigliano nuclear power plant.

Jeffrey, A., 103-105. Boundary conditions in diffusion theory.

Nucl. Sci. and Engng.,Vol. 5, No. 6 (1959).

Jordan, P., and G. Leppert, 349-359. Nucleate boiling characteristics of organic reactor coolants.

Goad, W., and R. Johnston, 371-375. Use of the Monte Carlo technique for solving the criticality problem.

Brown, H., et al., 376-381. Analysis of reactor power oscillations to determine temperature coefficients of reactivity.

McWhorter,R., et al., , 382-389. Use of thermal block control sheets.

Poppendiek, H., 390-404. Turbulent liquid-metal heat transfer in channels.

Gyftopoulos, E., and H. Smets, 405-414. Transfer functions of distributed-parameter nuclear reactor systems.

Volpe, J., et al., 360-370. Two-region studies in slightly enriched water-moderated uranium and uranium-water lattices.

Nucl. Sci. and Engng.Vol. 6, No. 2 (1959).

Sandmeier, H., 85-92. Nonlinear treatment of large perturbation in studies of power reactor stability problems.

Johnston, H., et al., 93-96. Relative worth of rare-earth oxide control elements.

Fritsch, A., and B. Levy, 97-99. Distribution and elution of fission products upon ThO_2-UO_3 slurry at simulated reactor conditions.

Stoughton, R., and J. Halperin, 100-118. Heavy nuclide cross sections of particular interest to thermal reactor operation: Conventions, measurements, preferred values.

Ruane, T., and M. Storm, 119-127. Epithermal hafnium parameters for calculation of control rod worth in thermal reactors.

Greebler, P., et al., 128-134. Neutron thermalization calculations for a heterogeneous lattice containing uranium and plutonium fuel in water.

Gyftopoulos, E., and L. de Sobrino, 135-139. Variational calculation of control rod reactivity.

Chappell, D., 140-146. Permissible voids in photon shields.

Jacobs, A., 147-151. Use of two-group albedo theory applied to temperature coefficient calculation.

Ash, M., 152-156. On control of reactor shutdown involving minimal xenon poisoning.

Tralli, N., et al., 157-158. Multigroup diffusion theory applied to calculation of K_∞ for heavy-water lattices.

Moore, L., 157. Transfer function for boiling water reactors.

Mullin, C., 160-162. Approximate solution of the Boltzmann equation.

Nucleonics, Vol. 17, No. 8 (1959).

92-96. Statistical calculation of hot-spot factors.

Hauser, L., 97-99. Limited-leakage pumps vs. canned motor pumps.

Nucleonics, Vol. 17, No. 9 (1959).

Meinke, W., 86-89. Pneumatic tubes speed activation analysis.

Banks, W., 96-102. Future of gas-cooled reactors.

Goosey, M. 104. Candia discriminator permits simplified monitor circuit.

Nukleonika, Vol. 4, No. 4 (1959).

Filipczak, W., and M. Sztainholer, 395-404. Electrical analog simulates reactor kinetics.

III. NUCLEAR FUEL AND MATERIALS

Geol. Rudn. Mestorozhdenii, No. 4 (1959).

Rekharskii, V. I., et al., 103-110. Redeposition of molybdenum and uranium by hydrothermal bicarbonate solutions.

Doklady Adad. Nauk SSSR, Vol. 127, No. 5 (1959).

Krongauz, V. A., Bagdasar'yan, Kh. S., 1047-1050. Transfer of energy of excitation and sensitization of chemical reactions in the radiolysis of solutions of aromatic compounds.

Doklady Akad. Nauk SSSR, Vol. 127, No. 6 (1959).

Savvin, S. B., 1231-1234. Photometric assay of throim and uranium, using the arsenazo-III reagent.

Zhur. Anal. Khim., Vol. 14, No. 4 (1959).

Grishina, T. N., 427-430. Determination of small amounts of rare-earth elements in preparations of praseodymium .neodymium, samarium, terbium, dysprosium, holmium, erbium, and thulium.

Gerkhardt, L. I., 434-439. The extraction-photometric method for determinations of thorium in natural materials.

87

Zaikovskii, F. V., 440-444. Complexometric and photometric determinations of thorium in minerals and ores.

Sinikova, S. I., Klassova, I. S., 451-456. Spectrophotometric investigation of uranium solutions. Note 2.

Zvenigorodskaya, V. M., Rinicheva, M. I., 457-462. Uranium determination by the fluoride method, with dead-stop titration.

Zhur. Neorganizh. Khim., Vol., 4, No. 8 (1959).

Badaeva, T. A., Alekseenko, G. K., 1873-1880. Phase diagram of the thorium-zirconium system.

Zapiski Vsesoyuz. Min. Obsh-va, No. 88, 4 (1959)

Bilibina, T. V., et al., 369-376. On uranium mineralization of the sedimentary-metamorphic type in Precambrian marbles and skarnlike rocks.

Izvestiya Akad. Nauk SSSR, Otdel. Tekh. Nauk. Metallurgiya i toplivo, No. 3 (1959).

Nesmeyanov, A. N., Firsova, L. P., 150-151. Vapor pressure of lithium, beryllium, boron, silicon, and lead oxides.

Izvestiya Akad. Nauk SSSR, Seriya Geol., No. 8 (1959).

Rekharskii, V. I., 20-23. Contribution to the problem of regularities in the distribution of molybdenum and uranium in mineralized zones.

Izvestiya Akad. Nauk SSSR, Seriya Geofiz., No. 7 (1959).

Vorob'ev, V. A., 995-1002. On the possibility of using shielded detectors in airborne radiometric surveys.

Izmeritel'naya Tekhnika, No. 8 (1959).

Sokolov, V. N., 25-26. High-speed method for determining concentrations of solutions.

Radiokhimiya, Vol. 1, No. 3 (1959).

Shevchenko, V. B., et al., 257-269. On the effect of the nature of a diluent on extraction of uranyl nitrate by TBP.

Nikol'skii, B. P., et al., 283-289. Adsorption of zirconium and niobium on silica gel.

Grinberg, A. A., et al., 300-308. Contribution to the production and properties of salts of uranooxalic acid with rare-earth elements.

Starik, I. E., et al., 321-324. On the forms of occurence of uranium and thorium in ground-ice deposits in the Antarctic.

Vdovenko, V. M., et al., 364. A method for purifying radioactive Zr^{95} tracer of Nb^{95} impurities.

Khim. Nauk. i Promyshlennost', No. 4 (1959).

Vinogradov, A. P., 418-422. Fundamental problems in radiochemistry.

Atomwirtschaft, IV, No. 9 (1959).

Ziehr, H., 365-368. Uranium deposits in Italy, and their exploration.

Dolle, L., 388-392. Steel research and nuclear engineering (II).

Chem. Process Engng., Vol. 40, No. 8 (1959).

Paulsen, F., 271-273. Review of plutonium separation processes.

Chem. Process Engng., Vol. 40, No. 9 (1959).

Harries, D., 313-316. Technology of zirconium and its alloys.

Industries Atomiques, III, No. 7-8 (1959).

Fisher, C., 49-54. The chemistry of artificial radioelements.

Gauzit, M., and R. Danon, 63-72. Activity of fission products of U^{235} bombarded by thermal neutrons.

J. Appl. Phys., Vol. 30, No. 8 (1959).

Brooks, H., 1118-1124. Radiation effects in materials.

Schweinler, H., 1125-1126. Some consequences of thermal neutron capture in silicon and germanium.

Fan, H., and A. Ramdas, 1127-1134. Infrared absorption and photoconducticity in irradiated silicon.

Reiss, H., 1141-1152. Diffusion-controlled reactions in solids.

Geballe, T., 1153-1157. Radiation effects in semiconductors. Thermal conductivity and thermoelectric power.

Willardson, R., 1158-1165. Transport properties of silicon and gallium arsenide.

Wertheim, G., 1166-1174. Recommendation properties of bombardment effects in semiconductors.

Curtis, O., 1174-1180. Radiation effects on recombination in germanium.

Loferski, J., and P. Rappaport, 1181-1183. Electron-bombardment-induced recombination centers in germanium.

Sonder, E., 1186-1194. Magnetic and electrical properties of reactor-irradiated silicon.

Bemski, G., 1195-1198. Paramagnetic resonance in electron-irradiated silicon.

Watkins, G., et al., 1198-1203. Spin resonance in electron-irradiated silicon.

Crawford, J., and J. Cleland, 1204-1213. Nature of bombardment damage and energy levels in semiconductors.

Gossick, B., 1214-1218. Disordered regions in semiconductors bombarded by fast neutrons.

Blount, E., 1218-1221. Energy levels in irradiated germanium.

Wertheim, G., and D. Buchanan, 1232-1234. Electron-bombardment damage in oxygen-free silicon.

Lint, V., and H. Roth, 1235-1238. High-energy electron irradiation of germanium and tellurium.

Aukerman, L., 1239-1244. Radiation-produced energy levels in compound semiconductors.

Simmons, R., and R. Balluffi, 1249-1258. X ray and expansion effects produced by imperfections in solids: deuteron-irradiated germanium.

Brown, W., et al., 1258-1268. Annealing of radiation defects in semiconductors. Deuteron-irradiated germanium.

MacKay, J. and E. Klontz, 1269-1274. Low-temperature annealing studies in Ge.

Truell, R., p. 1275-1278. Ultrasonic methods and radiation effects in solids.

Noggle, T., and J. Stiegler, 1279-1288. Electron microscope studies on the etching of irradiated germanium.

Oen, O., and D. Holmes, 1289-1295. Cross sections for atomic displacements in solids by gamma rays.

Loferski, J., and P. Rappaport, 1296-1299. Displacement thresholds in semiconductors.

Cahn, J., 1310-1316. Irradiation damage in germanium and silicon due to electrons and gamma rays. Memoires Scient. Rev. Metallurgie, Vol. 56, No. 3 (1959).

Calais, D., et al., 261-272. Dependence of recrystallization of imperfect single crystals of uranium grown by the method of the β→α phase transition, on the mode of plastic deformation.

Hérenguel, 273-284. Use of standard metallurgical processes in applications to cladding materials for fuel elements: Aluminum and magnesium.

Bellot, J., et al., 301-306. Contribution to the study of uranium alloys by thermal analysis in vacuum.

Langeron, J., and P. Lehr, . 307-315. Study of the α⇌β allotropic transformation in zirconium. Nucl. Power, Vol. 4, No. 42 (1959).

Butcher, B., 105-106. Deformation of α-uranium.

— 108-109. Plutonium production at the Argonne National Laboratory. Nucleonics, Vol. 17, No. 8 (1959).

Effect of alpha-beta thermal cycling on uranium and its alloys. Nukleonika, IV, No. 4 (1959).

Przewlocki, K., 417-439. The development of nuclear geophysics. Phys. Rev. Letters, Vol. 3, No. 3 (1959).

Blewitt T., et al., 132-137. Latent energy of irradiated copper.

IV. NUCLEAR RADIATION SHIELDING
Biokhimiya Plodov i Ovoshchei, Symposium No. 5 (1959).

Rubin, B. A., et al., 5-101. Use of ionizing radiations in controlling the quiescent stage of potato tubers during storage. Doklady Akad. Nauk Arm. SSSR, Vol. 28, No. 5 (1959).

Ananyan, V. L., 217-221. On beta-radioactive soils in Armenia. Doklady Akad. Nauk Uzbek SSR, No. 8 (1959).

Rozhdestvenskaya, L. F., et al., 11-13. The effect of gammas emitted by Co^{60} on the nutritive properties of mulberry leaves. Doklady Vsesoyuz. Akad. Sel'sko-khoz. Nauk, No. 9 (1959).

Mukhin, E. N., et al., 14-17. Effect of ionizing radiation on the resistance of potato tubers to the fungus Fusarium sp. Vestnik Rentgenologii i Radiologii, No. 4 (1959).

Nikitin, N. S., 59-65. On the use of photographic film for individual dosimetric monitoring of beta-particle flux.

Deev, Yu. S., et al., 66-68. Gamma-radiation indicators utilizing photoconductive cells.

Gel'fman, A. Ya., Vasyurenko, V. V., 68-69. An instrument for calibrating solutions of radioactive isotopes. Vestnik Sel'sko-khoz. Nauki, No. 8 (1959).

Kalashnikov, A. I., et al., 47-50. Experience in the use of small doses of radioactive radiations in incubation. Kolloidnyi Zhurnal, Vol. 21, No. 4 (1959).

Dunski, V. F., Smirnov, N. S., 436-441. Contribution to the question of the effect ionizing radiations on the degree of dispersion of aerosols. A. M. A. Arch. Industr. Health, Vol. 20, No. 2 (1959).

Guyton, H., et al., 9-13. Emergency measures for protection of respiratory tract from radiological and biological aerosols. A. M. A. Arch. Industr. Health, Vol. 20, No. 3 (1959).

Lippmann, M., 39-54. Irradiation exposure of personnel working with uranium compounds. Atompraxis, Vol. 5, Nos. 7-8 (1959).

Glubrecht, H., 276-280. Radiobiology and isotope applications in applied botany.

Herbst, W., . 280-284. Study of radioactive contamination of the environment. I. Plant-growing soil.

Neuwirt, R., . 284-288. Radioactivity measurements of atmospheric precipitates in air at Erlangen-Brucke.

Feldt, W., 316-319. Sensitive beta counters with low zero effect. Chem. and Process Engng., Vol. 40, No. 8 (1959).

-279-281 Safety procedures at a plutonium plant.

Chleck, D., and C. Ziegler, 287. A system for measuring concentrations of nonradioactive gases. Energia Nucl., Vol. 6, No. 9 (1959).

Cottini, C., et al., 588-594. Linear accelerator for scintillation and proportional counters. Industries Atomiques, III, Nos. 7-8 (1959).

Roubault, M., 37-47. The center of radiological research at the University of Nancy.

Jaderna Energie, Vol. 5, No. 8 (1959).

Beránek, J., et al., 261-265. Localization of radioactive wastes by fusing them with silicates.

Behounek, F., et al., 266-267. Measurement of thermal neutron dose with the aid of ionization chambers.

Jaderna Energie, Vol. 5, No. 9 (1959).

Rado, R., 303-308. Ionizing radiations and polymers.

Šilar, J., . 309-313. Pulsed methods for measuring relative scintillator efficiency.

Nucl. Instrum. and Methods, Vol. 5, No. 2 (1959)

DePancher, J., 61-74. Double-moderator neutron dosimeter.

Nucl. Power, Vol. 4, No. 42 (1959)

Wells, F, 92-96. Use of electronics to record radiation. 2. Dicriminators and coincidence circuits.

Nucleonics, 17, No. 8 (1959).

Mix, T., et al., 84-86. Neutron gage measures liquid level in intense γ-rays fields.

Brown, H., and J. Rogers, 88-90. Transistorized area monitor uses GI ion chamber probe.

— 100-101. Radiation protection standards revised.

Harlan, J. and E. Hart, 102, 10 -11. Ceric dosimetry: accurate measurements at 10^8 rads.

Taimuty, S., et al., 103-105, 107. Ceric dosimetry: routine use at 10^5-10^7 rads.

V. RADIOACTIVE AND STABLE ISOTOPES USES OF RADIOACTIVE RADIATIONS

Avtomat. Telemekh. i Svyaz', No. 8 (1959).

Belov, K. P., 13-14. Atomic light sources and their application to light signaling (in railways).

Voprosy Ékonomiki, No. 9 (1959)

Letenko, V., et al., 132-136. Some problems in the economics of the industrial use of radioactive isotopes.

Zhelezno- Doroshnyi Transport, No. 8 (1959).

Tatarinov, B. P., Arkhangel'skii, A. A., 34-38. Possibilities in the use of radioactive isotopes in railway transportation.

Izvestiya Vyssh. Ucheb. Zaveden. Priborostoenie, No. 1 (1959).

Shumilovskii, N. N., et al., 133-138. Use of radio-

active radiations for automatic control of liquid flow-rate in closed conduits.

Nauka i Zhizn', No. 9 (1959).

Furman, K. S., 12-16. Atomic instruments for automation.

Tekstil'naya Promyshlennost', No. 7 (1959).

Vlasov, P. V., 45-49. Use of radioactive isotopes in weaving.

Trudy Bashkir. Nauchno-issled. Inst. po Pererabotke Nefti, No. 12 (1959).

Yablonskii, V. S., Khizgilov, I. Kh., et al., 16-24. Determination of the amount of radioactive isotopes to be used for monitoring of flow of petroleum and petroleum products at pipeline pumping stations.

Trudý Moskv. Inst. Inzh. Zhelez.-Dor. Transport., No. 108 (1959).

Hsi Chung-heng, 327-335. Experimental research using radioactive isotopes on the process of breaking up rocks by introduction of wedges and aggregate, for driving tunnels.

Atompraxis, Vol. 5, No. 9 (1959).

Kühn, W., 335-342. Neutrons determine moisture on basis of material density measurements.

Energia Nucl., Vol. 6, No. 9 (1959).

Parolini, G., 571-587. Radioluminescence in response to β radiation.

Jaderna Energie, Vol. 5, No. 7 (1959).

Kovanic, P., 227-231. Economics of radioactive isotope production in nuclear reactors.

Nucl. Power, Vol. 4, No. 42 (1959).

Hall, G., 97-99. The criticality problem in the design of chemical plants for work with fissionable isotopes.

— 110-111. The Wantage irradiation facility.

Nukleonika, Vol. 4, No. 4 (1959).

Jurkiewicz, L., 347-363. Using radioactive isotopes in mechanical and metallurgical research.

Czernowa, A., Minc, S., 365-370. On the reduction of ferric oxide ions by gamma bombardment of aqueous solutions containing certain organic substances.

Smulek, W., 371-380. Tritium, the radioactive isotope of hydrogen.

Herczyńska, E., 381-388. Measurements of activity of tritium in the gaseous phase.

Czuchnik, A., et al., 389-394. Some problems related to the synthesis of tagged organic compounds.

RESEARCH by Soviet EXPERTS

Translated by Western Scientists

SPECTRA AND ANALYSIS
by A. A. Kharkevich

The first handbook directed toward acousticians and others working in those fields which require the analysis of oscillations—ultrasonics, electronics, shock and vibration engineering. This volume is devoted to the analysis of *spectral concepts* as they are applied to oscillations in acoustics and electronic engineering, and to a discussion of the methods of spectral analysis. Contents include KOTEL'NIKOV'S theorem for bounded spectra, the spectra and analysis of random processes, and (in connection with the latter) the statistical compression of spectra.

cloth   **236 pages**   **$8.75**

ULTRASONICS AND ITS INDUSTRIAL APPLICATIONS
by O. I. Babikov

This work is concerned with ultrasonic control methods which are applied in industry, and also with the action of high-intensity ultrasonic oscillations on various technological processes. Considerable attention is devoted to ultrasonic pulse methods of flaw detection and physicochemical research. It is an invaluable aid to scientific researchers, engineers, and technicians working in fields which make use of ultrasonic methods industrially, as well as being a convenient reference for a broad category of readers who might wish to become acquainted with the current state of ultrasonic instrumentation.

cloth   **265 pages**   **$9.75**

Tables of contents upon request

CONSULTANTS BUREAU
227 West 17th Street ● New York II, N.Y. ● U.S.A.

*An important new series published in cooperation with the
American Geophysical Union . . .*

SOVIET RESEARCH IN GEOPHYSICS

(TRANSACTIONS OF THE GEOPHYSICAL INSTITUTE
OF THE USSR ACADEMY OF SCIENCES)

IN ENGLISH TRANSLATION

Volume 1 A COLLECTION OF ARTICLES ON DYNAMIC METEOROLOGY

TRUDY No. 37, edited by I. A. Kibel'

The seven papers presented are the results of original investigations, including a newly proposed theory for the calculation of soil temperature at various depths from a given air temperature; a solution to the problem of the distribution with depth of a steady current in a baroclinic ocean layer; a new method of calculating the advective heat influx, and other reports on recently accumulated data in the field.

cloth   228 pages $8.00

Volume 2 ISOSTASY AND ISOSTATIC HYPOTHESES

TRUDY No. 38   by E. N. Lyustikh

The classic theories of Airy, Pratt, Dutton, and others are discussed, criticized, and amplified in the light of new data. The methods of gathering this information, the means of analysis, and the applications of original Soviet research are expounded fully both in the text and on related maps. Present theories related to isostatic rebound, compensation and overcompensation, gravitational anomalies showing concentrations of density, etc., are illustrated with accompanying pertinent data. Designed to produce a clearer and more up-to-date picture of the isostatic status of the earth.

cloth   150 pages $6.50

Volume 3 THE MICROSTRUCTURE AND MACROSTRUCTURE OF ELASTIC WAVES
IN ONE-DIMENSIONAL CONTINUOUS NONHOMOGENEOUS MEDIA

TRUDY No. 39   by B. N. Ivakin

This book discusses the problems of the structure of waves propagating in continuous nonhomogeneous and generally absorbing media, with a single spatial coordinate, over intervals infinitesimally small or comparable with a wavelength (microstructure) and over intervals larger or appreciably larger than a wavelength (macrostructure). The solutions of the wave problems posed are presented in operator notation, making it possible to study nonsteady-state oscillations, although detailed calculations and graphs are given for steady-state sinusoidal oscillations as well.

cloth   120 pages $6.00

Volume 4 INVESTIGATION OF THE MECHANISM OF EARTHQUAKES

TRUDY No. 40   by O. D. Gotsadze

The results of work conducted by the Geophysics Institute of the Academy of Sciences, USSR, since 1948 on the investigation of fault plane displacements are documented in this volume. During this period a method was evolved which makes it possible to determine the mechanical type of fractures at the focus, the dip and strike of the fault plane, and the direction of the displacement and order of the relative intensity of the first shock. Many of the methodological conclusions and results of interpretations are being published for the first time.

cloth   208 pages $7.50

CONTENTS UPON REQUEST

You may order on approval from

CONSULTANTS BUREAU

227 West 17th St.   ·   New York 11, N. Y.